

Probabilistic Finite Element Analysis &
Design Optimization for Structural Designs

by

Arumugam Deivanayagam

A Thesis Presented in Partial Fulfillment
of the Requirements for the Degree
Master of Science

Approved October 2012 by the
Graduate Supervisory Committee:

Subramaniam D.Rajan, Chair
Barzin Mobasher
Narayanan Neithalath

ARIZONA STATE UNIVERSITY

December, 2012

ABSTRACT

This study focuses on implementing probabilistic nature of material properties (Kevlar® 49) to the existing deterministic finite element analysis (FEA) of fabric based engine containment system through Monte Carlo simulations (MCS) and implementation of probabilistic analysis in engineering designs through Reliability Based Design Optimization (RBDO).

First, the emphasis is on experimental data analysis focusing on probabilistic distribution models which characterize the randomness associated with the experimental data. The material properties of Kevlar® 49 are modeled using experimental data analysis and implemented along with an existing spiral modeling scheme (SMS) and user defined constitutive model (UMAT) for fabric based engine containment simulations in LS-DYNA. MCS of the model are performed to observe the failure pattern and exit velocities of the models. Then the solutions are compared with NASA experimental tests and deterministic results. MCS with probabilistic material data give a good prospective on results rather than a single deterministic simulation results.

The next part of research is to implement the probabilistic material properties in engineering designs. The main aim of structural design is to obtain optimal solutions. In any case, in a deterministic optimization problem even though the structures are cost effective, it becomes highly unreliable if the uncertainty that may be associated with the system (material properties, loading etc.) is not represented or considered in the solution process. Reliable and optimal

solution can be obtained by performing reliability optimization along with the deterministic optimization, which is RBDO. In RBDO problem formulation, in addition to structural performance constraints, reliability constraints are also considered. This part of research starts with introduction to reliability analysis such as first order reliability analysis, second order reliability analysis followed by simulation technique that are performed to obtain probability of failure and reliability of structures. Next, decoupled RBDO procedure is proposed with a new reliability analysis formulation with sensitivity analysis, which is performed to remove the highly reliable constraints in the RBDO, thereby reducing the computational time and function evaluations. Followed by implementation of the reliability analysis concepts and RBDO in finite element 2D truss problems and a planar beam problem are presented and discussed.

To My Family and Friends...

ACKNOWLEDGEMENTS

I would like to thank and express my sincere gratitude to my advisor and committee chair, Dr. Subramaniam D. Rajan, for mentoring, motivating and guiding through all my research work and course works. I would also like to extend my gratitude to Dr. Barzin Mobasher and Dr. Narayanan Neithalath for being in my thesis committee.

I would like to thank Peter Goguen for his technical assistance and guidance regarding the experimental works and Thomas Fujibayashi for his technical support associated with the lab machines.

I would like to thank my friends for all their support and motivation throughout the studies and I am very glad to acknowledge all my classmates and colleagues, especially Jon Fein, Erblina Vokshi, and Canio Hoffarth for their support. I would also like to express my gratitude to all the CEE and ASU administrative staffs for their kind help and support.

I dedicate this thesis to my father, Deivanayagam, my mother, Meenambal, my sister, Kalaiselvi, my aunt, Manimozhi and to all my family and friends especially Thendral and Rajesh.

TABLE OF CONTENTS

	Page
LIST OF TABLES	viii
LIST OF FIGURES	xi
1. INTRODUCTION	1
1.1 Literature Review.....	3
1.1.1 Probabilistic Distribution Models	4
1.1.2 Probabilistic Finite Element Analysis through Weibull Models.....	5
1.1.3 Reliability Analysis and Implementation.....	7
1.1.4 Reliability-based Design Optimization.....	8
1.2 Thesis Objectives & Overview	14
1.2.1 Thesis Objectives	14
1.2.2 Thesis Overview	15
2. PROBABILISTIC FINITE ELEMENT ANALYSIS & DESIGN.....	16
2.1 Introduction.....	16
2.2 Probabilistic Distribution Models	19
2.2.1 Normal Distribution	25
2.2.2 Log-Normal Distribution	27
2.2.3 Weibull Distribution	29
2.2.4 Generalized Exponential Distribution.....	34

	Page
2.2.5	Gamma Distribution.....36
2.3	Goodness of Fit Tests.....38
2.3.1	Kolmogorov-Smirnov (KS) Test38
2.3.2	Chi-Square test.....39
2.3.3	Anderson-Darling (AD) Test39
2.3.4	Maximum Likelihood Criterion.....40
2.4	FORM Method.....41
2.5	SORM Method.....44
2.6	MCS Method.....47
2.7	RBDO Method47
3.	EXPERIMENTAL DATA.....52
3.1	Introduction.....52
3.2	Sampling53
3.3	Experimental Results56
3.3.1	Kevlar® 49 -Swath Data.....58
3.3.2	Yarn Data63
3.4	Parameter Response of Swath.....66
3.5	Compliance Test69
3.6	Digital Image Correlation72
4.	FINITE ELEMENT AND MATERIAL MODELING.....74
4.1	Introduction.....74

	Page
4.2	NASA Ballistic Tests76
4.3	Finite Element Model76
4.4	Material Model.....77
4.5	Finite Element Program83
5.	NUMERICAL EXAMPLES.....88
5.1	Fabric Based Engine Containment System.....88
5.1.1	Experimental Data - Distributions88
5.1.2	Monte Carlo Simulations101
5.2	Truss Designs.....109
6.	CONCLUSIONS AND FUTURE WORK126
6.1	Conclusions.....126
6.2	Future Work127
	Appendix A.....130
	REFERENCES133

LIST OF TABLES

Table	Page
Table 2-1. Weights of W1, W2 [9].	34
Table 2-2. Weights of W3[9].	34
Table 2-3. Anderson-Darling Test - Critical Values.	40
Table 3-1. Operational Characteristic Curve Parameters.	55
Table 3-2. Yarn Experimental Data (psi).	55
Table 3-3. Sample Size Calculation With $\alpha = 0.05$.	55
Table 3-4. Kevlar® 49 Swath (2" x 8").	59
Table 3-5. Kevlar® 49 Swath (2" x 11").	60
Table 3-6. Kevlar® 49 Swath (2" x 14").	61
Table 3-7. Kevlar® 49 Yarn (8").	64
Table 3-8. Kevlar® 49 Yarn (11").	64
Table 3-9. Kevlar® 49 Yarn (14").	65
Table 4-1. Summary of UMAT Parameters.	81
Table 4-2. Damping Coefficient Values.	84
Table 4-3. Energy Checks.	87
Table 5-1. Weibull Comparison Results.	89
Table 5-2. Results Using EDP Software- Kevlar® 49-Swath (E).	91
Table 5-3. Maximum Likelihood Criterion Results - Kevlar® 49-Swath (E).	91
Table 5-4. Results Using EDP Software- Kevlar® 49-Yarn (E).	95
Table 5-5. Maximum Likelihood Criterion Results - Kevlar® 49-Yarn (E).	96

Table	Page
Table 5-6. Results of Data Analysis Using EDP.	100
Table 5-7. Test Case I Results.	102
Table 5-8. Simulations vs. Probability of failure.	103
Table 5-9. Flat_Impact Model Description.	104
Table 5-10. Parameters and Distribution Models.	105
Table 5-11. Simulation Results of Flat Impact Model.	106
Table 5-12. Simulation Results of Engine Containment Models.	107
Table 5-13. 2-Bar Truss Problem Data.	111
Table 5-14. 2-Bar Truss Results ($\sigma_x = 5\%$)	112
Table 5-15. 6 Bar-Truss Problem Data.	114
Table 5-16. 6-Bar Truss Results ($\sigma_x = 5\%$)	115
Table 5-17. 31-Bar Truss Problem Data.	117
Table 5-18. 31 Bar Truss Results ($\sigma_x = 5\%$)	117
Table 5-19. Beam Problem-Random Variable Data.	120
Table 5-20. Beam Problem RBDO Results.	121
Table 5-21. 3-Bar Truss Problem Data (RBDO).	121
Table 5-22. 3 Bar Truss-Random Variable Data.	122
Table 5-23. 3 Bar Truss-Reliability Analysis Results.	123
Table 5-24. 3 Bar Truss-RBDO Results	124
Table 5-25. 6 Bar Truss-Random Variables Data.	124

Table	Page
Table 5-26. 6 Bar Truss-Reliability Analysis Results.	125
Table 5-27. 6 Bar Truss – RBDO Results	125

LIST OF FIGURES

Figure	Page
Figure 1-1. Kevlar® 49 fabric	3
Figure 2-1. Limit surface [20].....	18
Figure 2-2. CDF $F(x)$ []	20
Figure 2-3. PDF $f(x)$ [39].....	21
Figure 2-4. Survival function $S(x)$ [39]	22
Figure 2-5. Effect of shape parameter in Weibull distribution [39]	24
Figure 2-6. Effect of scale parameter in normal distribution [39]	24
Figure 2-7. Effect of location parameter in normal distribution.....	25
Figure 2-8. Normal distribution - PDF	26
Figure 2-9. Log-normal distribution - PDF	27
Figure 2-10. Weibull distribution – PDF.....	29
Figure 2-11. Generalized exponential distribution - PDF.....	35
Figure 2-12. Gamma distribution - PDF.....	37
Figure 2-13. Flowchart for FORM method	44
Figure 2-14. Flowchart for SORM method	46
Figure 2-16. Flowchart for RBDO method.....	48
Figure 2-17. Flowchart for RBDO with sensitivity analysis	50
Figure 3-1. Operational characteristic curve [45]......	54
Figure 3-2. Piecewise linear approximation of true stress vs. true strain curve ...	57
Figure 3-3. Grip plates a) side view b) inner view	58

Figure	Page
Figure 3-4. True stress vs. true strain curve -Kevlar® 49-swath (2” x 8”).....	60
Figure 3-5. True stress vs. true strain curve -Kevlar® 49-swath (2” x 11”).....	61
Figure 3-6. True stress vs. true strain curve -Kevlar® 49-swath (2” x 14”).....	62
Figure 3-7. True stress vs. true strain curve - various gage lengths (Kevlar® 49-Swath)	62
Figure 3-8. True stress vs. true strain – various gage lengths (Kevlar® 49-yarn)	65
Figure 3-9. Parameters vs. gage length (Kevlar® 49-swath) (load, modulus, toughness & strain at ultimate stress – clockwise)	66
Figure 3-10. Ultimate stress vs. gage length (Kevlar® 49-swath)	67
Figure 3-11. Parameters vs. gage length (Kevlar® 49-yarn) (load, modulus, ultimate stress, strain at ultimate stress & toughness- clockwise)	68
Figure 3-12. Compliance test for Kevlar® 49-swath.....	71
Figure 3-13. Compliance test for Kevlar® 49-yarn.....	71
Figure 3-14. Experimental setup for DIC	72
Figure 3-15. Image correlation [46].....	73
Figure 4-1. Modeling the fabric as continuum	74
Figure 4-2. High speed NASA-ballistic test setup (a) steel ring with Kevlar® 49 Wrap. (b) gas gun (c) typical projectile	76
Figure 4-3. Projectile, ring and fabric FE model	77
Figure 4-4. Spiral modeling scheme	79
Figure 5-1. PDF for Kevlar® 49-swath (E)	92

Figure	Page
Figure 5-2. CDF for Kevlar® 49-swath (E).....	93
Figure 5-3. PDF for Kevlar® 49-swath (σ_{ult}).....	94
Figure 5-4. CDF for Kevlar® 49-swath (σ_{ult})	95
Figure 5-5. PDF for Kevlar® 49-yarn (E)	97
Figure 5-6. CDF for Kevlar® 49-yarn (E).....	97
Figure 5-7. PDF for Kevlar® 49-yarn (σ_{ult}).....	98
Figure 5-8. CDF for Kevlar® 49-yarn (σ_{ult}).....	99
Figure 5-9. CDF plot for probabilistic analysis	101
Figure 5-10. Schematic diagram of the FE model	104
Figure 5-11. CDF plot of exit velocity for LG594	108
Figure 5-12. CDF plot of exit velocity for LG620	109
Figure 5-13. 2-bar truss FE model	111
Figure 5-14. Probability of failure vs. σ_X (% of mean)-2-bar truss.....	113
Figure 5-15. 6-bar truss FE model	114
Figure 5-16. Probability of failure vs. σ_X (% of mean) - 6-bar truss.....	115
Figure 5-17. 31-bar truss FE model	116
Figure 5-18. Probability of failure vs. σ_X (% of mean) - 31-bar truss.....	118
Figure 5-19. Cantilever beam problem [53].	119
Figure 5-20. 3-bar truss FE model(RBDO)	121
Figure 6-1. Advanced MCS method	127

ABBREVIATIONS

ASTM	American Society for Testing Materials
ASU	Arizona State University
CDF	Cumulative Distribution Function
DIC	Digital Image Correlation
DO	Deterministic Optimization
EDF	Empirical Distribution Function
EDO	Engineering Design Optimization
FAA	Federal Aviation Administration
FEA	Finite Element Analysis
FORM	First Order Reliability Method
RBDO	Reliability Based Design Optimization
RIA	Reliability Index Approach
PDF	Probability Density Function
PMA	Performance Measure Approach
RO	Reliability Optimization
SORM	Second Order Reliability Method
MCS	Monte Carlo Simulation
MLE	Maximum Likelihood Estimation
MPPF	Most Probable Point of Failure

NOMENCLATURE

α, σ	Shape parameter
$\mathbf{\alpha}$	Vector of steepest descent direction
β^a	Reliability index allowable limit
β_j	Reliability index associated with j^{th} constraint
β_j^a	Allowable reliability index associated with j^{th} constraint
β_{FORM}	Reliability index using FORM method
β_{SORM}	Reliability index using SORM method
δ_a^x	Allowable deflection in x-direction
δ_a^y	Allowable deflection in y-direction
ε, σ	Engineering strain and engineering stress
ε_t, σ_t	True strain and true stress
$\varepsilon_{ult}, \sigma_{ult}$	Strain at ultimate stress and ultimate stress
$\dot{\varepsilon}$	Strain rate
λ	Scale parameter
κ	Curvature of the response function
μ	Mean or location parameter
μ_x	Mean of the random variable
μ_x^N	Equivalent normal mean
ϕ	Standard normal probability density function

σ_x	Standard deviation of the random variable
σ_a^t	Allowable tensile stress
σ_a^c	Allowable compressive stress
σ_y^t	Yield tensile stress
σ_y^c	Yield compressive stress
σ_x^N	Equivalent normal standard deviation
Φ	Standard normal cumulative distribution function
C, P	Cowper Symonds factor
D	Matrix of second order derivative of response function in the standard normal space
d	Direction vector
E	Young's modulus
F	Total number of function evaluations
$F(x)$	Cumulative distribution function (CDF)
$f(x)$	Probability density function (PDF)
g_j	j^{th} constraint
g^{rc}	Reliability constraint
G	Shear modulus
k	Iteration number
L	Log-likelihood Function
n, N	Sample size

n_{rc}	Total number of reliability constraints
n_{tc}	Total number of constraints
n_c	Number of inequality constraints
n_{dv}	Number of design variables (deterministic)
n_{rv}	Number of random variables (probabilistic)
N_f	Number of failure
P_f	Probability of failure
P_x, P_y	Load in x-direction and y-direction
s	Step size
$S(x)$	Survival (or, reliability) functions
T	Transformation matrix
U	Random variable vector in reduced (standard normal) space
x	Vector of design variables
X	Random variable vector in normal space
X, x	Values corresponding to the data
$\mathbf{x}^l, \mathbf{x}^u$	Vector of lower and upper bounds on the design variables
$\mathbf{X}^l, \mathbf{X}^u$	Vector of lower and upper bounds on the random variable in normal space

1. INTRODUCTION

The traditional deterministic optimization (DO) can be used to obtain optimal solutions to structural design problems involving considerations such as cost, serviceability, strength etc. A typical design optimization problem is posed as follows.

$$\begin{aligned} & \text{Find } \{\mathbf{x}\} \\ & \text{to minimize } f(\mathbf{x}) \\ & \text{subject to } g_i(\mathbf{x}) \leq 0 \text{ for } i=1, \dots, n_c \\ & \quad \quad \quad h_j(\mathbf{x}) = 0 \text{ for } j=1, \dots, (n_{tc} - n_c) \\ & \text{subject to } \mathbf{x}^l \leq \mathbf{x} \leq \mathbf{x}^u \end{aligned} \tag{1.1.1}$$

Vastly different solution techniques are available to solve such problems - gradient-based techniques that find the closest local optimal design point in a continuous design space to population-based techniques that can potentially be used to find the global optimal design point in continuous and discontinuous design space. In any case, in a deterministic optimization problem formulation the uncertainty that may be associated with the system (material properties, loading etc.) is not represented and considered in the solution process.

RBDO incorporates the stochastic nature of the random variables in evaluating the response of the system and an appropriate solution is found. In the problem formulation, in addition to structural performance constraints, reliability constraints are considered. The problem statement is posed as follows.

$$\begin{aligned}
& \text{Find } \{\mathbf{x}\} \\
& \text{to minimize } f(\mathbf{x}) \\
& \text{subject to } g_i(\mathbf{x}) \leq 0 \text{ for } i=1, \dots, n_c \\
& \quad h_j(\mathbf{x}) = 0 \text{ for } j=1, \dots, (n_{rc} - n_c) \\
& \quad \beta_k(\mathbf{X}) \geq \beta_k^a \text{ for } k=1, \dots, n_{rc} \\
& \quad \mathbf{x}^l \leq \mathbf{x} \leq \mathbf{x}^u \\
& \quad \mathbf{X}^l \leq \mathbf{X} \leq \mathbf{X}^u
\end{aligned} \tag{1.1.2}$$

In the above problem formulation, additional reliability based constraints are imposed that are computed from the random variables associated with the problem.

Structural analysis is an integral part of the design optimization problem statement and today, the analysis method of choice is the finite element method. In this thesis, two design examples are considered. The first is the design of planar trusses that serves to illustrate how RBDO can be potentially used in the optimal design of structural systems. The second example deals with implementation of the concept in fabric based engine containment system. Woven fabrics are widely used in the propulsion engine containment systems to mitigate the damaging effects from the fan blade out events. Kevlar® 49 is widely used in industrial products where large deformation and high energy absorption are required. A simple fabric weave using Kevlar® 49 fabric is shown in the Figure 1-1. It consists of warp yarns (in horizontal direction) and fill yarns (in vertical direction).



Figure 1-1. Kevlar® 49 fabric

To understand the deformation of the fabric under impact system and build a finite element model, many aspects have to be studied such as material properties of the constituent parts, projectile geometry, impact velocity, friction between fabric and projectile, friction between fabrics plies, and boundary conditions associated with the system. Material properties form the basis of the constitutive model. Tension tests on the material in warp and fill yarns show that the material is quite similar in both the directions and other tests such as picture frame shear test, friction test are conducted to characterize the shear and friction properties of the material [1]. Previous analyses [2, 3, 4, 5, 6 & 7] were based on the use of deterministic material properties (mean value from a set of experimental results) in the material model. In this study, some of the important material properties are modeled using probabilistic distribution models that are then used to randomly assign material properties to elements in the finite element model.

1.1 Literature Review

Considerable amount of research has been carried out by other researchers to analyze structural systems considering the stochastic nature of material properties, geometric nonlinearities or loading conditions.

1.1.1 Probabilistic Distribution Models

Basu et al. [8] studied the effects of using different types of statistical models in modeling the strength of ceramic materials such as monolithic ZrO_2 and ZrO_2 - TiB_2 composites, glass and Si_3N_4 . Goodness of fit tests are used with cumulative distribution function (CDF) and probability distribution function (PDF) of various distribution models to distinguish between a good fit and a better fit. The researcher used Weibull, Gamma, generalized exponential, normal and lognormal distributions with goodness of fit tests such as Kolmogorov Smirnov test, Anderson Darling test, Maximum likelihood criterion test and Chi-square test.

Cousineau [9, 10, 11] studied the importance of three parameter Weibull distribution by focusing on the change in the skew of the model with the change in the shape parameter. He compared the Weibull 2-parameter with Weibull 3-parameter model showing that for some data, model parameters are poorly estimated when the Weibull 2-parameter model is used instead of 3-parameter model. The studies also include different methods for estimating the parameters such as method of moments, maximum likelihood and mixed method (involving both method of moments and maximum likelihood). The results show that the mixed method which involves minimizing two equations simultaneously containing location and shape parameters is the one that consistently produces more accurate results. An unbiased estimation method for the Weibull 3-parameter distribution is demonstrated using MCS technique.

Gupta et al. [12, 13, 14 & 15] developed the generalized exponential distribution as a particular member of Weibull exponential distribution. The authors studied the closeness of the distribution with the other existing distributions frequently used in carrying out lifetime data analysis. They also compared the distribution with Gamma, lognormal and Weibull distributions, and the study reveals that the generalized distribution provides more accurate results compared to other distributions. The accuracy estimates are carried out using Maximum Likelihood Estimators (MLE), Method of Moment Estimators (MME), Least Square Estimators (LSE) and Unbiased Estimator (UBE) with UBE, MLE and MME being the superior methods.

1.1.2 Probabilistic Finite Element Analysis through Weibull Models

Dooraki et al. [16] studied the role of Weibull parameters on the strength of different yarns. Quasi-static tests and high rate tests were performed on Kevlar 129, Kevlar KM2, Kevlar LT, Twaron and Zylon with the gage length effect on Kevlar 129. The results from the study shows that the scale parameter obtained for various gage lengths is associated with the average strength of the yarn and the shape parameter is related to variation of the strength among the specimens. In addition, (a) Weibull parameters are dependent on the number of specimens that are used to model the data and (b) probability of defects increases with the increasing gage length. Finally, an exponential 3 parameter growth model is developed by considering the normalized volume and normalized failure stress of the material.

Bimodal Weibull distribution of strength of Kevlar-KM2 fabric has been used by Wang et al. [17] to determine the effect of fiber friction coefficient during ballistic impacts. Digital element approach, also known as sub-yarn modeling, is used where each yarn is divided into number of digital fibers. MCS is used to assign a unique material property at the element level based on the concept that the statistical property varies along the length and thickness of the yarn. The developed finite element model using MCS showed good results when compared with the experimental results using residual velocities.

Nilakantan et al. [18] used Monte Carlo approach at yarn level modeling (Kevlar KM2 fabric) in which all the elements modeling a yarn are assigned a unique set of material properties based on the probabilistic nature of elastic modulus, strength and failure strain. The FE model is broken into 50 zones and each zone is assigned a set of material properties. They do not specify the number of MCS runs made. However, they compare the MCS results with deterministic runs made using low, mean and high strength of the material.

Gu [19] simulated the ballistic penetration of conical steel projectile through plain Twaron fabric. The finite element method used the actual fabric structure (warp and weft yarns) in which yarns are modeled using three-dimensional elements having probabilistic-based material properties (Young's modulus). The results from the simulation show that the residual velocities are comparable to experimental results (varying number of fabric layers and projectile velocities).

1.1.3 Reliability Analysis and Implementation

Mahadevan and Haldar [20] illustrated the stochastic analysis of structures using first-order reliability method (FORM), second-order reliability method (SORM) and MCS. Various types of FORM analysis were studied such as Hasofer-Lind [21] method and Rackwitz & Fiessler [22] method. The Hasofer-Lind method can be applied to the problems involving only linear functions and normal variables whereas the Rackwitz and Fiessler approach can be applied to problems involving non-normal variables and nonlinear functions. Rackwitz and Fiessler explain the analysis using second order approximation where curvature of the associated performance function is considered. The second order approximation provides for a more accurate representation of nonlinear functions.

Kiureghian et al. [23] proposed the point-fitting method for computing the curvature of the nonlinear limit state functions. The method is based on fitting a paraboloid at discrete points. Erroneous results that are produced in curvature fitting method due to noise are reduced in this method. Kiureghian and Stefano [24] developed a better method for estimating the curvatures using the performance function gradient in an iterative way. The method computes the principal curvatures of the limit state function in the order of decreasing magnitude. The researchers show that both the above mentioned methods are efficient for problems involving large number of random variables.

Liu and Der Kiureghian [25] use various optimization methods for solving reliability analysis problem formulation. The optimization methods include

gradient projection method, penalty method, Augmented Lagrangian method, sequential quadratic programming, HL-RF method and modified HL-RF. The optimization techniques are compared based on accuracy, efficiency and robustness. Five test cases involving explicit functions of random variables were used, and the modified HL-RF method was found to be best considering number of function evaluations, gradient evaluations and time required for the analysis as the metrics.

1.1.4 Reliability Based Design Optimization

There are two types of approaches in RBDO and they are described next.

Mono-Level Approach (or) Double-Loop Approach: In this approach, reliability optimization (RO) is carried out within the DO (see Eqn.(1.1.10)). The process is stopped once the results converge.

Decoupling Approach: In this approach the RO and DO are carried out separately. DO is used to solve the optimization problem given by Eqn.(1.1.2) but without the reliability constraints. Once the DO solution is obtained, a reliability-based optimization problem (see Eqn.(1.1.8) and Eqn.(1.1.9)) is solved. Results from the DO are updated in the RO and vice versa. The iterative procedure is stopped once the results converge.

Thanedar and Kodiyalam [26] replaced deterministic constraints with probabilistic constraints as follows.

$$\begin{aligned}
 & \text{Find } \{\mathbf{x}\} \\
 & \text{to minimize } f(\mathbf{X}, \mathbf{x}) \\
 & \text{subject to } 1 - P_i(g_i(\mathbf{X}, \mathbf{x})) > R_i^a \text{ for } i=1, \dots, n_{rc}
 \end{aligned} \tag{1.1.3}$$

where R_i^a , the allowable reliability level between 0 and 1, is specified for all the constraints involving random variables and P_i is the probability function. Truss and cantilever beam problems involving linear functions, nonlinear functions, non-normal variables are solved using the proposed approach and the results are compared with results from deterministic models.

Royset et al. [27] proposed three different problem formulations with probabilistic constraints. They are (a) minimize the cost subject to reliability constraints, (b) maximize the reliability subject to cost and structure constraints and (c) minimize the initial cost and expected cost of failure subject to reliability and structural constraints. The last problem is reformulated by replacing the reliability constraints with the function that captures the minimum of limit state function within a ball of specified radius. In this approach, DO and RO are decoupled, and a series of system failure is considered in which failure of one constraint leads to the failure of the structure.

Enevoldsen and Sorensen [28] show the different formulations of reliability based design involving reliability constraints, reliability inspection and planning. Reliability based estimation is based on FORM analysis. Sensitivity of objective function, optimal design and constraints with respect to optimization variables and other deterministic parameters of the problem are also performed as post-analysis to study the effect of optimal solution.

Kuschel and Rackwitz [29] proposed mono-level formulation of reliability based cost optimization with the measure of reliability based on FORM analysis. The problem formulation is modification of the one proposed by Polak et al. [30].

$$\begin{aligned}
& \text{Find } \{\mathbf{x}\} \\
& \text{to minimize } f(\mathbf{x}) \equiv C^0 + C(p) + L(p) \sum_{i=1}^{n_{rc}} \Phi(-\|\mathbf{U}_i\|) \\
& \text{subject to } \Phi(-\|\mathbf{U}_i\|) \leq p_i^a \tag{1.1.4} \\
& \quad \mathbf{g}_i(\mathbf{U}_i) = 0 \\
& \quad \mathbf{U}_i^T \nabla_U g(\mathbf{U}_i) + \|\mathbf{U}_i\| \|\nabla_U g(\mathbf{U}_i)\| = 0 \\
& \quad \mathbf{H}(\mathbf{x}) \leq 0
\end{aligned}$$

where C^0 is the fixed cost, $C(p)$ is the variable cost, L is the failure cost associated with each failure mode and H is the structural equality and inequality constraints. This approach is used to design portal frames using sequential quadratic programming. The disadvantages of the method are that the method is not robust (final solution is a function of the initial guess) and that the second order derivative of response function ($g(\mathbf{U})$) is required.

Agarwal [31] shows how to use a combination of deterministic and probabilistic optimization in a decoupled RDBO approach. The deterministic optimization problem is posed as follows.

$$\begin{aligned}
& \text{Find } \{\mathbf{x}\} \\
& \text{to minimize } f(\mathbf{X}, \mathbf{x}) \\
& \text{subject to } g_i^{rc}(\mathbf{X}, \mathbf{x}) \leq 0 \quad i = 1, \dots, n_{rc} \tag{1.1.5} \\
& \quad g_j(\mathbf{x}) \leq 0 \quad j = 1, \dots, n_{soft} \\
& \quad \mathbf{x}^l \leq \mathbf{x} \leq \mathbf{x}^u
\end{aligned}$$

The probabilistic optimization problem is posed as follows.

$$\begin{aligned}
& \text{Find } \{\mathbf{X}\} \\
& \text{To minimize } g_j^{rc}(\mathbf{U}_j) \\
& \text{subject to } \beta_j - \beta_j^a = 0 \\
& \beta_j = \|\mathbf{U}_j\|
\end{aligned} \tag{1.1.6}$$

The random variable from probabilistic optimization is updated in the deterministic optimization as follows.

$$\mathbf{U}_i^{k+1} = \mathbf{U}_i^k + \sum_{j=1}^{n_{dv}} \frac{\partial \mathbf{U}}{\partial \mathbf{X}_j} (\mathbf{x}_j^{k+1} - \mathbf{x}_j^k) \text{ for } i=1, \dots, n_{rc} \tag{1.1.7}$$

The steps are repeated until the results converge.

Tu et al. [32] studied two different types of reliability optimization formulations - Reliability Index Approach (RIA) and the Performance Measure Approach (PMA). The former is described as follows.

$$\begin{aligned}
\text{RIA: } & \text{minimize } \|\mathbf{U}_j\| \\
& \text{subject to } g_j^{rc}(\mathbf{X}_j) = 0
\end{aligned} \tag{1.1.8}$$

The latter is described as follows (see Eqn.(1.1.6)).

$$\begin{aligned}
\text{PMA: } & \text{minimize } g_j^{rc}(\mathbf{X}_j) \\
& \text{subject to } \|\mathbf{U}_j\| = \beta_j^a
\end{aligned} \tag{1.1.9}$$

The study shows that the RIA approach is more suitable for violated constraints, PMA for inactive constraints and both the approaches yield the same results when the constraint is active.

Mahadevan and Haldar [33] proposed new methodology for RBDO involving reliability based constraints at system level and component level in an

iterative manner. Element level reliabilities are also estimated using Monte Carlo (variation reduction technique). The problem formulation is as given as follows.

$$\begin{aligned}
& \text{Find } \{\mathbf{x}\} \\
& \text{To minimize } f(\mathbf{x}) \equiv \text{Weight} \\
& \text{subject to } \beta_i^l \leq \beta_i \leq \beta_i^u \text{ for } i=1, \dots, n_{rc} \\
& \quad \quad \quad g_j(\mathbf{x}) \leq 0 \text{ for } j=1, \dots, n_c
\end{aligned} \tag{1.1.10}$$

where β_i^l, β_i^u are the lower and upper bounds on reliability corresponding to the i^{th} constraint. The proposed method is based on linear objective function and nonlinear reliability constraints. Design examples include the design of portal frames.

Zou and Mahadevan [34] proposed a variation of the decoupling approach. The problem formulation is based on minimization of cost function subject to reliability constraints and structural performance constraints. RO is done separately before each DO and it is updated by its first order approximation.

$$\begin{aligned}
& \text{To find } \{\mathbf{x}\} \\
& \text{minimize } C(\mathbf{x}) \\
& \text{subject to } g_i(\mathbf{x}) \leq 0 \text{ for } i=1, \dots, n_{rc} \\
& \quad \quad \quad h_j(\mathbf{x}) = 0 \text{ for } j=1, \dots, (n_{rc} - n_c) \\
& \quad \quad \quad \beta_i^k + \sum_{j=1}^{n_{dv}} \frac{\partial \beta_j}{\partial \mu_j} (\mu_j^{k+1} - \mu_j^k) \geq \beta_i^a \text{ for } i=1, \dots, n_{rc} \\
& \quad \quad \quad \beta_s^k + \sum_{j=1}^{n_{dv}} \frac{\partial \beta_j}{\partial \mu_j} (\mu_j^{k+1} - \mu_j^k) \geq \beta_s^a \\
& \quad \quad \quad \mathbf{x}_j^l \leq \mathbf{x}_j \leq \mathbf{x}_j^u \\
& \quad \quad \quad \mu_j^l \leq \mu_j \leq \mu_j^u
\end{aligned} \tag{1.1.11}$$

where β_s is the reliability index at the system level and μ is the mean of the random variables. The methodology employs RIA for reliability analysis and MCS for nonlinear reliability constraints. The problem also employs identification of potentially active constraints and thereby significantly reducing the computational time involved. Here the random variables and design variables are common (same) in both the deterministic and probabilistic optimization. And the proposed method is more efficient than the decoupled approach based on PMA approach.

Chen and Du [35] proposed another variation of the decoupled approach - sequential approximation and reliability assessment. In each cycle, the DO is updated based on the information from the most probable point of failure (MPPF).

The problem formulation is as follows.

$$\begin{aligned}
 & \text{Find } \{\mathbf{x}\} \\
 & \text{to minimize } f(\mathbf{x}, \boldsymbol{\mu}) \\
 & \text{subject to } g_i^{rc}(\mathbf{x}, \boldsymbol{\mu} - \mathbf{s}_i) \geq 0 \text{ for } i=1, \dots, n_{rc} \\
 & \mathbf{s}_i = \boldsymbol{\mu}^k - \mathbf{X}^k
 \end{aligned} \tag{1.1.12}$$

where \mathbf{s} is the shifting distance updated after PMA based reliability assessment to increase the feasibility on the deterministic constraints. The mean of the random variable from the reliability based assessment is used. The method is implemented in vehicle crashworthiness problems and truss problems [36].

Frangopol [37, 38] presented different problem formulations for life cost and utility optimization concepts with applications in civil and aerospace structures, the history of probabilistic structural optimization, its applications in

life cycle cost analysis and how the problem formulations can be used to solve problems in the future. The survey papers shed light on the available methods for reliability based optimization and provide a comprehensive view of probabilistic structural optimization.

1.2 Thesis Objectives & Overview

1.2.1 Thesis Objectives

The major objectives of the research works are as follows.

- a. Study available statistical models and develop the relevant equations and algorithms in implementing them as a computer program.
- b. Develop a computer program to obtain parameters (scale, shape, location) associated with various distribution models.
- c. Use the developed program for selection of suitable statistical model for different types of material properties that are obtained from Kevlar® 49 uniaxial tension test. The material properties include Young's modulus, crimp strain, strain at ultimate stress, stress at nonlinear post-peak region, failure strain, etc.
- d. Implement FORM, SORM and MCS in a computer program to obtain the reliability of a given structural system.
- e. Develop a computer program to perform RBDO using planar truss and beam finite elements involving linear constraints, nonlinear constraints, normal and non-normal random variables.

- f. Use MCS to carry out the analysis of fabric-based engine containment system that is typically modeled using deterministic FE model in LS-DYNA.

1.2.2 Thesis Overview

Chapter 2 provides an introduction to probabilistic analysis, discusses the available probabilistic distribution models (normal, lognormal, gamma, generalized exponential, Weibull), compares the goodness of fit tests that are performed to select the best distribution models, shows how estimation of reliability using FORM, SORM, and MCS can be carried out, and discusses the theory and implementation of the RBDO procedure.

Experimental data used in this thesis is discussed in Chapter 3. First, measurement error and sampling of experimental data are discussed. Then, results from uniaxial tension test of Kevlar® 49 fabrics and yarns are presented, analyzed and discussed.

In Chapter 4, finite element modeling, material modeling of Kevlar® 49, recent improvements to the existing model, comparison of material parameters over various phases of the research, and energy checks are explained.

In Chapter 5, several numerical examples are presented. First, the fabric model data used with engine containment systems is analyzed. This data is then used in the MCS of two NASA-GRC ballistic tests. Second, five planar truss models are used in illustrating the developed FORM, SORM, MCS & RBDO procedures. Finally, a planar beam model is used to illustrate the RBDO procedure.

2. PROBABILISTIC FINITE ELEMENT ANALYSIS & DESIGN

In this chapter the background on probabilistic analysis is presented followed by available probabilistic distribution models (normal, lognormal, gamma, generalized exponential, Weibull), comparison of various the goodness of fit tests, estimation of reliability using FORM, SORM, and MCS, and the theory and implementation of the RBDO procedure.

2.1 Introduction

The classical way of designing steel structures is to follow the provisions of either Allowable Stress Design (ASD) or Ultimate Strength Method. In ASD method, the yield stress of the material is divided by a factor of safety, i.e. factor of safety is used for resistance alone. In the Ultimate Strength Method, the maximum load is multiplied by a factor of safety, i.e. factor of safety is used for the load acting on the system. In Load Resistant Factor Design (LRFD) method, factor of safety is used for both the load and resistance provided by the structure. Some of the quantities such as load acting on the system and material properties that are used in the system are random in nature and cannot be accurately captured using factor of safety as in deterministic analysis. By considering the random nature of these values, we can more accurately capture the response of the structure and hence decrease the probability of failure. Examples of the random variables are shown below.

Load: Live loads, wind loads and seismic loads are random in nature.

Material Properties: Material properties such as Young's modulus (E), strain at ultimate stress (ε_{ult}), yield stress (σ_y) and ultimate stress (σ_{ult}) are random.

These properties are either computed using experiments (material properties) or are obtained from historical data (wind and seismic loads). The distribution of these values can be modeled as explained later in Section 2.2.

Failure of the system is defined based on the performance functions. The performance functions are based on service limit states and strength limit states failure criteria. Service limit states correspond to the performance of system considering occupancy of the structures (e.g. maximum displacements, cracking, vibrations etc.), and strength limit states are concerned with load carrying capacity of the structure (e.g. allowable compressive stress, allowable tensile stress, Euler buckling criteria etc.). A structure (or) system is considered to have failed if any of the performance criteria is violated. A typical performance function is given by

$$g(R,S) = R(\mathbf{x}, \mathbf{X}) - S(\mathbf{x}, \mathbf{X}) \quad (2.1.1)$$

$$\begin{aligned} g(R,S) > 0 &\Rightarrow \text{Safe} \\ g(R,S) < 0 &\Rightarrow \text{Failure} \end{aligned} \quad (2.1.2)$$

where R is resistance of the structure and S is the load acting on the structure. Figure 2-1 explains the difference between failure and safe zones. The reliability index β is the distance of the design point (MPPF) from the origin when the random variables are expressed in standard normal space. The closer the limit

surfaces are to the origin, the higher the probability of failure. The probability of failure is computed as follows (assuming the variables are independent)

$$\iint_{g(\mathbf{U}) < 0} f(U_1)f(U_2)dU_1dU_2 \quad (2.1.3)$$

The probability of failure is based on the joint probability density function of the variables that are random in nature. Joint probability density function is the probability function when there is more than one random variable associated with it. Since the computation of joint probability density function is extremely complicated, the probability of failure is computed using either reliability methods involving Taylor series approximation (1st & 2nd order) of the performance function or simulation techniques are used. The commonly used reliability methods and simulation techniques include the following:

- I. First Order Reliability Method (FORM)
- II. Second Order Reliability Method (SORM)
- III. Monte Carlo Simulation (MCS)

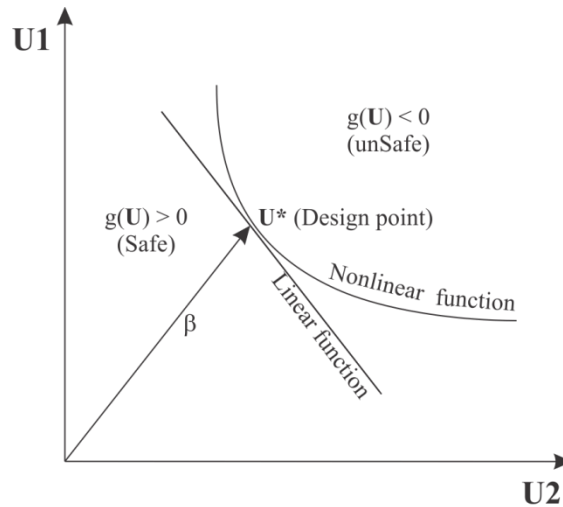


Figure 2-1. Limit surface [20]

Procedure in Probabilistic Analysis

In a typical probabilistic analysis, the following steps are used in the computations.

1. Problem-specific random variables are identified.
2. Random variable data are collected based on the experiments or historical data. A distribution that best fits the data is selected and parameters associated with the distribution are computed (Section 2.2 &2.3).
3. Performance of the structure is described using service limit state or strength limit state criterion.
4. Performance evaluation and computation of reliability and probability of failure of the system can then be undertaken (Section 2.4 through Section 2.6).

These steps are discussed next.

2.2 Probabilistic Distribution Models

Using experimental data in analytical or numerical models requires a careful analysis of the underlying data. This section explains how one can categorize and analyze this data using probabilistic analysis. Specifically, examples are taken from solid mechanics but the ideas and procedures are applicable for other data sources. Some of the terms used in this section are defined first before they are used in data analysis.

Cumulative Distribution Function

Cumulative Distribution Function (CDF), $F(x)$ is the probability that the variable takes a value less than or equal to x .

$$F(x) = \text{prob}[X \leq x] = \alpha \quad (2.2.1)$$

CDF plot for a normal distribution is shown in Figure 2-2. For continuous distributions, the above function is expressed mathematically as

$$F(x) = \int_{-\infty}^x f(\mu) d\mu \quad (2.2.2)$$

where μ corresponds to the dataset values and the integral represents the area under the curve up until x .

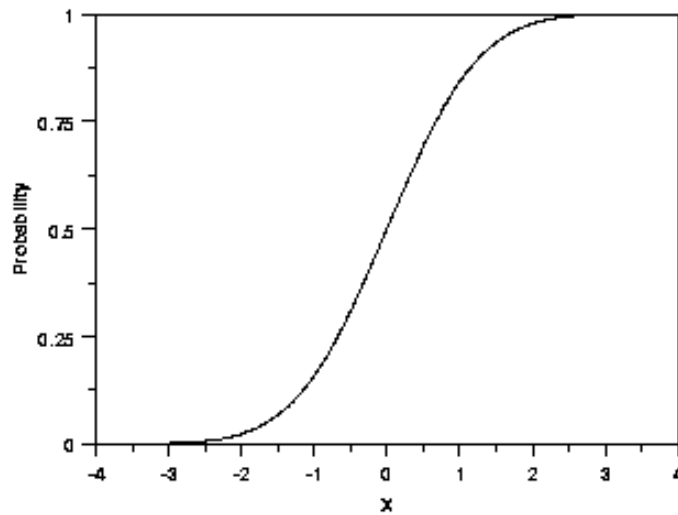


Figure 2-2. CDF $F(x)$ [39]

Probability Density Function

Probability Density Function (PDF) $f(x)$ is a function that describes the relative likelihood for this random variable to occur at a given point. The probability for the random variable to fall within a particular region is given by

the integral of this variable's density over the region. The PDF is nonnegative everywhere, and its integral over the entire space is equal to one¹.

$$f(x) = \frac{d(F(x))}{dx} \quad (2.2.3)$$

$$\text{Prob}[x_L < X \leq x_U] = \int_{x_L}^{x_U} f(x) dx \quad (2.2.4)$$

The PDF plot for a normal distribution is shown in the Figure 2-3.

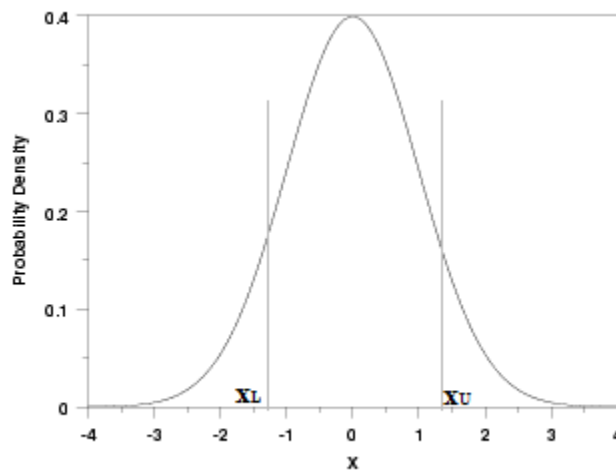


Figure 2-3. PDF $f(x)$ [39]

Survival Function

Survival function $S(x)$ (Figure 2-4) is the probability that the variate takes a value greater than x and is given as

$$S(x) = \text{prob}[X > x] = 1 - F(x) \quad (2.2.5)$$

¹ http://en.wikipedia.org/wiki/Probability_density_function.

It captures the probability that the system will survive beyond a specified time. The term *reliability function* is common in engineering while the term *survival function* is used in a broader range of applications, including human mortality².

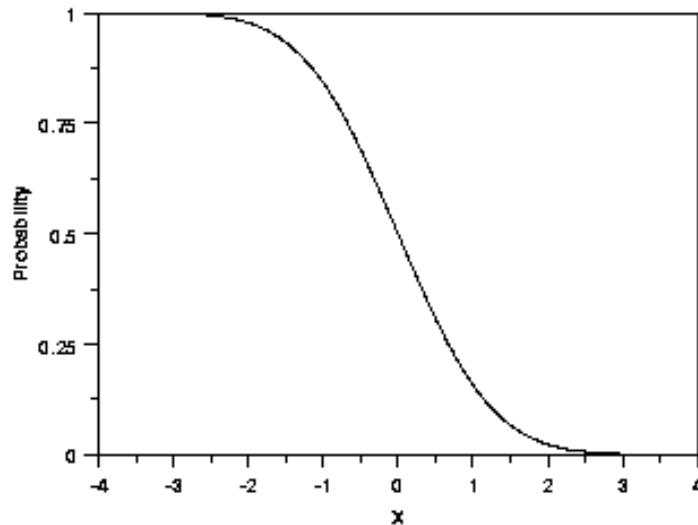


Figure 2-4. Survival function $S(x)$ [39]

Maximum Likelihood Estimation

Maximum Likelihood Estimation (MLE) is one of several methods of estimating the parameters of a statistical model. When applied to a data set and given a statistical model, MLE provides estimates for the model's parameters³. MLE starts with the likelihood function of a given data. For example $x_i (i=1,2,\dots,n)$ constitutes a sample size with relative frequency $f(x, \theta_1, \dots, \theta_k)$, where $\theta_1, \dots, \theta_k$ are the unknown parameters. The likelihood function is given as

² http://en.wikipedia.org/wiki/Survival_function

³ http://en.wikipedia.org/wiki/Maximum_likelihood_estimation

$$L(\theta_1, \theta_2, \dots, \theta_k) = \prod_{i=1}^n f(x, \theta_1, \theta_2, \dots, \theta_k) \quad (2.2.6)$$

The unknown parameters are the ones that maximize the likelihood function. The parameters are estimated by taking natural logarithm of the likelihood function, then differentiating with respect to the unknown parameters and equating the result to zero, e.g.

$$\theta_j = \frac{d \ln L}{d \theta_j} = 0 \quad (2.2.7)$$

Scale Shape and Location Parameters

Scale, shape and location parameters are the three parameters that are associated with the distribution function.

The shape parameter allows the distribution to take variety of shapes, and this helps in modeling a variety of datasets. Figure 2-5 shows the effect of shape parameter in Weibull distribution.

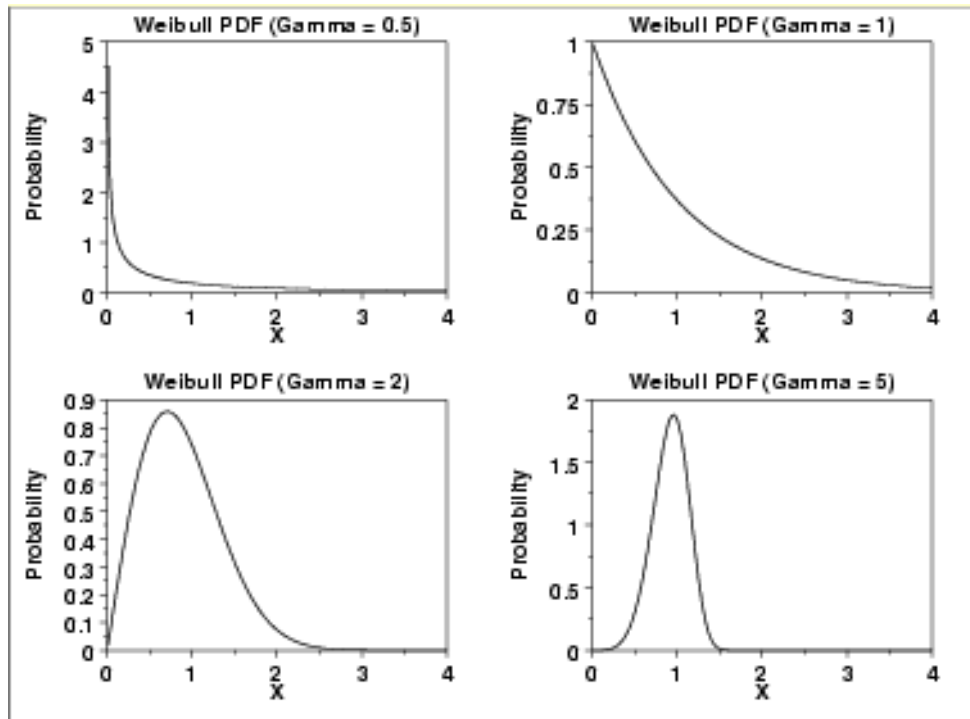


Figure 2-5. Effect of shape parameter in Weibull distribution [39]

The scale parameter helps to stretch out the graph. The greater the magnitude, greater the stretching effect. A scale parameter (Figure 2-6) value less than 1.0 compresses the PDF and a value equal to 1.0 leaves the PDF unchanged.

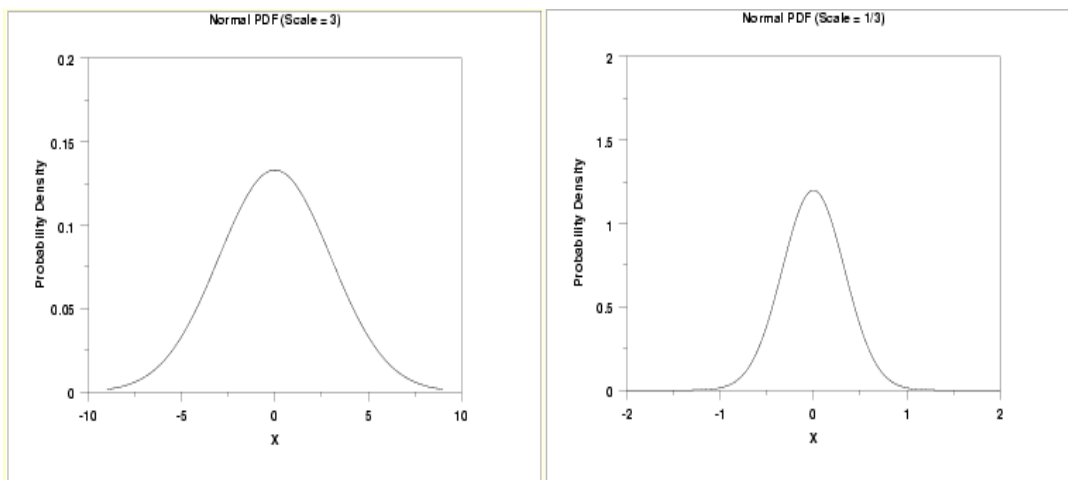


Figure 2-6. Effect of scale parameter in normal distribution [39]

The location parameter helps to translate the graph. It shifts the graph right or left depending on the value. Figure 2-7 shows the effect of location parameter in a selected distribution.

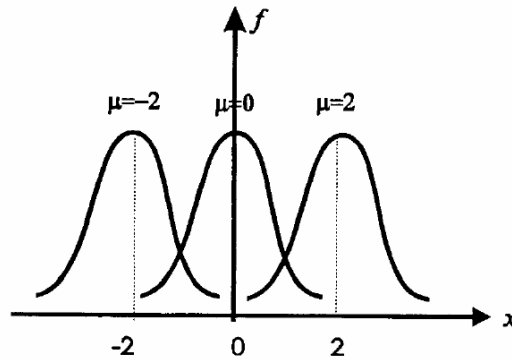


Figure 2-7. Effect of location parameter in normal distribution

In the distributions explained in the subsequent sections, unless otherwise specified, the location parameter is assumed to be zero.

2.2.1 Normal Distribution

Normal distribution is the one that resembles a bell shaped curve. The curve is symmetric with most of the data situated around probability's mean value and decreasing values on the either side (Figure 2-8). It has less of tendency to produce extreme values. Observation error in experimental data is a good example of normal distribution.

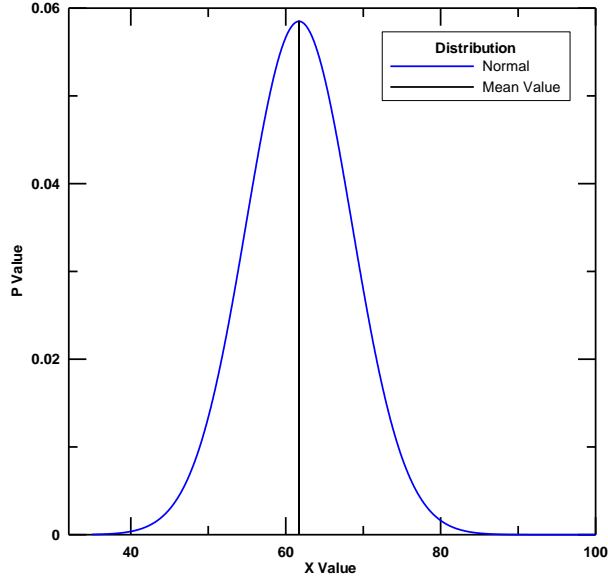


Figure 2-8. Normal distribution - PDF

Normal distribution is sometimes called Gaussian distribution or bell curve. The PDF of the normal distribution is given as

$$f(x) = \frac{1}{\sqrt{(2\pi)} \sigma} e^{-\frac{(x-\mu)^2}{2\sigma^2}} \quad (2.2.8)$$

where μ is the location parameter and σ is the scale parameter. The values of the parameters are found by differentiating the log-likelihood function with respect to the parameters and equating to zero. The log-likelihood function is given as

$$L_N = -\frac{n}{2} \ln(2\pi\sigma^2) - \sum_{i=1}^n \frac{(x_i - \mu)^2}{2\sigma^2} \quad (2.2.9)$$

Using Eqn.(2.2.9), the parameters that maximize the function can be computed as

$$\mu = \frac{\sum_{i=1}^n x_i}{n} \quad (2.2.10)$$

$$\sigma = \frac{\sum_{i=1}^n (x_i - \mu)}{n-1} \quad (2.2.11)$$

The CDF of the normal distribution is given as

$$F(x) = \frac{1}{\sqrt{(2\pi)\sigma^2}} \int_0^x \exp\left(-\frac{(x-\mu)^2}{2\sigma^2}\right) dx \quad (2.2.12)$$

2.2.2 Log-Normal Distribution

Lognormal distribution is a probability distribution of a random variable whose logarithm is normally distributed. The distribution is skewed with a lower mean value and large variance (Figure 2-9).

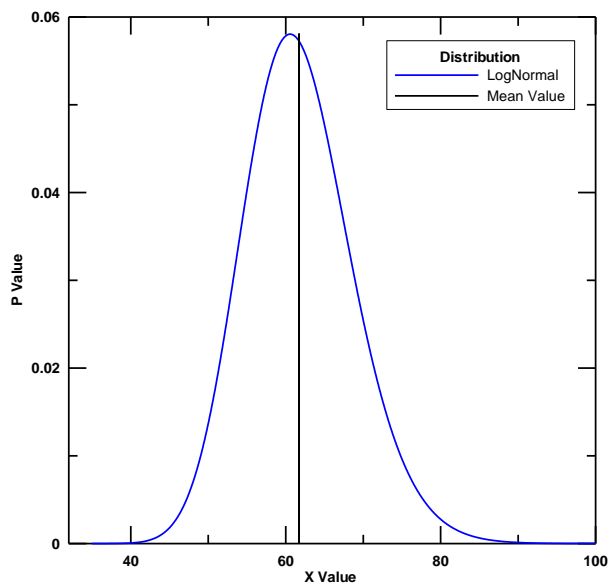


Figure 2-9. Log-normal distribution - PDF

The main difference between normal and lognormal distributions is that the effect is additive and multiplicative for normal and lognormal distributions, respectively. The PDF of the lognormal distribution is given as

$$f(x) = \frac{1}{\sqrt{(2\pi)\sigma x}} e^{-\frac{(\ln x - \ln \lambda)^2}{2\sigma^2}} \quad (2.2.13)$$

The log-likelihood function is given as

$$L_{LN} = -\frac{n}{2} \ln(2\pi\sigma^2) - \sum_{i=1}^n \ln x_i - \frac{\sum_{i=1}^n \ln x_i^2}{2\sigma^2} + 2 \frac{\sum_{i=1}^n \ln x_i \ln \lambda}{2\sigma^2} - \frac{n \ln(\lambda^2)}{2\sigma^2} \quad (2.2.14)$$

The values of the parameters are found by differentiating the log-likelihood function with respect to the parameters and equating to zero. This results in the following equations:

$$\frac{dL_{LN}}{d\lambda} = \frac{\sum_{i=1}^n \ln x_i}{\lambda\sigma^2} - \frac{n \ln(\lambda)}{\lambda\sigma^2} = 0 \quad (2.2.15)$$

$$\lambda = e^{\left(\frac{\sum_{i=1}^n \ln x_i}{n} \right)} \quad (2.2.16)$$

$$\frac{dL_{LN}}{d\sigma} = -\frac{n}{\sigma} - \frac{\sum_{i=1}^n \ln x_i^2}{\sigma^3} - 2 \frac{\ln \lambda \sum_{i=1}^n \ln x_i}{\sigma^3} - \frac{n \ln(\lambda^2)}{\sigma^3} = 0 \quad (2.2.17)$$

Substituting the scale parameter in Eqn.(2.2.14), we get the shape parameter as

$$\sigma = \left(\frac{\sum_{i=1}^n (\ln x_i - \ln \lambda)^2}{n-1} \right)^{\frac{1}{2}} \quad (2.2.18)$$

The CDF of the lognormal distribution is given as

$$F(x) = \frac{1}{\sqrt{(2\pi)\sigma}} \int_0^x \frac{1}{x} \exp\left(-\frac{\ln(x/\sigma)^2}{2\sigma^2}\right) dx \quad (2.2.19)$$

2.2.3 Weibull Distribution

Weibull distribution (Figure 2-10) is a widely used distribution that can be used for modeling data in reliability and lifetime modeling. The function is extremely versatile and several types of distributions can be modeled (see Figure 2-5). For example, with $\alpha=1$ is Weibull distribution is identical to the exponential distribution, with $\alpha=2$ the distribution is identical to Rayleigh distribution, with $\alpha=2.5$ the distribution approximates lognormal distribution, with $\alpha=3.6$ the distribution approximates normal distribution, and with $\alpha=5$ the distribution approximates peaked normal distribution.

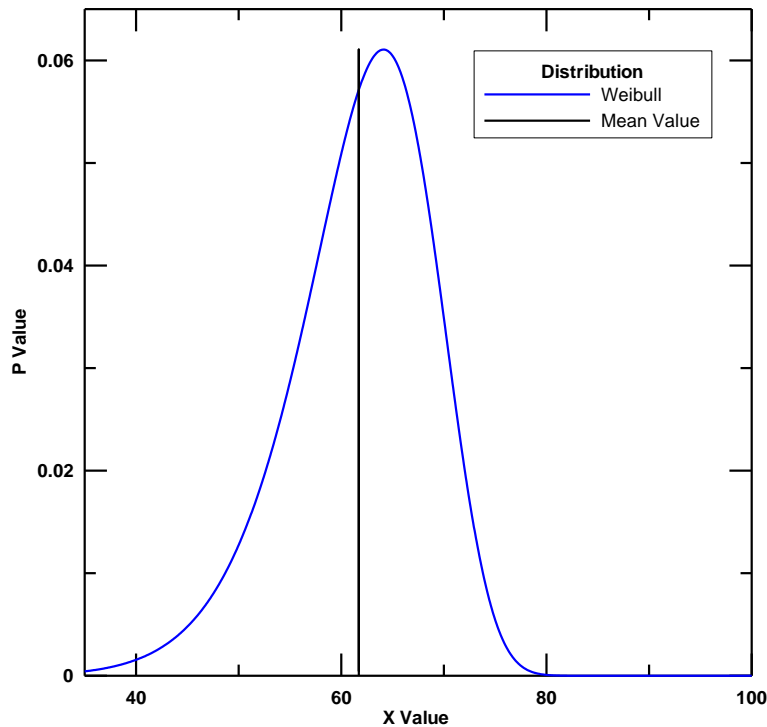


Figure 2-10. Weibull distribution – PDF

Weibull 2-Parameter Model

The PDF of Weibull 2-parameter distribution is given as

$$f(x) = \frac{\alpha}{\lambda} \left(\frac{x}{\lambda} \right)^{\alpha-1} e^{-(x/\lambda)^\alpha} \quad (2.2.20)$$

The Weibull distribution with $\alpha > 1$ characterizes a life that deteriorates with time. On the other hand, when $\alpha > 1$, Weibull becomes an exponential distribution and the failure rate is constant. When $\alpha < 1$, there is reliability growth where the failure rate decreases with the time. Maximum log-likelihood function is given as

$$L_{WE} = n \ln \alpha - \alpha n \ln \lambda + (\alpha - 1) \sum_{i=1}^n \ln x_i - \frac{1}{\lambda^\alpha} \sum_{i=1}^n x_i^\alpha \quad (2.2.21)$$

MLE of the parameters are found by differentiating the maximum log-likelihood function with respect to the parameters and equating to zero, resulting in the following equations [9]

$$\{\hat{\alpha}\} = \left\langle \arg \min \left(\frac{1}{\alpha} + \frac{\sum_{i=1}^n \log(x_i)}{n} - \frac{\sum_{i=1}^n \log(x_i) x_i^\alpha}{\sum_{i=1}^n x_i^\alpha} \right) \right\rangle \quad (2.2.22)$$

$$\lambda = \left(\frac{\sum_{i=1}^n x_i^\alpha}{n} \right)^{1/\alpha} \quad (2.2.23)$$

The shape parameter can be obtained by solving Eqn.(2.2.22) and the scale parameter is obtained using Eqn.(2.2.23). The CDF is given as

$$F(x) = 1 - e^{-(x/\lambda)^\alpha} \quad (2.2.24)$$

Weibull 3-Parameter Model

Additional flexibility in modeling the data is available in the Weibull 3-parameter model. Sometimes the first value or observation of the data occurs at the location other than zero. Such a shifted distribution can be modeled using the Weibull 3-parameter distribution [11]. In addition to shape and scale, the location parameter is used in the model (Figure 2-7). The PDF is given as

$$f(x) = \frac{\alpha}{\lambda} \left(\frac{x-\gamma}{\lambda} \right)^{\alpha-1} e^{-((x-\gamma)/\lambda)^\alpha} \quad (2.2.25)$$

where γ is the location parameter. The MLE function for this distribution is given as

$$\{\hat{\alpha}, \hat{\lambda}\} = \arg \min \left(\left(\frac{1}{\alpha} + \frac{\sum_{i=1}^n \log(x_i - \gamma)}{n} - \frac{\sum_{i=1}^n \log(x_i - \gamma)(x_i - \gamma)^\alpha}{\sum_{i=1}^n (x_i - \gamma)^\alpha} \right)^2 + \left(\frac{1}{n} \sum_{i=1}^n \frac{1}{(x_i - \gamma)} \frac{\sum_{i=1}^n (x_i - \gamma)^\alpha}{\sum_{i=1}^n (x_i - \gamma)^{\alpha-1}} - \frac{\gamma}{\gamma - 1} \right)^2 \right) \quad (2.2.26)$$

From Eqn.(2.2.26) the shape and location parameters which minimize the function are obtained and from those parameters, scale parameter is computed as follows.

$$\lambda = \left(\frac{\sum_{i=1}^n (x_i - \gamma)^\alpha}{n} \right)^{1/\alpha} \quad (2.2.27)$$

The CDF is given as

$$F(x) = 1 - e^{[-(x-\gamma)/\lambda]^\alpha} \quad (2.2.28)$$

Estimation of Weibull Parameters

The Weibull parameters can be estimated using Eqn.(2.2.22) and Eqn.(2.2.26) with or without weights (W_1, W_2 & W_3).

- a) Two-step iterative MLE method with no weights: Eqn.(2.2.22), (2.2.23), (2.2.26) and (2.2.27) are used without any change and the parameter values are obtained through iterative procedure.
- b) Weighted two-step iterative MLE method: In this method Eqn.(2.2.22), (2.2.23), (2.2.26) and (2.2.27) are modified by introducing weights as shown below.

$$\{\hat{\alpha}\} = \left\langle \arg \min \left(W_2 + \frac{\sum_{i=1}^n \log(x_i)}{n} - \frac{\sum_{i=1}^n \log(x_i) x_i^\alpha}{\sum_{i=1}^n x_i^\alpha} \right) \right\rangle \quad (2.2.29)$$

$$\lambda = \left(\frac{\sum_{i=1}^n x_i^\alpha}{n W_1} \right)^{1/\alpha} \quad (2.2.30)$$

$$\{\hat{\alpha}, \hat{\lambda}\} = \left(\arg \min \left[\left(W_2 + \frac{\sum_{i=1}^n \log(x_i - \gamma)}{n} - \frac{\sum_{i=1}^n \log(x_i - \gamma)(x_i - \gamma)^\alpha}{\sum_{i=1}^n (x_i - \gamma)^\alpha} \right)^2 + \left(\frac{1}{n} \sum_{i=1}^n \frac{1}{(x_i - \gamma)} \frac{\sum_{i=1}^n (x_i - \gamma)^\alpha}{\sum_{i=1}^n (x_i - \gamma)^{\alpha-1}} - W_3 \right)^2 \right] \right) \quad (2.2.31)$$

$$\lambda = \left(\frac{\sum_{i=1}^n (x_i - \gamma)^\alpha}{nW_1} \right)^{1/\alpha} \quad (2.2.32)$$

The weights (W_1, W_2 & W_3) used in the above equations are given as follows [9].

$$W_1 = \frac{1}{n} \sum_{i=1}^n \log \left(\frac{1}{1 - F(x_i)} \right) \quad (2.2.33)$$

$$W_2 = \frac{\sum_{i=1}^n \log \left(\frac{1}{1 - F(x_i)} \right) \log \left(\log \left(\frac{1}{1 - F(x_i)} \right) \right)}{\sum_{i=1}^n \log \left(\frac{1}{1 - F(x_i)} \right)} - \frac{1}{n} \sum_{i=1}^n \log \left(\log \left(\frac{1}{1 - F(x_i)} \right) \right) \quad (2.2.34)$$

$$W_3 = W_1 \frac{\sum_{i=1}^n \log \left(\frac{1}{1 - F(x_i)} \right)^{-1/\gamma}}{\sum_{i=1}^n \log \left(\frac{1}{1 - F(x_i)} \right)^{(\gamma-1)/\gamma}} \quad (2.2.35)$$

The estimation of weights depends on the CDF ($F(x_i)$) which can be obtained using cumulative frequency. However, the results are indeterminate when $F(x_i)$ is 1 (See Eqn.(2.2.33) through Eqn.(2.2.35)). Hence the weights are assumed as

random variables and assigned a suitable distribution model and then MCS is performed. The mean/median/geometric mean value of the random variable from MCS can be used as weights [9]. In this study the median value from MCS is used as weights for further calculations. The weight W_3 (median) and the MLE weights approach the same value as the shape parameter increases. For $\gamma > 2.5$, $W_3 = \frac{\gamma}{\gamma-1}$ is used. The weights used are given in Table 2-1 and Table 2-2.

Table 2-1. Weights of W1, W2 [9].

n	1	2	3	4	5	6	7	8	9	10
W1	0.693	0.839	0.891	0.918	0.934	0.945	0.953	0.959	0.963	0.967
W2	0	0.275	0.517	0.638	0.711	0.759	0.791	0.817	0.838	0.853

Table 2-2. Weights of W3[9].

n	γ				
	0.5	1.0	1.5	2.0	2.5
8	7.150	3.114	2.105	1.722	1.525
10	8.643	3.365	2.180	1.758	1.552

2.2.4 Generalized Exponential Distribution

Generalized exponential distribution has a more recent history [12, 13] and its PDF (Figure 2-11) defined as

$$f(x) = \alpha \lambda e^{-\lambda x} (1 - e^{-\lambda x})^{\alpha} \quad (2.2.36)$$

When $\alpha = 1$, then the distribution is exponential. One major advantage of a generalized exponential distribution is the simple structure of distribution and survival function.

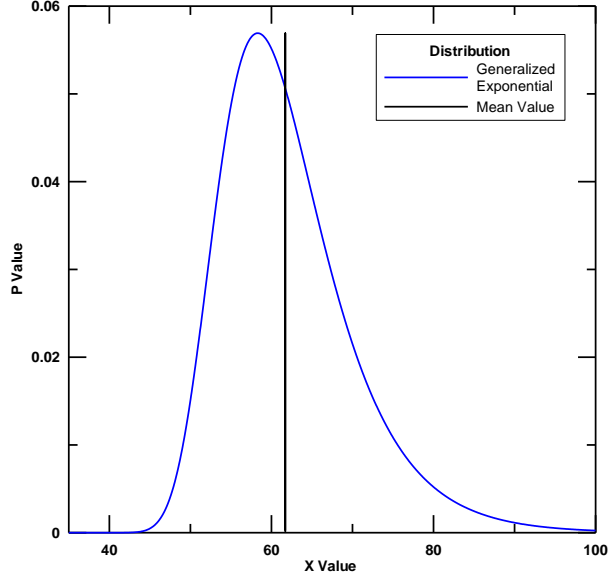


Figure 2-11. Generalized exponential distribution - PDF

Log-likelihood function is given by Eqn.(2.2.37).

$$L_{GE} = n \ln(\alpha) + n \ln(\lambda) - \lambda \sum_{i=1}^n x_i + (\alpha - 1) \sum_{i=1}^n \ln(1 - e^{-\lambda x_i}) \quad (2.2.37)$$

MLE of the parameters are found by differentiating the log-likelihood function with respect to the parameters and equating to zero.

$$\frac{dL_{GE}}{d\alpha} = \frac{n}{\lambda} - \sum_{i=1}^n x_i + (\alpha - 1) \sum_{i=1}^n \frac{x_i e^{-\lambda x_i}}{1 - e^{-\lambda x_i}} = 0 \quad (2.2.38)$$

$$\frac{dL_{GE}}{d\lambda} = \frac{n}{\alpha} + \sum_{i=1}^n \ln(1 - e^{-\lambda x_i}) = 0 \quad (2.2.39)$$

From Eqn.(2.2.39), the shape parameter can be obtained as

$$\alpha = - \frac{n}{\sum_{i=1}^n \ln(1 - e^{-\lambda x_i})} \quad (2.2.40)$$

By substituting the Eqn.(2.2.40) in Eqn.(2.2.38), the scale parameter can be obtained. The obtained scale parameter is used to estimate the shape parameter.

The CDF is given by

$$F(x) = (1 - e^{-\lambda x})^\alpha \quad (2.2.41)$$

2.2.5 Gamma Distribution

Gamma distribution, like the lognormal distribution, can be used to represent a skewed distribution. The PDF (Figure 2-12) of two parameter gamma distribution is given as

$$P_G = \frac{\left(\frac{x}{\lambda}\right)^{\alpha-1} e^{-\frac{x}{\lambda}}}{\lambda \tau(\alpha)} \quad (2.2.42)$$

where $\tau(\alpha)$ is given by

$$\tau(\alpha) = \int_0^{\infty} e^{-x} x^{\alpha-1} dx \quad (2.2.43)$$

The Figure 2-12 shows a sample gamma distribution.

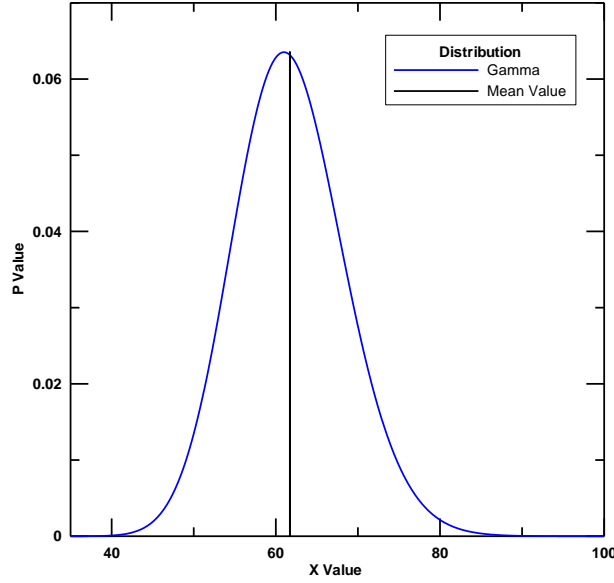


Figure 2-12. Gamma distribution - PDF

The log likelihood function from which the parameters are estimated is given as

$$L_G = -\alpha n \ln(\lambda) - n \ln(\tau(\alpha)) - \frac{1}{\lambda} \sum_{i=1}^n x_i + (\alpha - 1) \sum_{i=1}^n \ln(x_i) \quad (2.2.44)$$

Differentiating the Eqn.(2.2.44) with respect to scale parameter and equating to zero we obtain

$$\lambda = \frac{\sum_{i=1}^n x_i}{\alpha n} \quad (2.2.45)$$

The shape parameter is estimated by substituting the scale parameter in Eqn.(2.2.44).

$$\hat{\alpha} = -\alpha n \ln \left(\frac{\sum_{i=1}^n x_i}{\alpha n} \right) - n \ln(\tau(\alpha)) - \alpha n + (\alpha - 1) \sum_{i=1}^n \ln x_i \quad (2.2.46)$$

The shape parameter is obtained by maximizing the above function and then is used in Eqn.(2.2.45) to compute scale parameter. The CDF of the gamma distribution is given by

$$F(x) = \frac{1}{\tau(\alpha)} \int_0^x x^{\alpha-1} e^{-x} dx \quad (2.2.47)$$

2.3 Goodness of Fit Tests

Goodness of fit tests are used to find quality of fit arising from the distribution functions. Some of the tests that are used to compare the models [14, 15,40] are presented in this section and all the tests explained here can be applied to the various distribution functions.

2.3.1 Kolmogorov-Smirnov (KS) Test

Among competing models, it is natural to choose a particular model for a given sample which has the distribution function closest to the empirical distribution function (EDF) of the data according to some distance measure between the two distribution functions. KS test is measure of that distance between EDF and CDF of the selected distribution. Empirical distribution function is given as

$$E_N = \frac{n_{(i)}}{N} \quad (2.3.1)$$

where $n_{(i)}$ is the number of points less than x_i , where x_i is the ordered data from smallest to largest value. K-S distance [39] is defined as

$$D = \sup(\hat{F}(x) - F_0(x)) \quad (2.3.2)$$

where $F_0(x)$ is the CDF of the selected distribution and $\hat{F}(x)$ is the empirical cumulative distribution for the given dataset. The distribution with the smallest K-S distance is considered as the best fit. Eqn.(2.3.2) can be written as

$$D = \max_{1 \leq i \leq n} \left[\left| F_0(i) - \frac{(i-1)}{n} \right|, \left| F_0(i) - \frac{i}{n} \right| \right] \quad (2.3.3)$$

2.3.2 Chi-Square test

This is one of the oldest methods used for goodness of fit test or for model discrimination. The basic idea is very simple. First divide the samples into different groups and count the number of observations in each group. Second, compute the corresponding frequencies and then compare against its distribution function. The Chi-square formula is given as

$$\chi^2 = \sum_{i=1}^n \frac{(\text{Expected} - \text{Observed})^2}{\text{Expected}} \quad (2.3.4)$$

where χ^2 is the Chi-square test statistic. The distribution with the least Chi-square value is the best fit model for the data.

2.3.3 Anderson-Darling (AD) Test

AD test is used to test if a sample of data came from a specific distribution. It is modification of K-S test and gives more weight to the tails than the KS test. The AD test makes use of critical values of each specific distribution, and the computed distance is then compared with the critical value which is given in the Table 2-3. The AD test statistic is defined as

$$A^2 = -N - S \quad (2.3.5)$$

where N is the number of samples and S is given as

$$S = \sum_{i=1}^n \frac{(2i-1)}{N} [\ln(F(Y_i)) + \ln(1 - F(Y_{N+1-i}))] \quad (2.3.6)$$

where $F(Y_i)$ is the theoretical CDF and Y_i are the ordered data. The test statistic A^2 is compared with the critical values (see Table 2-3) corresponding to the specific distribution. If the test statistic is greater than critical value then the distribution is rejected.

Table 2-3. Anderson-Darling Test - Critical Values.

Statistic (T)	Percentage Points for T				
	15	10	5	2.5	1
A^2	1.610	1.933	2.492	3.070	3.857

2.3.4 Maximum Likelihood Criterion

Cox (1962) [41] proposed choosing the model which yields the largest likelihood function as the optimal model. Maximum likelihood criterion compares the given two distributions and finds the best fit between the two as shown in Eqn.(3.45).

$$T = \sum_{i=1}^n \ln \left(\frac{f(x_i)}{g(x_i)} \right) \quad (2.3.7)$$

where $f(x_i)$ and $g(x_i)$ are the PDF from two distributions. If $T > 0$, then the distribution $f(x)$ is considered as the best fit, else the distribution $g(x)$ is taken as the best fit.

2.4 FORM Method

The FORM method uses first order Taylor series approximation of the performance function. The algorithm, developed by [42] is being used along with Method of Feasible Directions (MFD) to compute the reliability and probability of failure.

Normal to Standard Normal Space: The given random variables are always in their respective space, i.e. original space. For FORM analysis, the random variables have to be expressed in standard normal space as

$$U_i = \frac{X_i - \mu_{X_i}^N}{\sigma_{X_i}^N} \quad (2.4.1)$$

Non-Normal to Standard Normal Space: Computation of mean and standard deviation for the non-normal variable is given by [43]. CDF and PDF of the non-normal variables and standard normal variables are equated to find the statistical data for non-normal distribution as

$$\sigma_x^N = \frac{\phi\{\Phi^{-1}[F_X(X)]\}}{f_X(X)} \quad (2.4.2)$$

$$\mu_x^N = X - \Phi^{-1}[F_X(X)]\sigma_x^N \quad (2.4.3)$$

Based on the above relations, mean and standard deviation computed are then used to express the variables in standard normal space as given by Eqn.(2.4.1).

Reliability Index & Probability of Failure: Reliability index (β) is used to compute probability of failure (p_f) and is called distance from the origin to the design point (MPPF) which is computed as follows.

$$\beta = \sqrt{(\mathbf{U}^T \mathbf{U})} \text{ (or) } \boldsymbol{\alpha}^T \mathbf{U} \quad (2.4.4)$$

$$p_f = 1 - \Phi(\beta) \quad (2.4.5)$$

Reliability Problem Formulation: The reliability analysis focuses on minimizing the reliability subject to the active limit surface ($g = 0$) and the solution gives the probability of failure, reliability index along with the most probable point of failure of random variables corresponding to the performance function. The problem formulation focuses on finding the most probable point of failure by minimizing the distance (β) from the origin. Available two types of reliability analysis problem formulation have already been explained in Eqn.(1.1.8) and Eqn.(1.1.9).

Method of Feasible Directions: MFD is used for the reliability analysis to find the variables. The steepest descent direction is used in MFD which is based on the performance function gradient and given as

$$\boldsymbol{\alpha} = \left[-\frac{\nabla g(\mathbf{U}_k)}{\|\nabla g(\mathbf{U}_k)\|^2} \right] \quad (2.4.6)$$

$$\nabla g(\mathbf{U}_i) = \nabla g(\mathbf{X}) \sigma_{x_i}^N \quad (2.4.7)$$

The search direction is updated based on the Taylor series approximation of the performance function. The approximated performance function is used to compute the new design point by equating it to zero. This gives the new point in a single iteration provided the performance function is linear.

$$g(\mathbf{U}_{k+1}) = g(\mathbf{U}_k) + \nabla g(\mathbf{U}_k)(\mathbf{U}_{k+1} - \mathbf{U}_k) = 0 \quad (2.4.8)$$

$$\mathbf{U}_{k+1} = \left[\frac{\nabla \mathbf{g}(\mathbf{U}_k) \mathbf{U}_k - g(\mathbf{U}_k)}{\|\nabla \mathbf{g}(\mathbf{U}_k)\|^2} \right] \nabla \mathbf{g}(\mathbf{U}_k) \quad (2.4.9)$$

Direction is computed based on the new point and old point in standard normal space

$$\mathbf{d} = \left[\frac{\nabla \mathbf{g}(\mathbf{U}_k)^T \mathbf{U}_k - g(\mathbf{U}_k)}{\|\nabla \mathbf{g}(\mathbf{U}_k)\|^2} \right] \nabla \mathbf{g}(\mathbf{U}_k) - \mathbf{U}_k \quad (2.4.10)$$

where k is the iteration number, from the above Eqn.(2.4.10), direction for given set of variables are computed. New design point is calculated based on the search direction (d) and step size (s). The s is between 0 and 1 and is computed based on the merit function as given below.

$$\mathbf{U}_{k+1} = \mathbf{U}_k + s_k \mathbf{d}_k \quad (2.4.11)$$

$$f_m(\mathbf{U}_k) = 0.5 \|\mathbf{U}_k\|^2 + C |g(\mathbf{X})| \quad (2.4.12)$$

$$C = \frac{2 \|\mathbf{U}_k\|}{\|\nabla \mathbf{g}(\mathbf{X})\|} + 10 \quad (2.4.13)$$

Step size is selected such that $f_m(\mathbf{U}_{k+1}) < f_m(\mathbf{U}_k)$. Initial value for s is

1.0. The overall algorithm for the FORM analysis is shown in Figure 2-13.

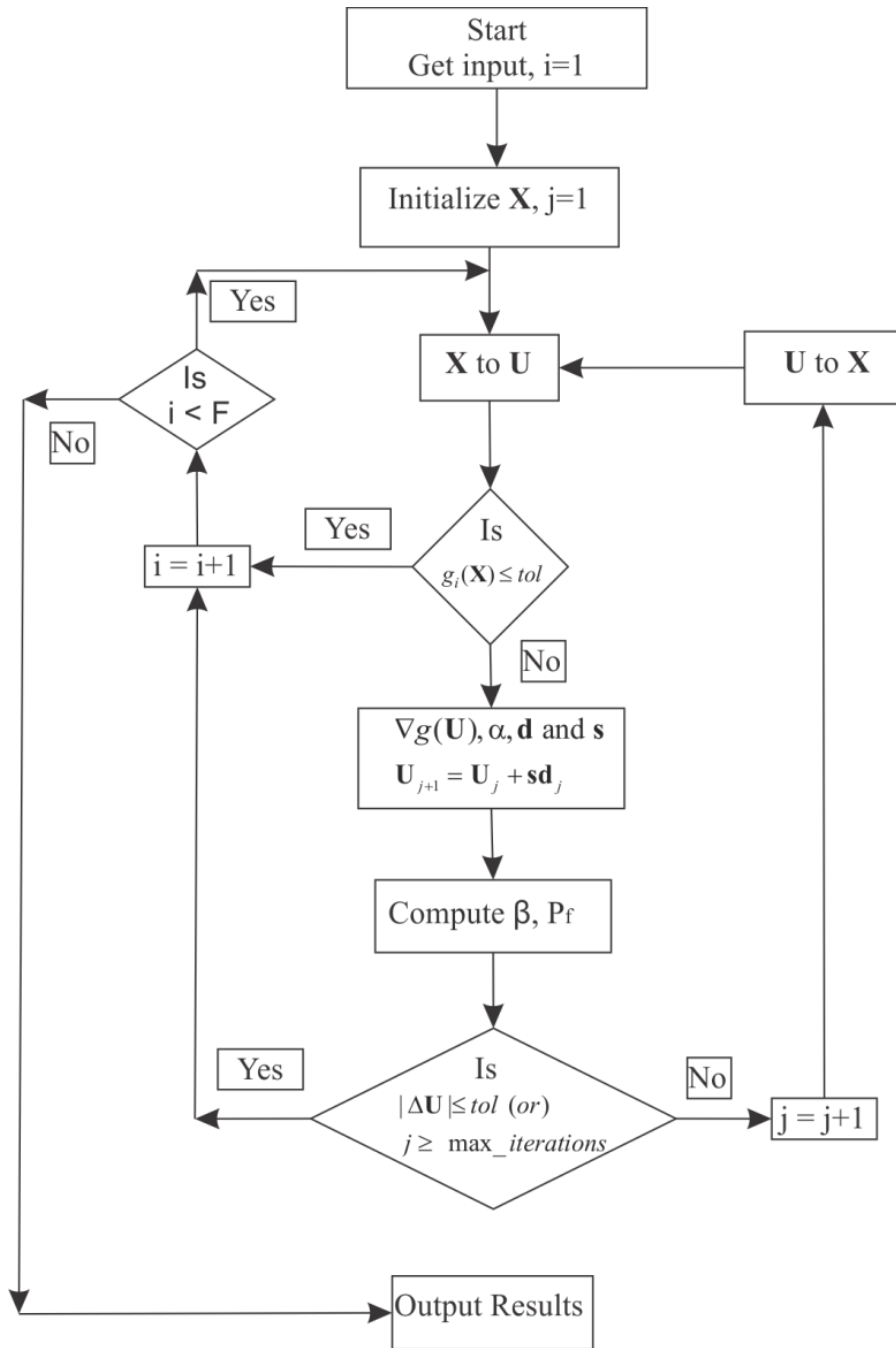


Figure 2-13. Flowchart for FORM method

2.5 SORM Method

The results from the FORM analysis holds true for all the linear limit state functions, but it fails to provide accurate results when the function is highly non-

linear. The accuracy can be increased by taking into account the curvature of the functions. In the SORM method, second order Taylor series approximation of the response function is done [20 & 43]. Nonlinear response function increases/decreases the failure domain based on the type of the curvature (see Figure 2-1). The response function becomes nonlinear when there are non-normal variables or the function by itself is nonlinear. The closed form expression for computing probability of failure [44] is given as

$$p_f = \Phi(-\beta_{FORM}) \prod_{i=1}^{n_{pdv}-1} (1 + \beta_{FORM} \kappa_i)^{-1/2} \quad (2.4.14)$$

where n is number of random variables, κ is the curvature of the response function associated with each variable. And from the probability of failure, β_{SORM} is updated as

$$\beta_{SORM} = -\Phi(p_f) \quad (2.4.15)$$

In order to compute the curvature, the variables (U) are rotated to (U') so that the last variable coincide with (β) of the minimum distance point. The rotation matrix used for transformation is given as

$$\mathbf{R}_0 = \begin{pmatrix} 1 & 0 & 0 & 0 \\ 0 & 1 & 0 & 0 \\ \vdots & \dots & \ddots & \vdots \\ \frac{U_i}{|\mathbf{U}^T \mathbf{U}|} & \frac{U_{i+1}}{|\mathbf{U}^T \mathbf{U}|} & \dots & \frac{U_n}{|\mathbf{U}^T \mathbf{U}|} \end{pmatrix} \quad (2.4.16)$$

Gram-Schmidt Orthogonalization procedure is carried out to obtain \mathbf{R} matrix.

$$\mathbf{A} = \frac{\mathbf{RDR}^T}{\|\nabla \mathbf{g}(\mathbf{X})\|} \quad (2.4.17)$$

where \mathbf{D} is second order derivative of the response function in the standard normal space and is computed based on the variable in normal space as follows

$$\mathbf{D} = \begin{bmatrix} \frac{\partial(g)}{\partial X_i \partial X_j} \sigma_i^N \sigma_j^N & \frac{\partial(g)}{\partial X_i \partial X_{j+1}} \sigma_i^N \sigma_{j+1}^N & \cdots & \frac{\partial(g)}{\partial X_i \partial X_{n_{rv}}} \sigma_i^N \sigma_{n_{rv}}^N \\ \frac{\partial(g)}{\partial X_{i+1} \partial X_j} \sigma_{i+1}^N \sigma_j^N & \frac{\partial(g)}{\partial X_{i+1} \partial X_{j+1}} \sigma_{i+1}^N \sigma_{j+1}^N & \cdots & \frac{\partial(g)}{\partial X_{i+1} \partial X_{n_{rv}}} \sigma_{i+1}^N \sigma_{n_{rv}}^N \\ \vdots & \vdots & \vdots & \vdots \\ \frac{\partial(g)}{\partial X_{n_{rv}} \partial X_j} \sigma_{n_{rv}}^N \sigma_j^N & \cdots & \cdots & \frac{\partial(g)}{\partial X_{n_{rv}} \partial X_{n_{rv}}} \sigma_{n_{rv}}^N \sigma_{n_{rv}}^N \end{bmatrix} \quad (2.4.18)$$

Since the last variable coincide with β , the last row and last column of the matrix \mathbf{A} is removed and eigenvalues correspond to the curvatures of the function. Flowchart of the SORM procedure is given in Figure 2-14.

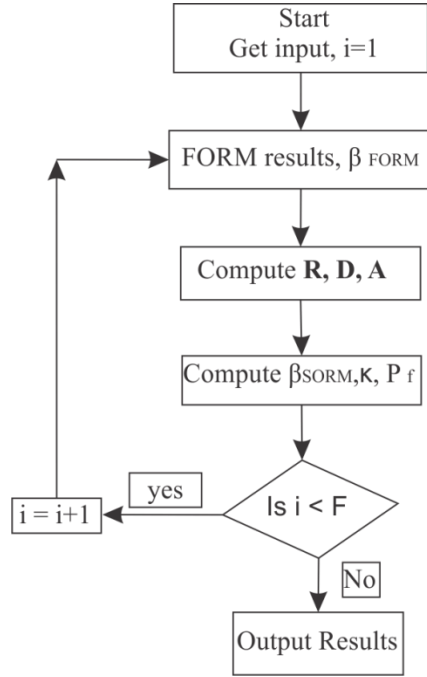


Figure 2-14. Flowchart for SORM method

2.6 MCS Method

Monte Carlo Simulation method is used to calculate the probability of failure of the system using just the values of performance functions (doesn't depend whether the performance function is explicit or implicit). The accuracy depends on the number of simulations that are carried out to determine the failure probability. Clearly this is computationally expensive procedure since a finite element analysis needs to be carried out for every simulation.

A set of random numbers is generated for each random variable. The random number generated values combined with the CDF of the respective random variables are used to obtain the random variable values. The process is repeated for each random variable and the probability of failure is computed as

$$p_f = \frac{N_f}{N} \quad (2.5.1)$$

where N_f is number of failures and N is total number of simulations.

2.7 RBDO Method

In deterministic based design optimization, the design is primarily based on deterministic variables without taking into account any uncertainties. As a result in most cases the design results have a high chances of failure because of the uncertainties associated with the material properties being used, load acting on the structure etc., In RBDO, the system along with the DO considers the uncertainties resulting in low probability of failure or high reliability. In RBDO, two types of optimizations DO and RO are done simultaneously to obtain the optimized values. The optimizations are decoupled and the method is Decoupled

methodology, implementation of the procedure is followed as proposed by [31].

The procedure is shown n Figure 2-15.

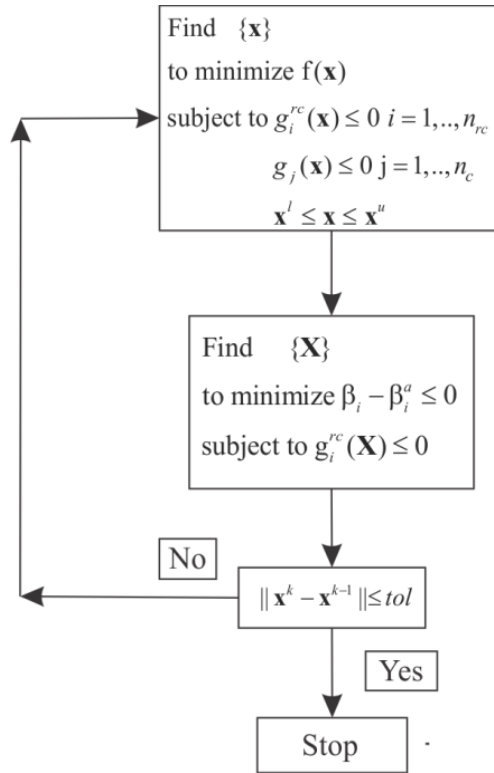


Figure 2-15. Flowchart for RBDO method

Sensitivity Analysis

In this RBDO procedure after the first design optimization, random variables associated with each constraint are identified by performing sensitivity analysis. Sensitivity of a single constraint with respect to one random variable is computed as

$$S = \frac{g(X) - g(X + \Delta X)}{\Delta X} \quad (2.5.2)$$

where S is the sensitivity value, if $S = 0$ then the corresponding random variable (X) is not considered for the given constraint in RO.

Reliability Optimization

Two types of approaches are available to implement the reliability analysis - RIA and PMA that were introduced in Eqn.(1.1.8) and Eqn.(1.1.9). Both the methods yield same results when the respective constraints are active, different results if the constraints are not active. If there are multi-constraints in a problem, both the approach yields singularity if the failure probability is zero or the obtained reliability index is greater than the allowable reliability index (β^a). In this study the RIA index approach is modified to include the β^a in the objective function and it is given as follows.

$$\begin{aligned} & \text{minimize } \beta_j - \beta_j^a \\ & \text{subject to } g_j^{rc}(\mathbf{X}_j) \leq 0 \end{aligned} \tag{2.5.3}$$

Usually the results obtained from the DO provide good reliability indices for constraints, but not all the constraints fall below the target reliability value and in that case either PMA or RIA yields singularity. So, the constraints with the high reliability value are not considered for the RO. After DO, reliability analysis FORM (or) SORM (or) MCS can be performed to find the reliability indices associated with each constraint and from then on only the concerned constraints which are less reliable are considered to avoid singularity results. The complete flowchart of the RBDO formulation is given in Figure 2-16.

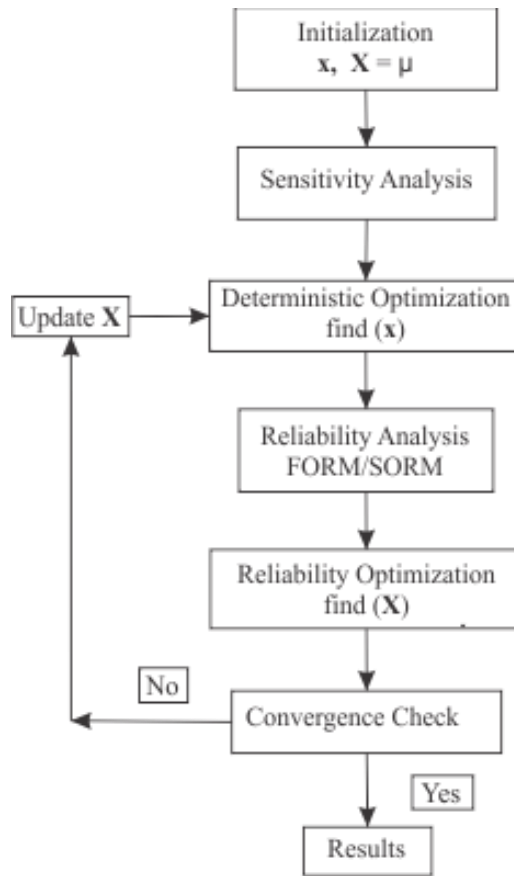


Figure 2-16. Flowchart for RBDO with sensitivity analysis

Algorithm:

1. Problem statement with design variables, random variables, inequality constraints and/or equality constraints with a target reliability value for each constraint is presented.
2. Conduct a deterministic optimization to find the design variables minimizing the given objective function subjected to constraints.
3. Perform sensitivity analysis on each constraint and identify the random variables associated with each constraint.

4. Conduct a reliability analysis using FORM/SORM/MCS on each constraint to find the constraints whose reliability values are less than their respective target reliability value.
5. Identify the less reliable constraints and conduct reliability optimization only to each of those constraints and find random variables of that concerned constraint following a reliability optimization problem formulation (see Eqn.(2.5.3)).
6. Once all the reliability optimizations (one for each constraint) are performed, update the random variables in each of the less reliable constraints that are obtained from their corresponding reliability optimization. Carry out design optimization.
7. Perform reliability optimization in the initially identified less reliable constraints same as step 5.
8. Perform convergence check by comparing design variables values in current and previous iteration. Steps 1 to 5 correspond to first iteration and steps 6 and 7 to second iteration. Repeat steps 6 and 7 until the design results converge.

3. EXPERIMENTAL DATA

Experimental data used in this thesis is discussed in this chapter. First, measurement error and sampling of experimental data are discussed. Then, results from uniaxial tension test of Kevlar® 49 fabrics and yarns are presented, analyzed and discussed.

3.1 Introduction

Measurement in any kind of experiment or process is always subject to uncertainties and errors. These errors are due to the following reasons.

Experimental/Systematic Error: This error is due to the uncertainties in the bias of the data. A simple example is initialization of the experiment, i.e., if the initial time or displacement is not set to zero. In tension test, improper aligning of the sample or improper gripping at the ends leads to the experimental error. The experimental error implies that all the measurements for a set of data in the same experiment are always shifted in same direction and by same amount. This is in contrast to the random error, where each measurement varies independently of other. There is no particular method for analyzing or eliminating systematic errors. It depends on the instrument/system and each has to be individually analyzed.

Random Error: Random errors are due to the instrument imprecision and inherent statistical nature of the phenomenon being observed. A particular parameter that is being observed in a specimen is not always a single value, and it is randomly distributed. For example, as Table 3-4 shows the material parameters are not the

same across replicates. This is due to the random distribution of defects in the samples.

3.2 Sampling

Before one starts carrying out the experimental tests, one has to determine the minimum sample size (or replicate data to generate). More reliable results are available with the larger sample size. Determining the sample size starts with identification of the effects of a particular experimental parameter on the test results, e.g. size of the specimen, gage length of the specimen, the compliance of the test machine etc. Null Hypothesis (H_0) is an theory⁴ put forward as

$$H_0 : \theta_1 = \theta_2 \quad (3.2.1)$$

where θ_1, θ_2 are the parameters corresponding to two separate data which are normally distributed.

Two kinds of errors are associated with the hypothesis. Type I error occurs if the null hypothesis is rejected when it is true and type II error occurs if null hypothesis is not rejected when it is false.

$$\begin{aligned} \alpha &= P(\text{Type I Error}) = P\{\text{Reject } H_0 \mid H_0 \text{ is true}\} \\ \beta &= P(\text{Type II Error}) = P\{\text{fail to Reject } H_0 \mid H_0 \text{ is false}\} \end{aligned} \quad (3.2.2)$$

Operational characteristics curve is used to estimate the sample size which is the plot of type II error probability of a statistical test for a particular sample

⁴ http://www.stats.gla.ac.uk/steps/glossary/hypothesis_testing.html#h0

versus a parameter that reflects the extent to which null hypothesis is false [45].

The type II error is given as

$$\beta = 1 - P\{\text{Reject } H_0 \mid H_0 \text{ is false}\} \quad (3.2.3)$$

A sample characteristic curve is shown in the Figure 3-1 and its parameters are explained in the Table 3-1. The parameter in the operating characteristic curve that type II error is plotted against is defined as

$$\Phi^2 = \frac{nD^2}{2a\sigma^2} \quad (3.2.4)$$

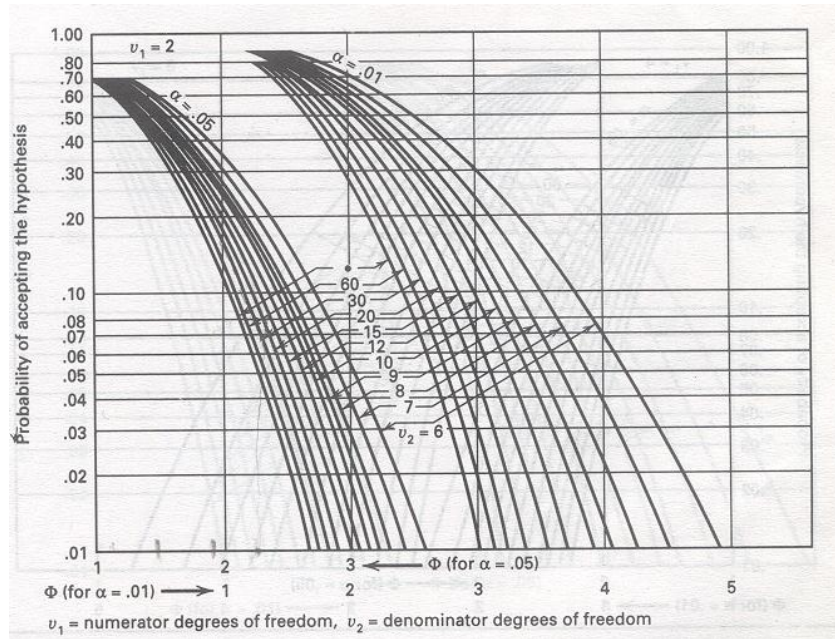


Figure 3-1. Operational characteristic curve [45].

where D is the smallest difference between any two treatments means, a is the total number of treatments, n is the sample size and σ is the standard deviation of all the treatments. The minimum value Φ for which null hypothesis is rejected would represent the sample size. The degree of freedom associated with sum of

squares between treatments and is called numerator degrees of freedom. The degree of freedom associated with the sum of squares of error within treatments is called denominator degrees of freedom.

Table 3-1. Operational Characteristic Curve Parameters.

Parameters	Φ^2	Numerator Degrees of Freedom	Denominator Degrees of Freedom
A	$\frac{nD^2}{2a\sigma^2}$	$a-1$	$a(n-1)$

Using Kevlar® 49, the minimum number of samples for the swath data can be calculated by considering the results from the tension tests on single yarn with gage length as the controlling parameter. Results are shown in Table 3-2.

Table 3-2. Yarn Experimental Data (psi).

Modulus (psi)	Gage length (in)			
	5	8	11	14
Mean	6341903	8399659	9740908	10702479
Standard Deviation	212750	174497	300843	388645

From the data above, we can compute D which is 961570, σ is taken as 400000 (based on the maximum value from Table 3-3 which is 388645), number of treatments is 4 (5, 8, 11 & 14 in specimens) and number of degrees of freedom is 3. Table 3-3 shows the calculation of sample size with level of significance as $\alpha = 0.05$.

Table 3-3. Sample Size Calculation With $\alpha = 0.05$.

Sample size	Φ^2	Φ	$a(n-1)$	β	$(1-\beta)$
5	3.61	1.90	16	0.18	0.82
6	4.33	2.08	20	0.12	0.88

7	5.06	2.25	24	0.09	0.91
8	5.78	2.40	28	0.04	0.96

3.3 Experimental Results

Experimental results of Kevlar® 49 both the swath and yarn are presented and analyzed in this section. The load-deformation results from the experimental results were used to calculate the true stress-strain response. The stress-strain curve of Kevlar® 49 is nonlinear and it is divided into four regions - crimp, elastic region, post peak linear and post peak nonlinear (see Figure 3-2). Details of the calculation of the various material properties from the true stress-strain curve are explained below.

Young's Modulus

The Young's modulus value is calculated based on the maximum slope in the linear elastic region.

$$E = \frac{\sigma_2 - \sigma_1}{\varepsilon_2 - \varepsilon_1} \quad (3.3.1)$$

where E is Young's modulus, σ_1, σ_2 and $\varepsilon_1, \varepsilon_2$ are the stress and strain at points 1 and 2 respectively in the elastic region.

Toughness

Toughness is the measure of the energy that is absorbed by the material and is computed by calculating area under the stress-strain curve.

Ultimate Stress

This is the maximum stress in the stress-strain curve and is also the end point of the linear elastic region.

Strain at Ultimate Stress

The strain value corresponding to the ultimate stress value is the strain at ultimate stress.

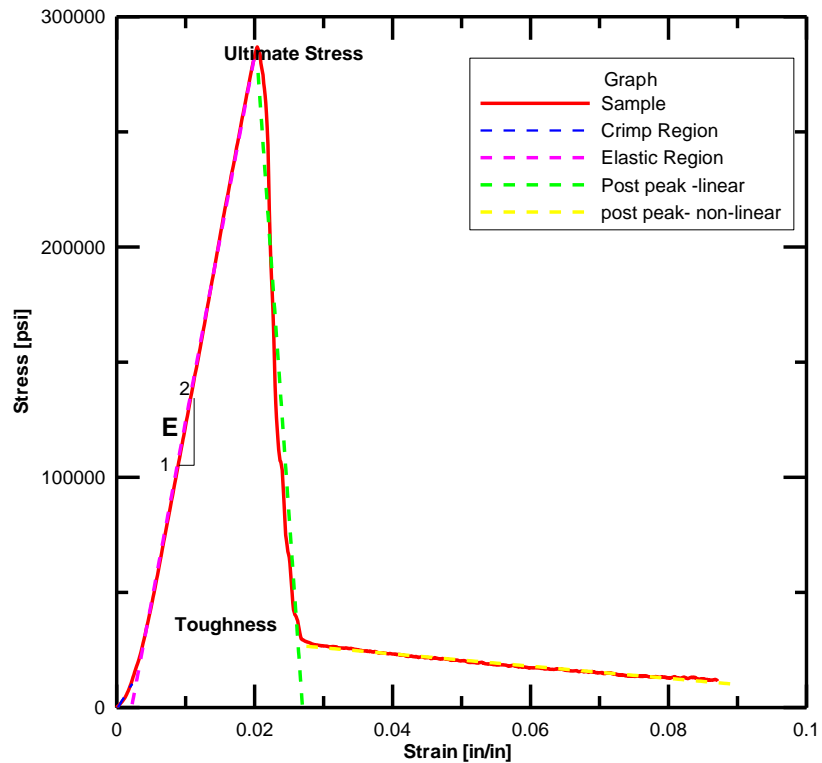


Figure 3-2. Piecewise linear approximation of true stress vs. true strain curve

True Stress and Strain

True stress and true strain are calculated from the engineering stress and strain as

$$\sigma_t = \sigma(1 + \epsilon) \quad (3.3.2)$$

$$\epsilon_t = \ln(1 + \epsilon) \quad (3.3.3)$$

where σ_t, ε_t are true stress and true strain and σ, ε are engineering stress and engineering strain.

3.3.1 Kevlar® 49 -Swath Data

In this sub-section, tests results of Kevlar® 49 swath are presented and discussed. Quasi-static tests were conducted as per American Society for Testing Material (ASTM) procedure, Tensile Testing of Polymer Matrix Composites – ASTM D 3039 “Standard Test Method for Tensile Properties of Fiber-Resin Composites” with the rate of loading as 0.1 in/min. The test was continued until complete failure of the specimen was achieved. In order to ensure that slipping of the specimens did not influence the deflection values, flat steel plates 2.5 in wide, 2 in long and 0.25 in thick (see Figure 3-3) are used to grip the specimen at both ends. At each end, one of the two pieces has a curved groove at the center of the plate throughout its width, which is half the thickness of the plate. The other plate has a V-notch cut in the same position about half the thickness of the plate.

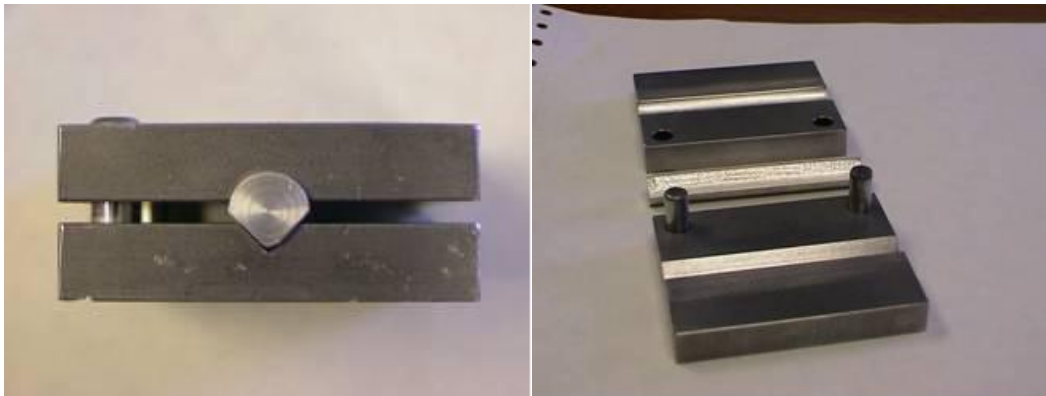


Figure 3-3. Grip plates a) side view b) inner view

A special step was taken during the specimen preparation. To create a strip of specimen, the fabric was first cut into rectangular strips, and then a number of

yarns along the fabric length are removed from both sides of the fabric width, thereby producing a sample without yarn crossovers along the edges. This step is necessary to ensure that the effects of edge defects are minimized and that the loaded yarns will not slip out of the cross yarns during the test. The total cross-sectional area of a specimen was defined as the cross-sectional area per yarn multiplied by the number of yarns within the width.

The specimen is clamped to the instrument using grip plates. One end of the specimen is fixed and the other end is subjected to the controlled displacement rate. The experiment is stopped once the load acting on the specimen falls below 5 lb. Experimental results and stress vs. strain plot of different specimen size are given in Figure 3-4 through Figure 3-7 and Table 3-4 through Table 3-6 respectively.

Table 3-4. Kevlar® 49 Swath (2" x 8").

Specimen #	Max Load (lb)	Modulus E (psi)	Toughness (psi)	Ultimate Stress σ_{ult} (psi)	Strain at Ultimate Stress, ϵ_{ult} (in/in)
1	1701	18770712	4674	286864	0.0204
2	1725	15556700	5654	291612	0.0229
3	1699	15940125	5597	286803	0.0219
4	1511	17881351	4731	255000	0.0215
5	1467	17052266	4558	247401	0.0203
6	1593	19323498	5791	268694	0.0209
7	1504	17425902	5348	253569	0.0204
8	1640	17168903	5495	276893	0.0215
Average Value	1605	17389932	5231	270855	0.0212
Standard Deviation	101	1282496	497	17250	0.0009

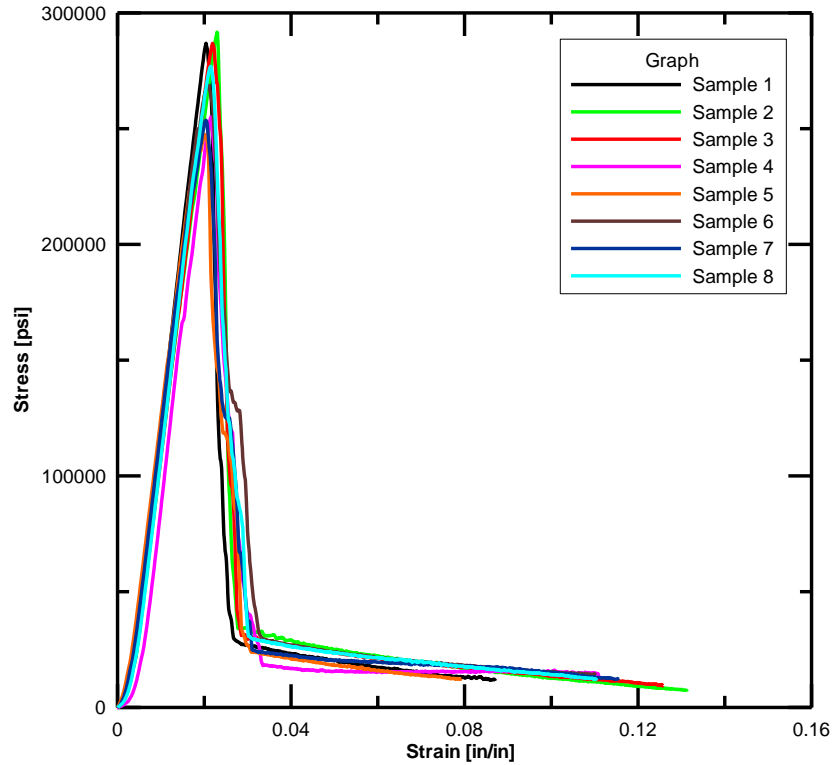


Figure 3-4. True stress vs. true strain curve -Kevlar® 49-swath (2'' x 8'')

Table 3-5. Kevlar® 49 Swath (2'' x 11'').

Specimen #	Max Load (lb)	Modulus E (psi)	Toughness (psi)	Ultimate Stress σ_{ult} (psi)	Strain at Ultimate Stress, ϵ_{ult} (in/in)
1	1440	18107096	4215	242699	0.0200
2	1670	18565086	4050	281595	0.0205
3	1609	18527485	3876	270852	0.0187
4	1500	20287396	3382	251887	0.0162
5	1539	20125640	3793	247401	0.0203
6	1546	19323498	3913	259542	0.0207
7	1486	20901273	4002	249938	0.0178
8	1684	18466929	4013	283374	0.0186
Average Values	1559	19288050	3906	260911	0.0191
Standard Deviation	88	1033304	711	15807	0.0016

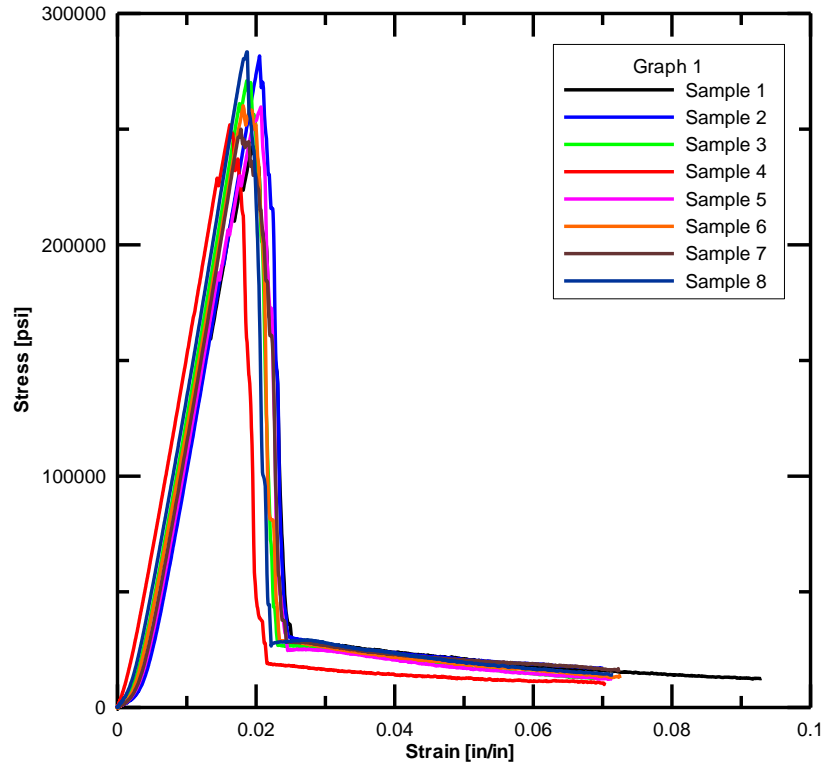


Figure 3-5. True stress vs. true strain curve -Kevlar® 49-swath (2'' x 11'')

Table 3-6. Kevlar® 49 Swath (2'' x 14'').

Specimen #	Max Load (lb)	Modulus E (psi)	Toughness (psi)	Ultimate Stress σ_{ult} (psi)	Strain at Ultimate Stress, ϵ_{ult} (in/in)
1	1605	20210093	4022	288454	0.0175
2	1648	20482200	3527	276976	0.0167
3	1548	19241991	3580	267070	0.0173
4	1600	22207602	4282	274173	0.0176
5	1523	20413049	4166	277472	0.0189
6	1564	21038781	3902	265868	0.0193
7	1678	20483410	3981	284646	0.0186
8	1545	19786473	3930	261559	0.0179
Average Values	1589	20482950	3924	274527	0.0180
Standard Deviation	54	877315	261	9334	0.0009

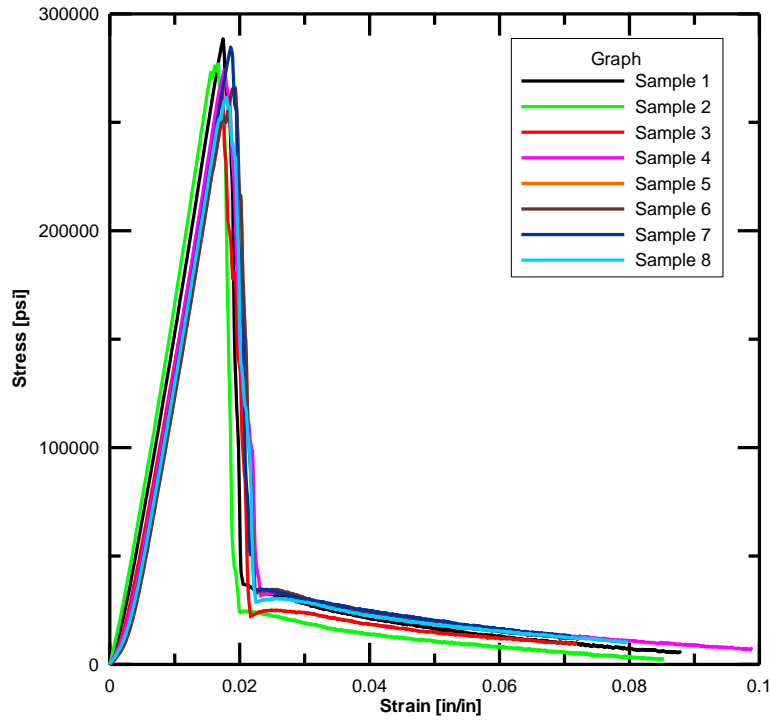


Figure 3-6. True stress vs. true strain curve -Kevlar® 49-swath (2'' x 14'')

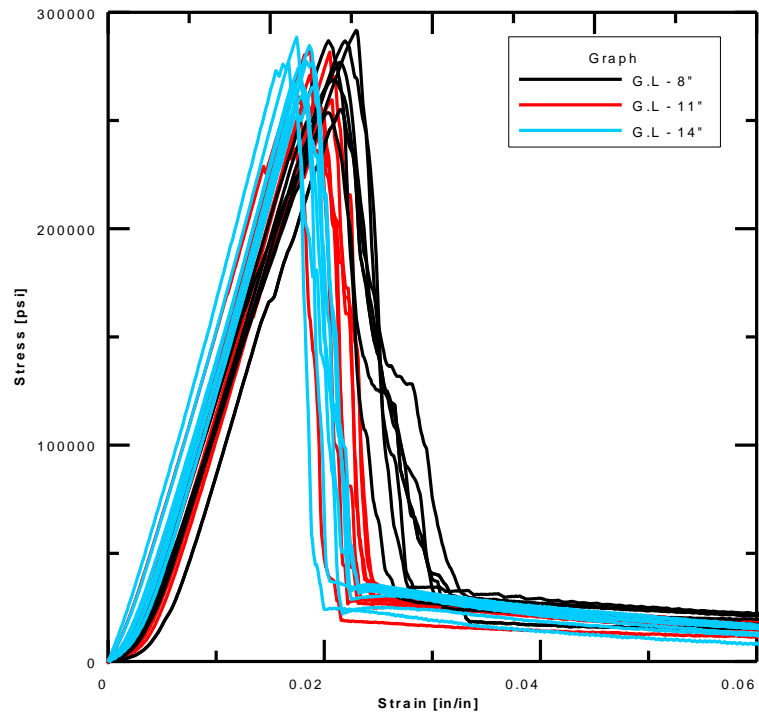


Figure 3-7. True stress vs. true strain curve - various gage lengths (Kevlar® 49-Swath)

3.3.2 *Yarn Data*

The samples for single yarn tensile tests were prepared by removing warp direction yarns from the woven fabric. Utmost care was taken to ensure that the yarns were removed without any damage [2]. To remove the warp yarns following steps were taken.

1. Cut the length of the fabric based on gage length required for the test sample.
2. Cut the sample from sides along the warp direction of the fabric so as to remove stitches on the fabric sample.
3. Remove fill yarns from both ends of the fabric. This ensures easy removal of warp yarns.
4. Apply crazy glue on both sides of the warp yarns to allow removal of the yarns without any damage and after glue is dried remove the warp yarn one by one with care.

The single yarn test specimen tested on MTS test frame under displacement controlled condition such that the strain rate for the specimen is 0.025 /min. Tests were conducted using 8", 11", 14" specimens [2] and the results are compared against the swath data. Experimental results and stress vs. strain plot of different specimen size are given in Table 3-7 through Table 3-9 and Figure 3-8 respectively.

Table 3-7. Kevlar® 49 Yarn (8”).

Specimen #	Max Load (lb)	Modulus E (psi)	Toughness (psi)	Ultimate Stress σ_{ult} (psi)	Strain at Ultimate Stress, ϵ_{ult} (in/in)
1	43	8740502	4773	241582	0.0410
2	43	9591447	5131	246909	0.0395
3	46	9941755	5129	260772	0.0405
4	43	9057741	4826	245310	0.0381
5	48	9304931	5629	273417	0.0447
6	44	9776610	5397	248641	0.0425
7	48	9479348	5838	271245	0.0441
8	47	10423857	5256	267427	0.0408
9	46	9369251	5167	261424	0.0437
10	42	10064157	4805	241077	0.0403
Average Values	45	9574960	5195	255780	0.0415
Standard Deviation	2	497061	353	12471	0.0021

Table 3-8. Kevlar® 49 Yarn (11”).

Specimen #	Max Load (lb)	Modulus E (psi)	Toughness (psi)	Ultimate Stress σ_{ult} (psi)	Strain at Ultimate Stress, ϵ_{ult} (in/in)
1	41	10718934	4042	231409	0.0299
2	47	10803698	4330	264975	0.0353
3	43	10363548	4027	242727	0.0318
4	44	10146075	4412	247469	0.0354
5	41	10830259	4056	235178	0.0340
6	49	11120894	4553	275696	0.0361
7	38	10877193	3749	216658	0.0337
8	45	10534750	4411	256674	0.0343
9	40	11078822	3789	229625	0.0319
10	45	10817346	4384	258351	0.0348
Average Values	43	10729152	4175	245876	0.0337
Standard Deviation	3	304183	280	18197	0.0019

Table 3-9. Kevlar® 49 Yarn (14”).

Specimen #	Max Load (lb)	Modulus E (psi)	Toughness (psi)	Ultimate Stress σ_{ult} (psi)	Strain at Ultimate Stress, ϵ_{ult} (in/in)
1	37	10770298	3910	208621	0.0246
2	46	11477332	4916	261403	0.0326
3	38	11628819	4274	217109	0.0271
4	50	11929564	5316	281943	0.0321
5	46	14396653	5087	263909	0.0323
6	37	12546649	3439	212425	0.0288
7	46	13282857	3732	263447	0.0291
8	42	14212865	3806	241275	0.0300
9	42	13042560	3804	241235	0.0300
10	43	14228247	3690	247081	0.0288
Average Values	43	12751585	4197	243845	0.0295
Standard Deviation	4	1287399	667	24750	0.0025

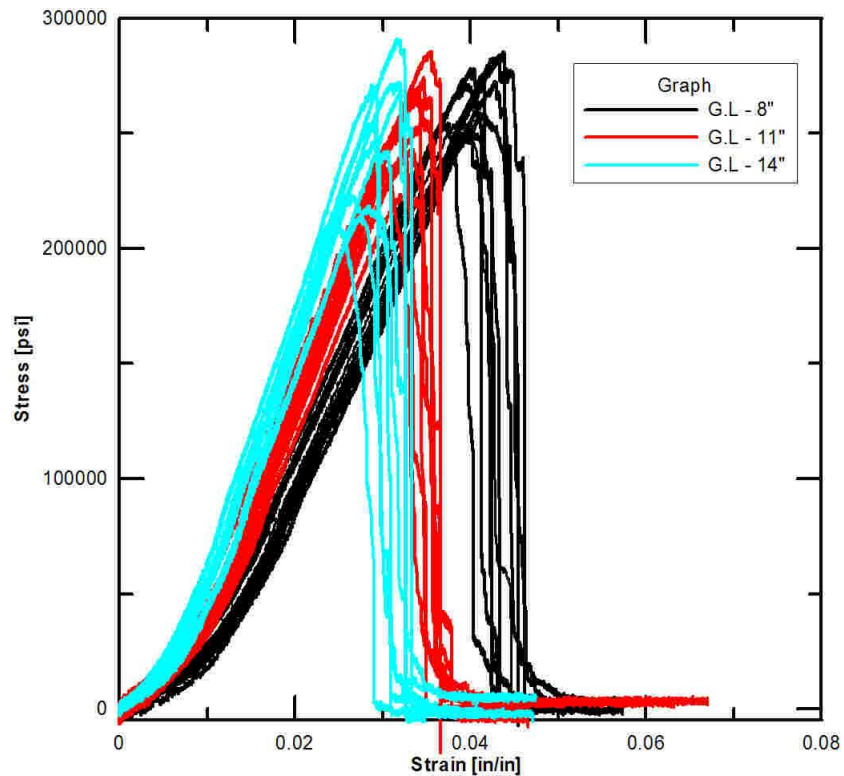


Figure 3-8. True stress vs. true strain – various gage lengths (Kevlar® 49-yarn)

3.4 Parameter Response of Swath

Experimental data from the swath and yarn specimens are considered for further analysis. Response of various parameters such as maximum load, Young's modulus in linear region, ultimate stress, strain at ultimate stress, toughness with respect to the gage lengths are plotted using Box plot (Figure 3-9, Figure 3-10 & Figure 3-11).

Kevlar® 49-Swath Data

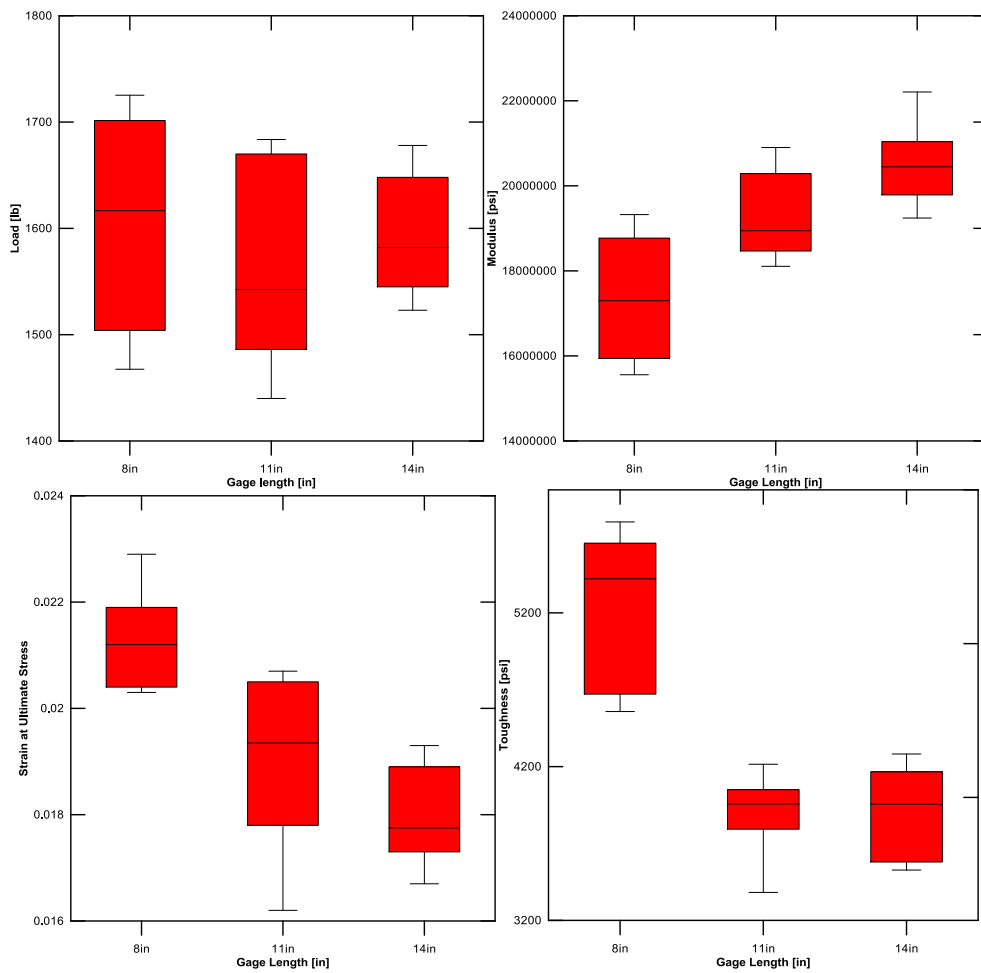


Figure 3-9. Parameters vs. gage length (Kevlar® 49-swath) (load, modulus, toughness & strain at ultimate stress – clockwise)

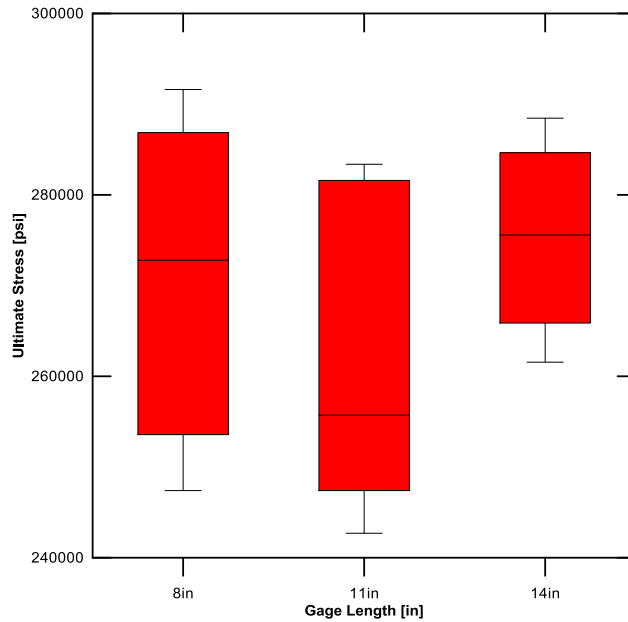


Figure 3-10. Ultimate stress vs. gage length (Kevlar® 49-swath)

From the above plots, the following points are observed.

1. Modulus increases as the gage length increases and bounds corresponding to each gage length are above the average value from the previous gage length.
2. Strain at ultimate stress decreases as gage length increases and bounds corresponding to each gage length are below the average value from the previous gage length.
3. Maximum load and ultimate stress decreases and then increases as the gage length increases.
4. Toughness decreases as the gage length increases from 8” to 11” and then remains the same when the gage length is increased to 14”

Kevlar® 49-Yarn Data

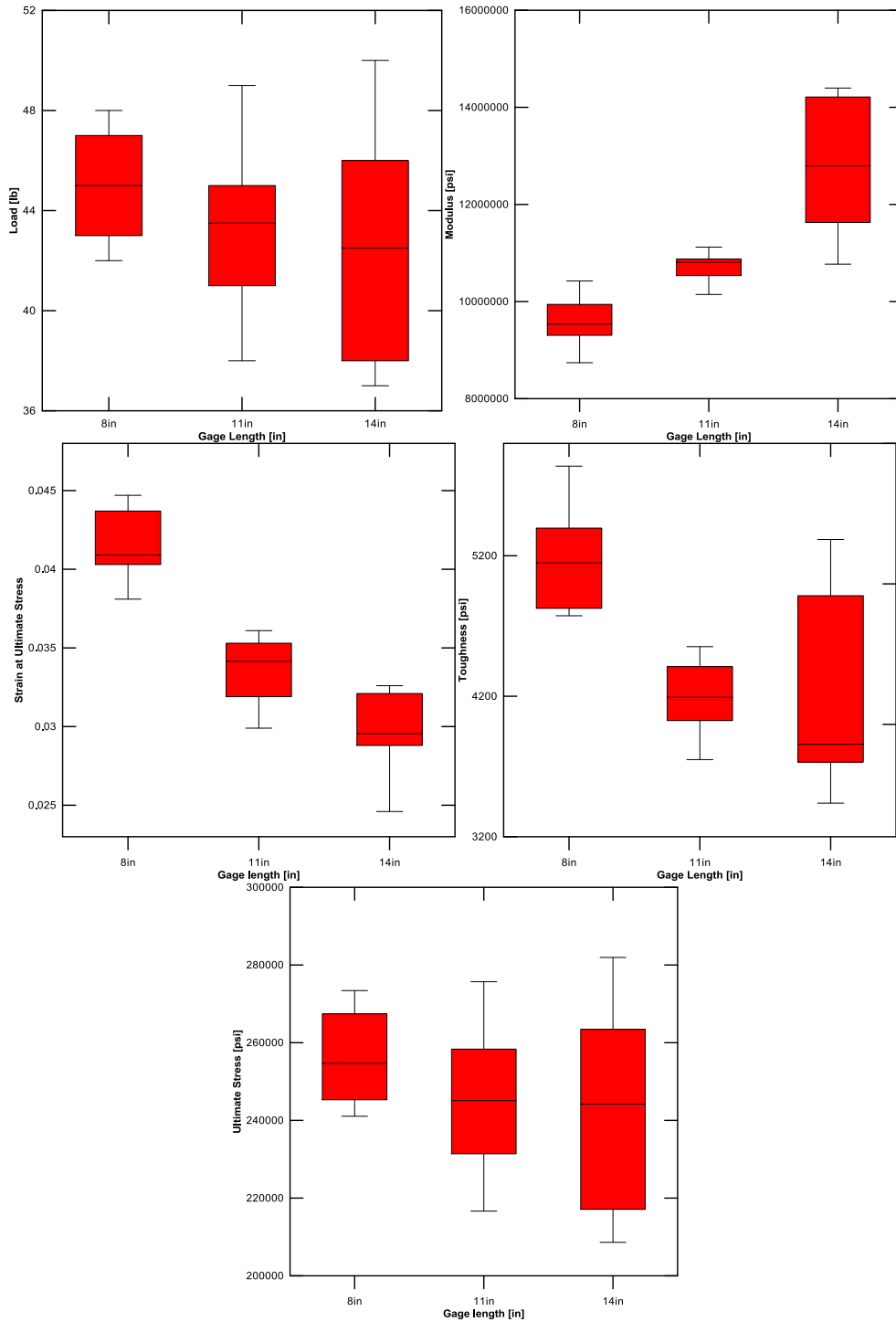


Figure 3-11. Parameters vs. gage length (Kevlar® 49-yarn) (load, modulus, ultimate stress, strain at ultimate stress & toughness- clockwise)

From the above plots, the following points are observed.

1. Modulus increases as the gage length increases and bounds corresponding to each gage length are above the average value from the previous gage length.
2. Strain at ultimate stress decreases as gage length increases and bounds corresponding to each gage length are below the average value from the previous gage length.
3. Mean value of toughness and load decreases as the gage length increases.
4. Mean value of ultimate stress decreases with the gage length from 8” to 11” and then remains the same.

Comparison:

1. Young’s modulus and strain at ultimate stress follow same pattern in both the swath and yarn data.
2. Decreasing trend (as the gage length increases) is observed in load and toughness parameters with respect to yarn data. Whereas in swath data, both the parameters decreases till the gage length 11”.
3. Wide range of bounds in parameters value is observed in all the yarn data corresponding to the gage length of 14” and no such wide range trend in swath data of particular gage length.

3.5 Compliance Test

The machine compliance is calculated based on the ASTM Standard 3379-75 “Standard Test Method for ASTM Standard and Young’s Modulus for High

Modulus Single-Filament Materials”. The inverse of the load-displacement slopes were plotted as a function of gage length. The plotted values are fitted using linear fit and equation from the fit is used to calculate the compliance. The equation of fit is given as

$$y = mx + c \quad (3.5.1)$$

where m is slope and c is the intercept. The c value gives the test machine compliance. Compliance calculations using Kevlar® 49 swath and yarn tests are given below.

Kevlar® 49-Swath Data

Equation of the fitted line (see Figure 3-12) is given by

$$\begin{aligned} y &= 8(10^{-6})x + 3(10^{-5}) \\ R^2 &= 0.9993 \end{aligned} \quad (3.5.2)$$

Compliance is estimated to be 0.00003 in/lb or the stiffness of the test frame is 33333.33 lb/in. The R^2 value is 0.9993 indicating an acceptable fit.

Kevlar® 49-Yarn Data

Equation of the fitted line (see Figure 3-13) is given by

$$\begin{aligned} y &= 0.0015x + 0.0141 \\ R^2 &= 0.9958 \end{aligned} \quad (3.5.3)$$

Compliance is estimated to be 0.015 in/lb or the stiffness of the test frame is 67 lb/in. The R^2 value is 0.9995 indicating an acceptable fit.

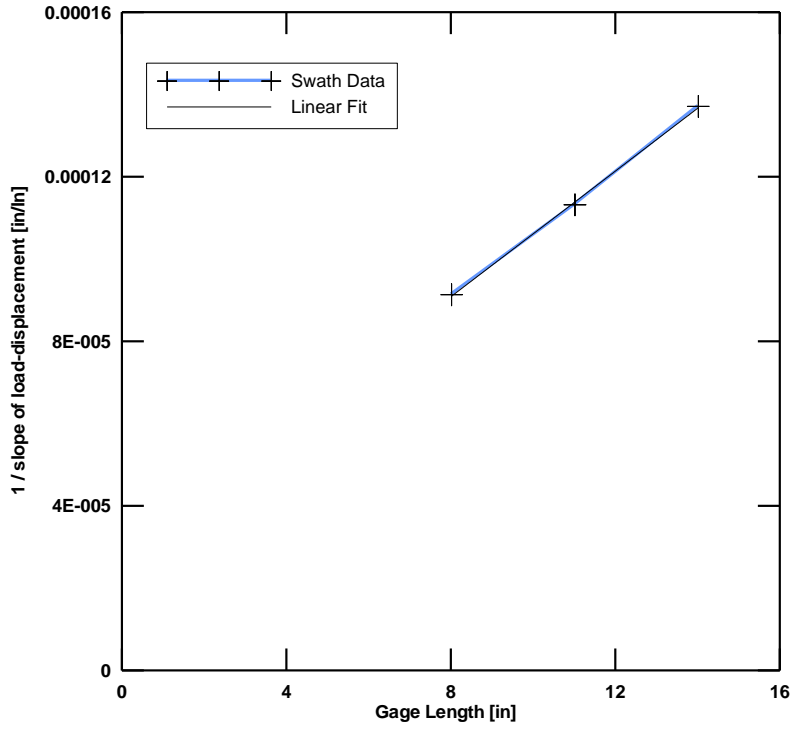


Figure 3-12. Compliance test for Kevlar® 49-swath

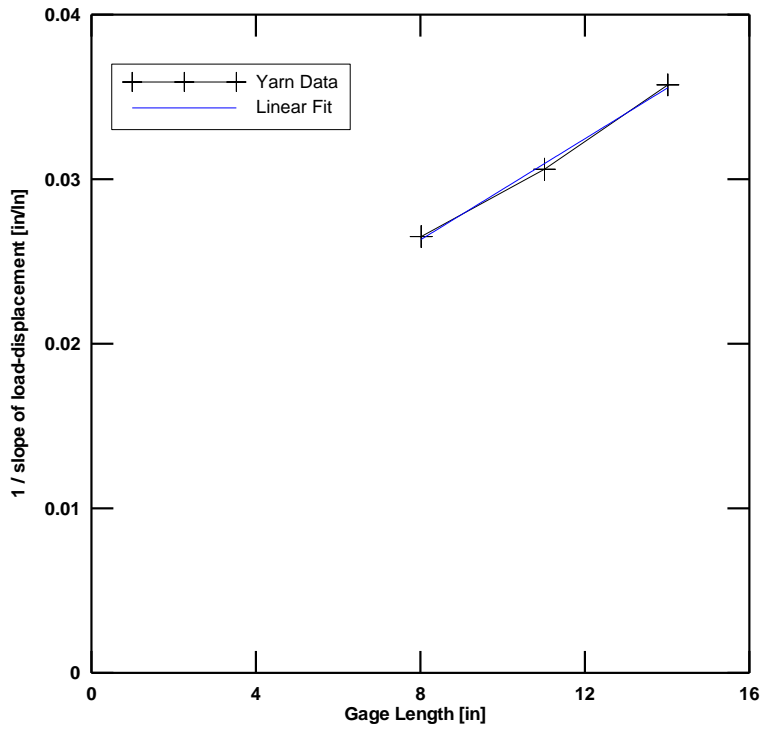


Figure 3-13. Compliance test for Kevlar® 49-yarn

3.6 Digital Image Correlation

Digital Image Correlation (DIC) is an optical method of measuring deformation or strain in 2D and 3D during an experimental test. It is a Non-interferometry technique (which uses gray intensity for image comparison) for measuring the in-plane and out-of-plane deformations using a non-contact optical method as opposed to the contact based gauging technique [46]. Deformation and full field strain are measured from the digital images captured before and after deformations. The schematic setup for DIC is shown in Figure 3-14.

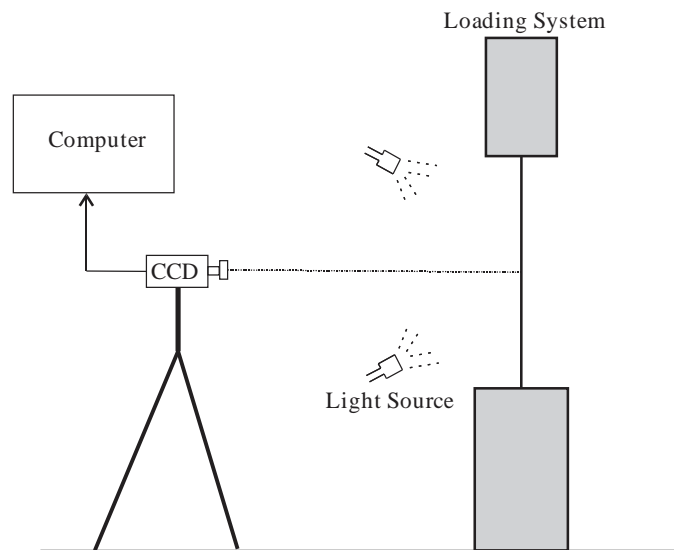


Figure 3-14. Experimental setup for DIC

The method employs the comparison of random gray intensity distribution of the images at different time steps. The basic idea is tracking of points in two images by selecting a subset of pixels which helps to track the deformation. The tracking of points is shown in Figure 3-15. Some of the careful considerations in conducting experiment are

- a) Vertical alignment of the camera and the loading instrument.

- b) The central horizontal axis from the camera should be perpendicular to the specimen to reduce the error in measurement.

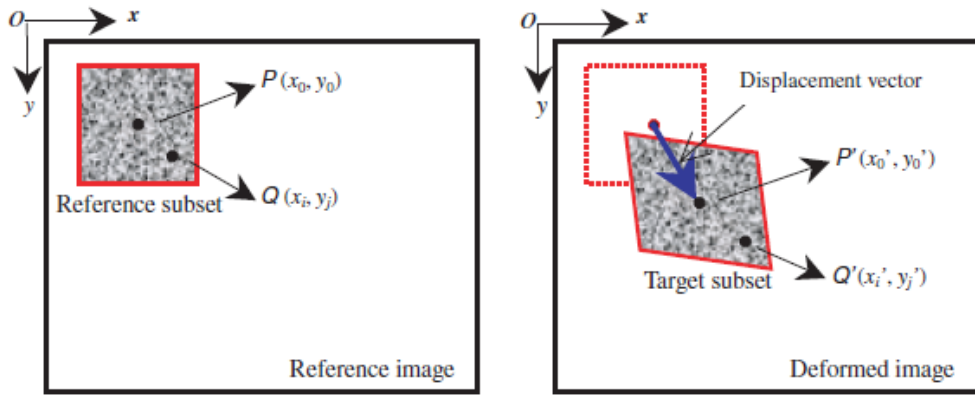


Figure 3-15. Image correlation [46]

The procedure for the DIC is as follows.

- 1) Specimen with random gray intensity distribution, if not use some paint source to obtain gray pattern in the specimen.
- 2) Alignment of CCD camera, light source and specimen vertically.
- 3) Record of digital images using CCD camera and correlation is done by transferring the image data to the computer.
- 4) Measurement of deformation and strain using DIC.

Out-of-plane deformation is measured using digital volume correlation which is called 3D-DIC [46]. Micro-scale and Nano scale measurement can also be made capable using DIC by combining it with a high spatial resolution microscope. The wider applications of the DIC are measurement of deformations and strains in various materials, fracture mechanics and for high speed applications.

4. FINITE ELEMENT AND MATERIAL MODELING

In this chapter, finite element modeling, material modeling of Kevlar® 49, recent improvements to the existing model, comparison of material parameters over various phases of the research, and energy checks are explained.

4.1 Introduction

Creating finite element models of dry fabrics that include yarn geometry details at a meso-scale level for use in the analysis is not practical. A more practical approach is to create an equivalent continuum model. The effective properties are needed for different weaves and weave geometries to be used in the model. Figure 4-1 shows the modeling of the fabric as an equivalent continuum shell. The experimentally obtained material properties are used in development of constitutive model of dry fabrics for use in an explicit finite element program.

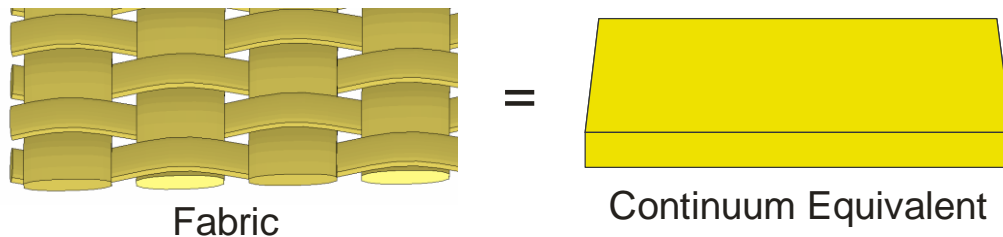


Figure 4-1. Modeling the fabric as continuum

Development of ASUumatv1.0 [3] material model started in 2006. In this model the stress–strain behavior extended only till the beginning of the post peak nonlinear region. Experimental data beyond this point was not available at that time. The failure criteria was combined for both the warp and fill directions. Only single layer (SL) concentric models were built. Simulations were run using LS-DYNA 970. Sensitivity analysis was carried out for various parameters assumed

in this model and the FE simulation trends were found to be consistent with experimental results.

In ASUumatv1.1 [4] the failure criteria were decoupled. An element was eroded if either the strain in warp or fill direction reached a pre-determined value or if the strain in both warp and fill directions reached ultimate strain. The simulations were run using LS-DYNA 971 version. Both multiple layer (ML) and SL concentric models were built to replicate the results of the ballistic tests. Quality assurance (QA) checks were carried out to ensure that the simulation results were acceptable. In ASUumatv1.2, the contact formulations were improved to include the contact and friction formulations between multiple layers. The shear behavior was also revised in the model.

In ASUumatv1.3 [5 & 6] regression analysis was used to obtain the values of a number of parameters that were difficult to characterize experimentally - strain rate behavior in tension, global damping parameters, and contact behavior between fabric layers and fabric and the steel ring. A new type of modeling the fabric called the Spiral Modeling Scheme (SMS) was implemented. This modeling scheme more closely represents the way the fabric is wrapped in the ballistic test. The FE model and the boundary conditions of the steel ring in the ballistic tests were changed to more closely reflect the experimental setup. The erosion criterion was refined. ML and SL simulations were run to validate the model. The analysis option was also updated and can be selected between probabilistic and deterministic analysis. The distribution model parameters

corresponding to the material property and random number generator were updated which are then used for probabilistic analysis.

4.2 NASA Ballistic Tests

Ballistic experimental data were generated at NASA-GRC. The tests consisted of shooting a steel projectile through multiple fabric layers wrapped around a 10.5" wide steel ring with the diameter of 40". A continuous 10" wide fabric is wrapped around the ring in one or more layers with the last part of the fabric is glued to the layer under it. The tests were repeated by changing the projectile orientation, projectile velocity, number of fabric layers and projectile geometry. In each test, velocity of the projectile is monitored using high speed cameras. Figure 4-2 shows components of the test setup.

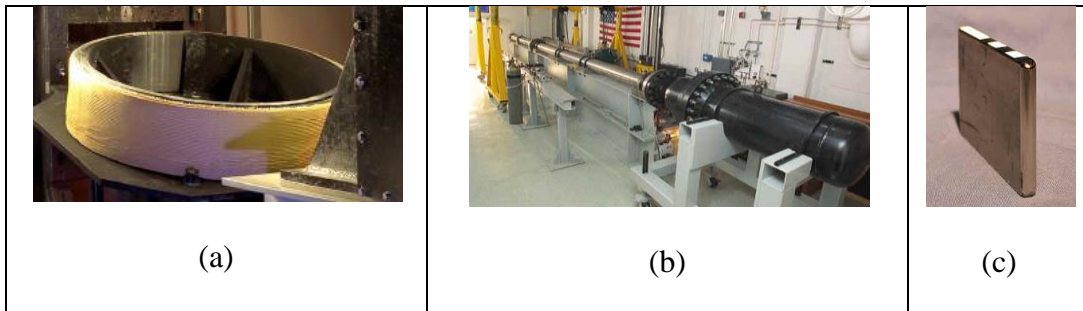


Figure 4-2. High speed NASA-ballistic test setup (a) steel ring with Kevlar® 49 Wrap. (b) gas gun (c) typical projectile

4.3 Finite Element Model

The fabric is modeled as shell elements, the ring and projectile are modeled as solid elements [6]. Two projectiles were used in the tests. The *old* projectile is modeled in two parts - the tip was meshed with 0.15" uniform tetrahedral elements and the body with 0.2" x 0.15625" x 0.2023" hexahedral elements. The *new* projectile had a mesh of 0.1" uniform tetrahedral elements for

tip and 0.15" x 0.1175" x 0.1495" hexahedral elements for the body. The steel ring was meshed with 0.25" x 0.25" x 1" hexahedral elements. A mesh convergence study [6] was conducted to seek a compromise between accuracy of the results and the computational time. Element size of 0.25 in was chosen based on the results. Figure 4-3 shows the FE model of the projectile, fabric and ring.

Fixed boundary conditions are used for nodes [7] at the bottom of the ring and the two bracings (stiffeners) that are placed on the either side of the opening mimicking the exact experimental boundary conditions. Fabric is modeled in two parts, flat and curved parts. The flat part represents the fabric portion where the projectile makes impact and the curved part represent the fabric which is wrapped around the ring.

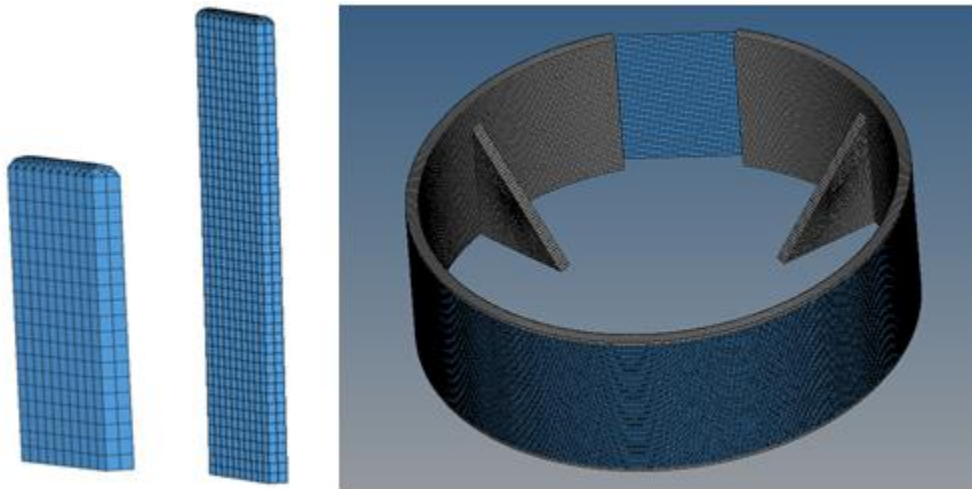


Figure 4-3. Projectile, ring and fabric FE model

4.4 Material Model

In this composite material each lamina is a thin layer and subjected to plane stress condition and the material is transversely orthotropic. We take material direction 11 as the main longitudinal direction of the fabric (warp

direction), direction 22 as the direction along the width of the fabric (fill direction), and direction 33 refers to the direction perpendicular to both warp and fill directions. The constitutive behavior suitable for use in an explicit finite element analysis in stiffness incremental form is shown in Eqn.(4.4.1). We assume that the stress-strain relationships are decoupled so that any stress component is a function of only one strain component.

$$\begin{bmatrix} \Delta\sigma_{11} \\ \Delta\sigma_{22} \\ \Delta\sigma_{33} \\ \Delta\sigma_{12} \\ \Delta\sigma_{31} \\ \Delta\sigma_{23} \end{bmatrix} = \begin{bmatrix} E_{11} & 0 & 0 & 0 & 0 & 0 \\ 0 & E_{22} & 0 & 0 & 0 & 0 \\ 0 & 0 & 0 & 0 & 0 & 0 \\ 0 & 0 & 0 & 2G_{12} & 0 & 0 \\ 0 & 0 & 0 & 0 & 2G_{31} & 0 \\ 0 & 0 & 0 & 0 & 0 & 2G_{23} \end{bmatrix} \begin{bmatrix} \Delta\varepsilon_{11} \\ \Delta\varepsilon_{22} \\ \Delta\varepsilon_{33} \\ \Delta\varepsilon_{12} \\ \Delta\varepsilon_{31} \\ \Delta\varepsilon_{23} \end{bmatrix} \quad (4.4.1)$$

Strain rate effects are implemented in the model using a modified Cowper-Symonds model [47] as

$$\bar{E} = E_0 \left[1 + \left(\frac{\dot{\varepsilon}}{C} \right)^P \right] \quad (4.4.2)$$

where \bar{E} is rate dependent modulus of elasticity, E_0 is warp or fill quasi-static modulus of elasticity, $\dot{\varepsilon}$ is the strain rate, C and P are the Cowper Symonds factors. Similar equation is used for computing the scaled peak stress and failure strain.

To validate the developed material model, finite element models are built to replicate the experimental ballistic impact tests as closely as possible. In the FE model, each layer is wound around the ring in the form of a spiral called spiral modeling scheme mimicking the experimental setup which is explained below.

Since the number of physical layers can be extremely large, multiple physical layers are modeled as an equivalent FE layer. For example, four physical layers are modeled as a single FE layer with an equivalent thickness as 0.044". Similarly, an 8 fabric layer model is represented by 2 FE layers each having a thickness of 0.044 in (4 x 0.011 in).

Spiral Modeling Scheme (SMS): In SMS modeling the fabric is wrapped around the ring in a continuous form. The wrapping starts at the end diametrically opposite of the cut out end in the ring. In this model each layer is connected to at least one more layer. Figure 4-4 shows the close up of the wrapping of the fabric around the ring. Note that a layer is represented by a single color. It starts at a lower radius and as it goes around the ring, the radius increases and it ends at the radius where the next layer is starting.

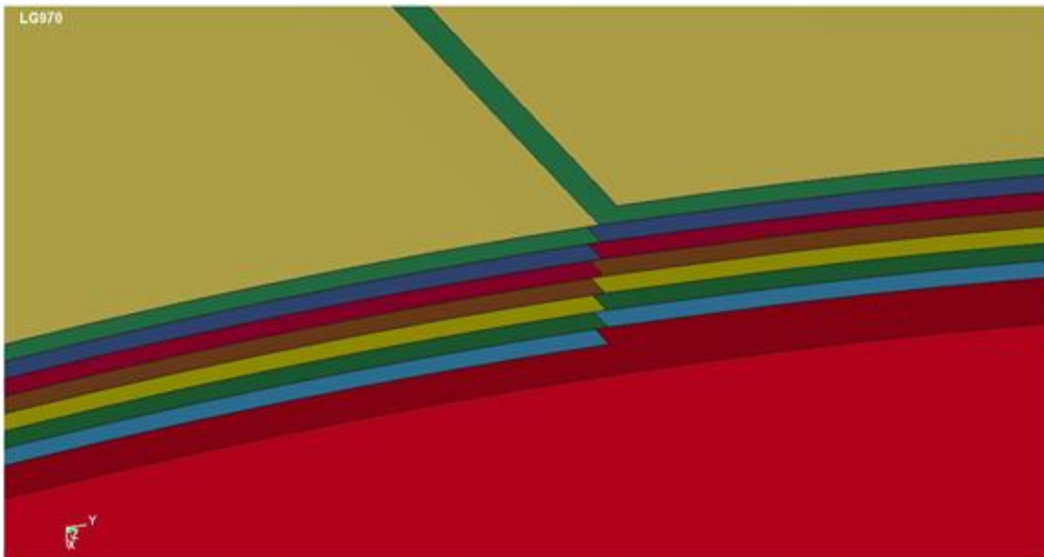


Figure 4-4. Spiral modeling scheme

This model more closely represents the wrapping conditions as different layers are connected in it. This is useful in better modeling the force transmission between different layers of the fabric. In the actual test the inner and the outer end of the fabric is glued to the ring and the fabric respectively.

*CONTACT_TIRBREAK_NODES card in LS DYNA [48]. In this card a contact is defined between a set of nodes and a surface by specifying a shear and tensile failure force. These forces define a failure criterion. If the criterion is not violated then the nodes and surface are tied together like glue but the moment the criterion is violated, they move separately.

The failure criterion is given by

$$\left(\frac{|f_n|}{F_n}\right)^{m_n} + \left(\frac{|f_s|}{F_s}\right)^{m_s} \geq 1 \quad (4.4.3)$$

where f_n is the normal interface force, f_s is the shear interface force, F_n is the normal failure force, F_s is the shear failure force, m_n, m_s are the exponents for normal and shear force. Regression analysis was carried out [6] to determine the tensile force and shear force for tie break and the optimum value of shear and tensile force between the ring and fabric is 500 and 1000 lb respectively

Equivalent Modulus of Elasticity: In computation of equivalent modulus of elasticity used in the FE model, we assume that the axial stiffness of the model and the material are equivalent.

$$E_{FE}A_{FE} = EA \quad (4.4.4)$$

where E_{FE}, A_{FE} are Young's modulus and area of the FE model and E, A are the Young's modulus and area of the material. Area of the material is number of yarns per one inch multiplied by area of each yarn and the corresponding area of the FE material model is obtained by multiplying width (w_{FE}) by thickness (t_{FE}).

$$E_{FE} = \frac{EA}{t_{FE}w_{FE}} = \frac{E*17*0.000178}{0.01075*1} \quad (4.4.5)$$

$$E_{FE} = 0.2815E \quad (4.4.6)$$

The summary of input parameters used in the ASUumatv1.3 is given in Table 4-1. The base units are million pounds (Mlb) for force, inches (in) for length and milliseconds (ms) for time.

Table 4-1. Summary of UMAT Parameters.

No.	Material Constant	UMAT Notation	Symbo 1	ASU UMAT v.1.0	ASU UMAT v.1.1	ASU UMAT v.1.2	ASU UMAT v.1.3
1	Warp Stiffness in Elastic Region (psi 10 ⁶)	Ex	E_{11}	3.2	3.2	3.2	4.68
2	Fill Stiffness in Elastic Region (psi 10 ⁶)	Ey	E_{22}	4.5	4.5	4.5	4.68
3	Warp Direction Crimp Stiffness Factor	Excrfac	E_1^{crp}	0.1	0.1	0.1	0.06
4	Fill Direction Crimp Stiffness Factor	Eycrfac	E_2^{crp}	N/A	N/A	N/A	0.20
5	Warp Direction Post-peak Linear Region Stiffness Factor	Exsoftfac	E_1^{soft}	-2.5	-2.5	-2.5	-2.2
6	Fill Direction Post-peak Linear Region Stiffness Factor	Eysoftfac	E_2^{soft}	N/A	N/A	N/A	-5.6
7	Unloading/Reloadi	Eunlfac	E^{unl}	1.5	1.5	1.5	1.5

	ng Stiffness Factor						
8	Compressive Stiffness Factor	Ecompfac	E^{comp}	0.005	0.005	0.005	0.005
9	Shear Stiffness (G_{23}) (psi 10^6)	G23	G_{23}	0.05	0.05	0.05	0.05
10	Shear Stiffness (G_{31}) (psi 10^6)	G31	G_{31}	0.05	0.05	0.05	0.05
11	Shear Stiffness Linear Region 1 (G_{12}) (psi 10^6)	G121	G_{12}	0.001	0.001	0.001	0.0006
12	Shear Stiffness Linear Region 2 (G_{12}) (psi 10^6)	G122	G_{12}	0.008	0.008	0.008	0.006
13	Shear Stiffness Linear Region 3 (G_{12}) (psi 10^6)	G123	G_{12}	0.040	0.040	0.04	0.050
14	Shear Stiffness Linear Region 4 (G_{12}) (psi 10^6)	G124	G_{12}	0.300	0.300	0.3	N/A
15	Shear Strain 1 (rad)	gamma ₁	γ_{12}	0.350	0.350	0.35	0.25
16	Shear Strain 2 (rad)	gamma ₂	γ_{12}	0.500	0.500	0.5	0.35
17	Shear Strain 3 (rad)	gamma ₃	γ_{12}	0.570	0.570	0.57	N/A
18	Warp Direction Crimp Strain (in/in)	ecrpx	ϵ_{11}^{crp}	0.0085	0.0085	0.0085	0.0065
19	Fill Direction Crimp Strain (in/in)	ecrpy	ϵ_{22}^{crp}	0.006	0.006	0.006	0.0025
20	Warp Direction Strain at Peak Stress (in/in)	emaxx	ϵ_{11}^{max}	0.0295	0.0295	0.0295	0.0223
21	Fill Direction Strain at Peak Stress (in/in)	emaxy	ϵ_{22}^{max}	0.0210	0.0210	0.021	0.0201
22	Stress at Post-peak Non-linearity (psi 10^6)	sigpost	σ^*	0.015	0.005	0.01	0.01
23	Warp Direction Failure Strain (in/in)	efailx	ϵ_{11}^{fail}	0.2	0.1	0.16	0.2
24	Fill Direction Failure Strain (in/in)	efailx	ϵ_{22}^{fail}	0.2	0.1	0.16	0.2
25	Cowper-Symonds	C(E)	C_E	0.005	0.005	0.005	0.005

	Factor for Stiffness (ms^{-1})						
26	Cowper-Symonds Factor for Stiffness (ms^{-1})	P(E)	P_E	40.0	40.0	40	40.0
27	Cowper-Symonds Factor for Strain (ms^{-1})	C(e)	C_e	0.005	0.005	0.005	0.005
28	Cowper-Symonds Factor for Strain (ms^{-1})	P(e)	P_e	40.0	40.0	40.0	40.0
29	Post-peak Non- linear Region Factor	dfac	$dfac$	0.3	0.35	0.3	0.3
30	Failure strain of element	fail_e	ϵ^{fail}	N/A	0.35	0.35	0.35
31	Analysis option (deterministic – 0)	-	-	N/A	N/A	N/A	0/1
32	Seed value	-	-	N/A	N/A	N/A	$\neq 0$

4.5 Finite Element Program

The developed constitutive model is implemented in LS-DYNA as a UMAT subroutine for use with shell elements. The computer simulations were run using the double precision LS-DYNA version 971 (Revision 5.1.1). The Intel FORTRAN 10.1 compiler was used for building the executable for Windows 7 OS. Apart from the mesh and material properties, it is necessary to specify other LS-DYNA specific parameters.

Contact Formulation. *CONTACT_AUTOMATIC_SURFACE_TO_SURFACE in LSDYNA is used to establish contact between the surfaces. For contact between ring and fabric, ring and projectile, fabric is chosen as the slave surface while the ring and projectile are chosen as master surface. For contact between the fabrics, outer layer of fabric is chosen as slave and inner layer is chosen as master

surface. In order to avoid oscillations between the elements, damping coefficient is provided. Viscous damping coefficient values of the model are given below in Table 4-2.

Table 4-2. Damping Coefficient Values.

Region	Damping Coefficient vale
Between flat parts of the fabric	10
Between curved parts of the fabric	20
Between ring and fabric	20
Between projectile and fabric	10

Friction. Static and dynamic coefficient of friction of 0.2 is assigned for the contact between fabric layers, 0.1 for contact between fabric and projectile, and between ring and fabric.

Hourglass Properties. A correct hourglass formulation is important in simulation to avoid zero energy mode which typically occur in an under integrated element. Flanagan-Belytschko stiffness form with hourglass coefficient of 0.1 is used for the fabric.

Shell Theory. The default Belytschko-Tsay shell theory was used with 1 through shell thickness integration point and other parameters related to shell theory were taken as default.

Material Properties. User defined material properties for fabric properties as discussed earlier are used. The steel ring and the projectile are characterized as an elasto-plastic material model (*MAT_JOHNSON_COOK).

Time Step. The *CONTROL_ACCURACY card [48] is used to control the time steps. This is recommended by LS DYNA for high velocity impact conditions.

The time step factor of 0.75 is used which means that the actual time step was 75 % of the time step computed by LS-DYNA.

To ensure that spurious results are not obtained, energy checks [3] are carried out as a part of the post-processing step. At any instant during the analysis, the sum of energies in the model must be equal to the sum of initial energies as given below⁵

$$E_K + E_I + E_S + E_H + E_{rw} + E_{damp} = E_K^0 + E_I^0 + W_{Ext} \quad (4.5.1)$$

where E_K is the kinetic energy, E_I is the internal energy, E_S is the sliding interface (contact) energy, E_H is the hourglass energy, E_T is the total energy, E_{rw} is the rigid wall energy, E_{damp} is the damping energy, E_K^0 is the initial kinetic energy, E_I^0 is the initial internal energy and W_{Ext} is external work. The total energy is the sum of the terms on the left-hand side

$$E_T = E_K + E_I + E_S + E_H + E_{rw} + E_{damp} \quad (4.5.2)$$

Internal Energy: Energy associated with elastic strain energy and work done in permanent deformation.

Kinetic Energy: Work done due to the motion of the nodes/elements with certain velocity.

External Work: Work done by the applied forces and pressure as well as work done by velocity, displacement or acceleration boundary conditions.

⁵ <http://www.dynasupport.com/tutorial/ls-dyna-users-guide/energy-data>

Sliding Energy: It is the work done by sliding interfaces and is the sum of *Slave Energy* (SE), *Master Energy* (ME), and *Frictional Energy* (FE), where slave and master energy are associated with the sliding energy of the slave and master parts of the model during the impact. Sliding energy is expected to be positive when friction between the surfaces is defined. Negative contact energy sometimes is generated when parts slide relative to each other. When a penetrated node slides from its original master segment to an adjacent though unconnected master segment and a penetration is immediately detected, negative contact energy is the result. Abrupt increases in negative contact energy may be caused by undetected initial penetrations.

Hourglass Energy: Under-integrated elements are used mainly to increase the computational efficiency and accuracy. However, in certain problems, spurious modes of deformations may result that are associated with the zero-energy modes of deformation (zero strain and no stress). To combat this problem, hourglass stabilization techniques are used. LS-DYNA provides several hourglass control options and the energy associated with these stabilization techniques can be computed. This nonphysical hourglass energy should be relatively small compared to peak internal energy for each part of the model.

Energy Ratio (ER): It is the ratio of total energy to the initial total energy and external work and is given below. The energy balance is perfect if the ratio is equal to 1.

$$ER = \frac{E_T}{E_I^0 + E_K^0 + W_{Ext}} \quad (4.5.3)$$

If the E_T rises above the right hand side, energy is being introduced artificially - for example, by numerical instability, or the sudden detection of artificial penetration through a contact surface. The latter condition is often shown by sudden jumps in the total energy. If the left hand side falls below the right hand side, energy is being absorbed artificially, perhaps by excessive hourglassing or by stonewalls or over-compliant contact surfaces. In Table 4-3 the values used in the energy checks are listed.

Table 4-3. Energy Checks.

Description	Acceptable Limit
Energy Ratio, ER	> 0.9 and < 1.1
Max. Sliding Energy Ratio, SER (sliding energy/total energy)	< 0.1
Max. Kinetic Energy Ratio, KER (kinetic energy/total energy)	< 1.0
Max. Internal Energy Ratio, IER (internal energy/total energy)	< 1.0
Max. Hourglass Energy Ratio, HER (hourglass energy/total energy)	< 0.1

5. NUMERICAL EXAMPLES

In this chapter, several numerical examples are presented. First, the fabric model data used with engine containment systems is analyzed. This data is then used in the MCS of two NASA-GRC ballistic tests. Second, five planar truss models are used in illustrating the developed FORM, SORM, MCS & RBDO procedures. Finally, a planar beam model is used to illustrate the RBDO procedure.

5.1 Fabric Based Engine Containment System

In this section, probabilistic modeling of experimental data and MCS of engine containment system are presented.

5.1.1 *Experimental Data - Distributions*

The EDP program [49] is enhanced with the capability to take experimental data and find the appropriate distribution function.

The program computes the scale parameter, shape parameter, PDF, CDF for each distribution and the goodness of fit tests values. Some results have been compared with DataPlot [39] results to make sure that the EDP program generates accurate results. The best fit model is selected based on statistics from the goodness of fitness tests. The test data from the uniaxial tension test as explained in the section 3.3 is considered.

Test Case I

In this test case, the Weibull model presented in the Section 2.2.3 is compared with the Weibull results from the source [50], in which CDF of the

model is normalized based on the volume of the specimen under consideration and is given by

$$F(x) = 1 - e^{V[-(x/\lambda)]^\alpha} \quad (5.1.1)$$

In the above Equation V is the characteristic parameter and given as follows.

$$V = \frac{\alpha + 3}{6(\alpha + 1)} V_0 \quad (5.1.2)$$

where V_0 is the volume of the specimen between the supports.

The comparison is done based on the experimental data (maximum stress) of the Kevlar® 49-yarn of gage length 8” data [2]. The scale parameter, shape parameter and the minimized function value are presented in the Table 5-1.

Table 5-1. Weibull Comparison Results.

Method	Parameter		Goodness of fit test		Function Value
	Scale [psi]	Shape	K-S Distance	AD	
Gage Length - 2 in					
M-1	280130	21.7	0.1632	0.2695	-
M-2	283880	27.8	0.1503	0.2523	0
M-3	280692	26.2	0.1253	0.1913	0
Gage Length - 5 in					
M-1	265140	11.5	0.1951	0.4507	
M-2	270530	14.3	0.2004	0.3505	0
M-3	268981	13.3	0.1760	0.2909	0
Gage Length - 8 in					
M-1	260160	14.3	0.3473	0.9999	
M-2	263756	24.8	0.2689	0.6260	0
M-3	263706	22.3	0.2393	0.5321	0
Gage Length - 11 in					
M-1	249790	11.9	0.2002	0.4977	

M-2	254841	14.6	0.1432	0.2505	0
M-3	254769	13.4	0.1210	0.2305	0
Gage Length - 14 in					
M-1	250160	7.9	0.2193	0.4879	
M-2	254190	10.9	0.1804	0.3559	0
M-3	254085	9.9	0.1539	0.1539	0
Gage Length - 17 in					
M-1	239370	8.8	0.2044	0.4551	
M-2	241389	10.9	0.2129	0.5206	0
M-3	241288	9.9	0.1980	0.4296	0

* M-1 – Model from source [50]

* M-2 – Weibull-2P Two Step Iterative MLE – No Weights

* M-3 - Weibull-2P Two Step Iterative MLE –Weighted

From the above results, it is clear that the weighted Weibull 2-parameter model gives good result compared to the other two models. The goodness of fit tests (KS and AD) which are associated with CDF of the model alone is considered here since only the CDF of the model [50] is available.

Test Case II

In this set of test, distributions such as Weibull, gamma, normal, lognormal, generalized exponential are considered, both the swath and yarn experimental data are considered for the analysis. Yarn and swath data are taken so that appropriate comparison can be made on the distribution models for different set of data.

Swath Data

Experimental data of Young’s modulus (E) and Ultimate Stress (σ_{ult}) from Swath specimen (Table 3-4) are analyzed here with results in Table 5-2 and Table 5-3.

Table 5-2. Results Using EDP Software- Kevlar® 49-Swath (E).

Distribution	Parameter		Goodness of fit test		
	Scale [psi]	Shape	K-S Distance	Chi-Square	AD
Young’s modulus (E)					
Weibull	17953600	15.9246	0.1620	0.1355	0.2460
Lognormal	17348500	0.0739	0.1580	0.2033	0.1875
Normal	1738990 (Mean/Location)	1282500 (Scale/S.D)	0.1463	0.1823	0.1853
Gamma	82958	210	0.2125	0.3250	0.2750
Generalized Exponential	9.18881×10^{-7}	5037390	0.2042	0.3178	0.2664
Ultimate Stress (σ_{ult})					
Weibull	261509	23.9464	0.2418	0.3903	0.5071
Lognormal	255508	0.048619	0.2119	0.406	0.4535
Normal	255780 (Mean/Location)	12470.9 (Scale/S.D)	0.216	0.4017	0.4559
Gamma	545.189	469.159	0.2242	0.1005	0.5343
Generalized Exponential	1.02×10^{-4}	1.09×10^{11}	0.2153	0.4836	0.5121

Table 5-3. Maximum Likelihood Criterion Results - Kevlar® 49-Swath (E).

Sample	The best distribution based on Maximum Likelihood Criterion									
	N/ LN	N/ WE	N/ GE	N/ G	LN/ WE	LN/ GE	LN/ G	WE/ GE	WE/ G	GE/ G
E	LN	WE	GE	-	WE	-	LN	GE	-	-
σ_{ult}	LN	WE	GE	-	WE	-	LN	GE	-	-

The PDF and CDF of all the distributions are shown in Figure 5-1 through Figure 5-4. From the results, it is clear that the normal distribution best fits the data (E & σ_{ult}).

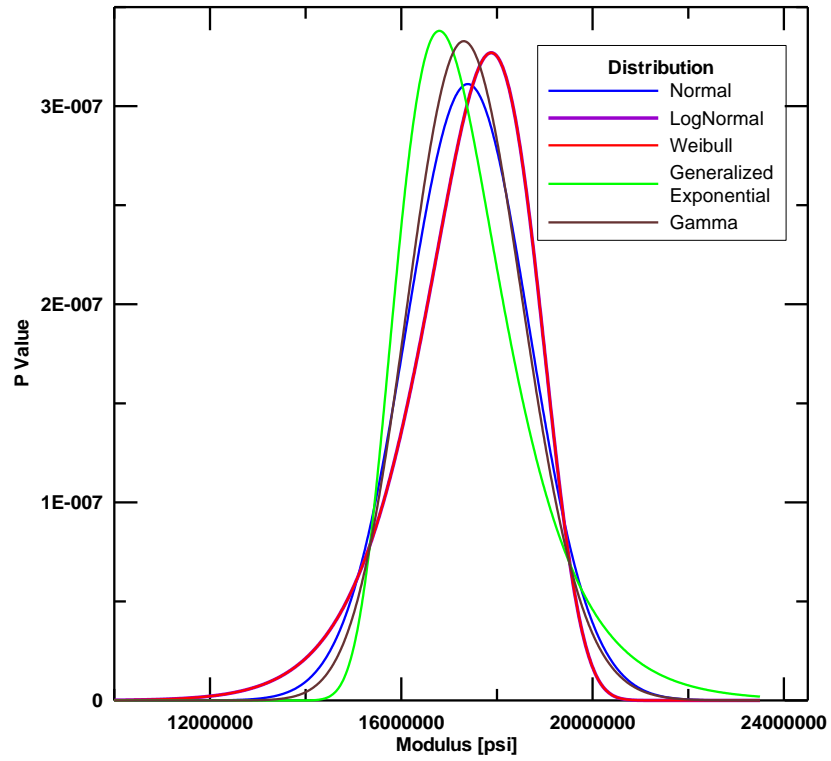


Figure 5-1. PDF for Kevlar® 49-swath (E)

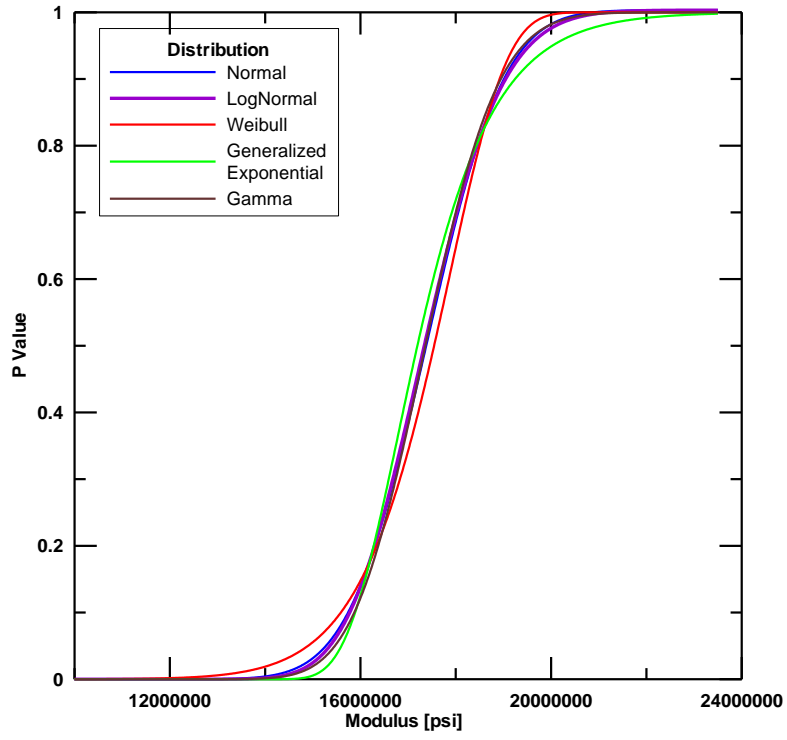


Figure 5-2. CDF for Kevlar® 49-swath (E)

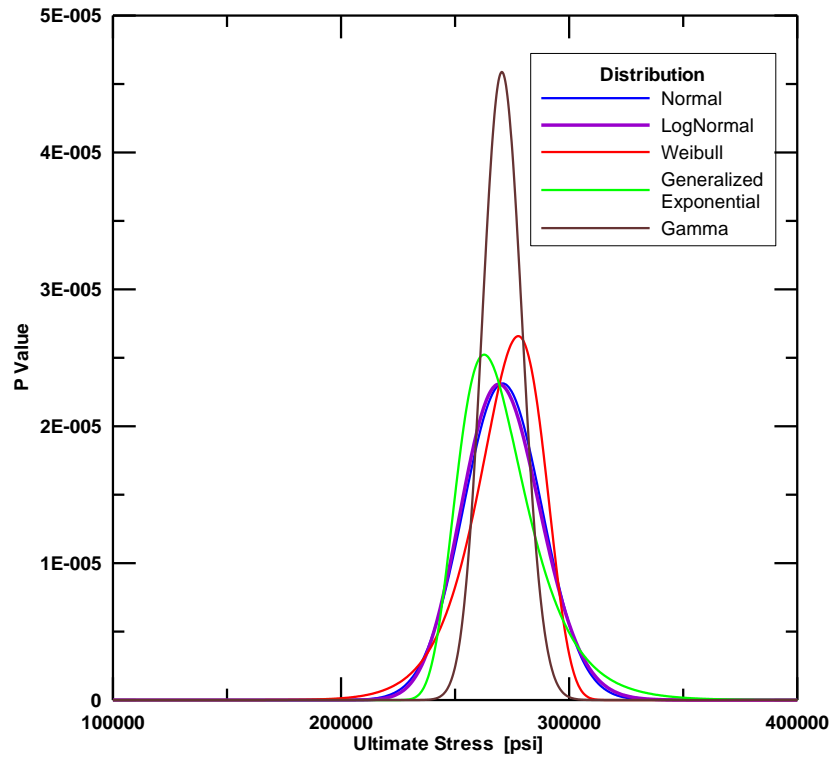


Figure 5-3. PDF for Kevlar® 49-swath (σ_{ult})

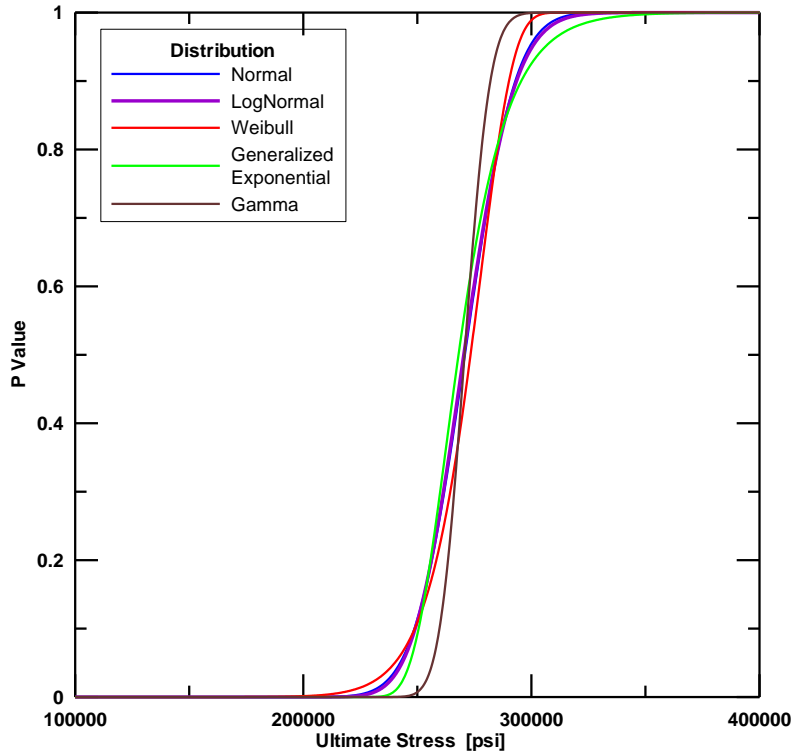


Figure 5-4. CDF for Kevlar® 49-swath (σ_{ult})

Yarn Data

Experimental data of Young's modulus (E) and Ultimate Stress (σ_{ult}) from (Table 3-7) are considered for the analysis and the results are presented in Table 5-4 and Table 5-5.

Table 5-4. Results Using EDP Software- Kevlar® 49-Yarn (E).

Distribution	Parameter		Goodness of fit test		
	Scale [psi]	Shape	K-S Distance	Chi-Square	AD
Young's modulus (E)					
Weibull	9800430	21.7858	0.1351	0.0484	0.1849
Lognormal	9563340	0.0519866	0.0993	0.0977	0.0995
Normal	9574960 (Mean/Location)	497060 (Scale/S.D)	0.0936	0.0995	0.0859
Gamma	23262.1	411.611	0.0874	0.0416	0.1087
Generalized Exponential	2.26×10^{-6}	1.48×10^9	0.1386	0.1942	0.1882

Ultimate Stress (σ_{ult})					
Weibull	261509	23.9464	0.2418	0.3903	0.5071
Lognormal	255508	0.048619	0.2119	0.4060	0.4535
Normal	255780 (Mean/Location)	12470.9 (Scale/S.D)	0.2160	0.4017	0.4559
Gamma	545.189	469.159	0.2242	0.1005	0.5343
Generalized Exponential	1.02×10^{-4}	1.09×10^{11}	0.2153	0.4836	0.5121

Table 5-5. Maximum Likelihood Criterion Results - Kevlar® 49-Yarn (E).

Sample	The best distribution based on Maximum likelihood criterion									
	N/ LN	N/ WE	N/ GE	N/ G	LN/ WE	LN/ GE	LN/ G	WE/ GE	WE/ G	GE/ G
E	LN	WE	GE	-	WE	GE	-	GE	-	-
σ_{ult}	LN	WE	GE	-	WE	GE	-	GE	-	-

The PDF and CDF of all the distributions are shown in Figure 5-5 through Figure 5-8. From the results, it is clear that the gamma distribution best fits E and normal distribution best fits σ_{ult} .

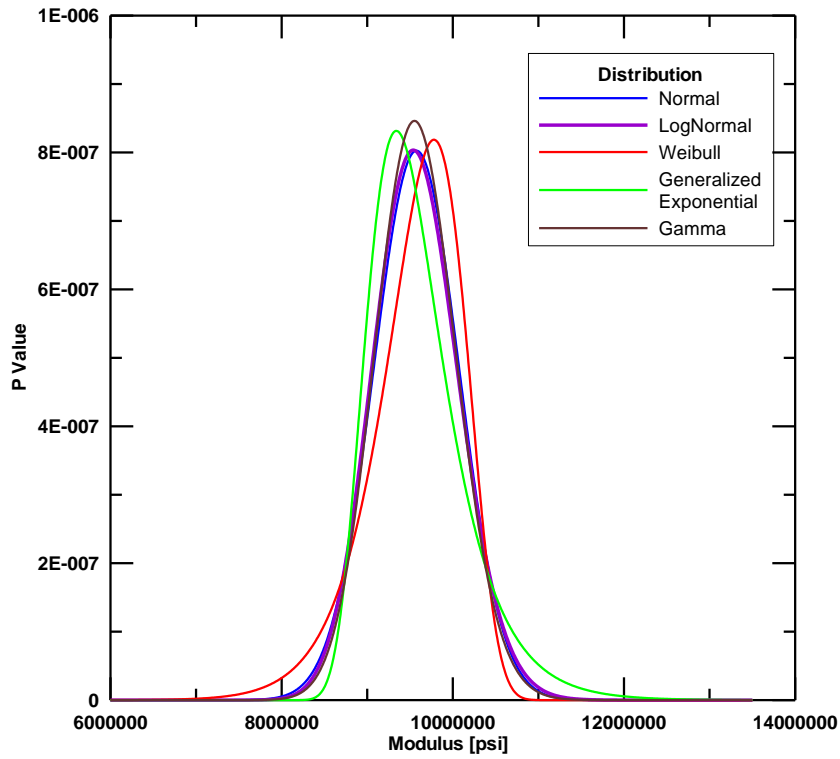


Figure 5-5. PDF for Kevlar® 49-yarn (E)

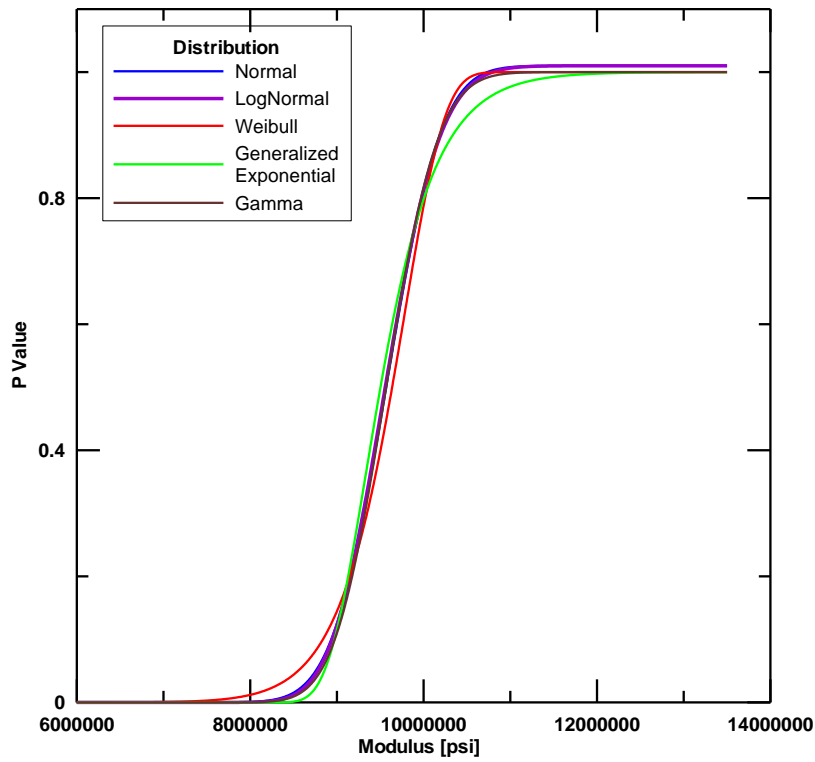


Figure 5-6. CDF for Kevlar® 49-yarn (E)

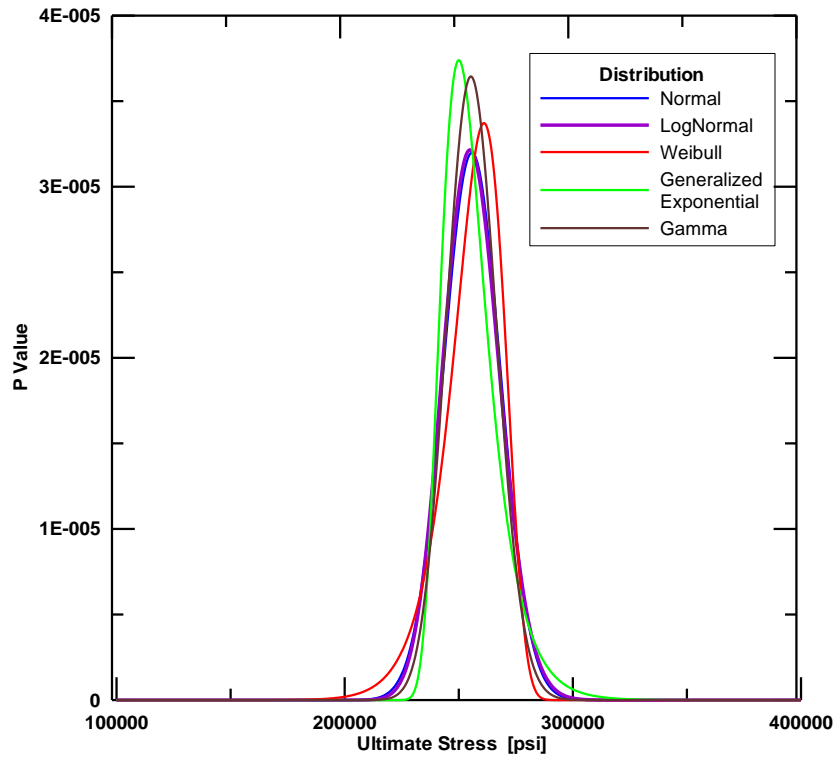


Figure 5-7. PDF for Kevlar® 49-yarn (σ_{ult})

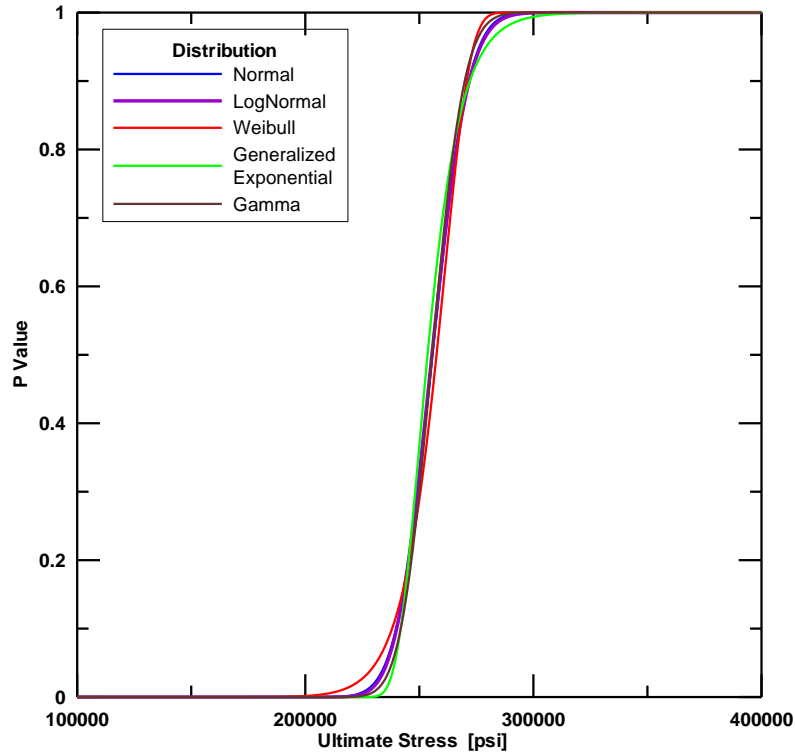


Figure 5-8. CDF for Kevlar® 49-yarn (σ_{ult})

Test Case III

Young's modulus as random variable in both the swath and yarn data are explained in this section. The test mainly focuses on comparing the different types of Weibull distributions with the other distributions. Results of parameters associated with each distribution and test statistics are provided below and the best fit solution/method is highlighted. The results (see Table 5-6) provide all the goodness of fit tests values and the distribution with the least value is the best fitted distribution for the data. The function value corresponds to the value of minimizing function at the optimum value of obtained parameters. The optimized parameters are computed by using a population-based on an optimization algorithm called Differential Evolution [42].

Table 5-6. Results of Data Analysis Using EDP.

Distribution	Method	Parameter		Goodness of fit test			Function Value
		Scale [psi]	Shape	K-S Distance	Chi-Square	AD	
Swath - E							
Weibull-2P	M-1	17953600	15.9246	0.162	0.1355	0.246	0
	M-2	17948400	14.1577	0.1428	0.0687	0.2188	0
Weibull-3P	M-1	44740000	40.0099	0.1690	0.1025	0.2606	1.53 x10 ⁻⁸
	M-2	47069800	39.8974	0.1669	0.0824	0.2435	1.18 x10 ⁻⁵
Lognormal	NA	17348500	0.0739	0.1580	0.0954	0.1875	NA
Normal	NA	1738990	1282500	0.1463	0.0954	0.1853	NA
		(Mean/Location)	(Scale/S.D)				
Gamma	NA	93303.3	209.623	0.2125	0.3250	0.275	NA
Generalized Exponential	NA	9.19 x10 ⁻⁷	5037390	0.2042	0.1085	0.2664	4.30 x10 ⁻¹³
Yarn – E							-
Weibull-2P	M-1	9800430	21.7858	0.1351	0.0484	0.1849	0
	M-2	9798770	19.9279	0.1205	0.0586	0.1812	0
Weibull-3P	M-1	18853700	42.0637	0.1392	0.0485	0.1985	1.83 x10 ⁻⁸
	M-2	19604500	41.9678	0.1380	0.0554	0.1974	7.03 x10 ⁻⁶
Lognormal	NA	9563340	0.0519866	0.0993	0.0977	0.0995	NA
Normal	NA	9574960	497060	0.0936	0.0859	0.0995	NA
		(Mean/Location)	(Scale/S.D)				
Gamma	NA	25585.5	411.611	0.0874	0.0416	0.1087	NA
Generalized Exponential	NA	2.26 x10 ⁻⁶	1.48 x10 ⁹	0.1386	0.1942	0.1882	1.28 x10 ⁻⁹

* M-1 - Two Step Iterative MLE – No Weights

* M-2 - Two Step Iterative MLE –Weighted

Goodness of fit tests explained was used to validate the model for the chosen variable. For the swath data, Weibull 2-parameter (weighted) distribution

is found to best fit the data. And in the yarn data, still the gamma distribution is the best fit. And moreover the weighted iteration method of the Weibull 2-parameter model shows even much better results as opposed to the two-step iteration method of the Weibull 2-parameter model (without weights).

5.1.2 Monte Carlo Simulations

Probabilistic analysis is implemented in the finite element models using MCS. Some of the test cases with the MCS are provided here. Before running the test cases, the random number generated for a single random variable is verified by running a sample test case. The CDF plot for the model was generated and is shown in Figure 5-9. The distribution shows that the random number generator is satisfactory.

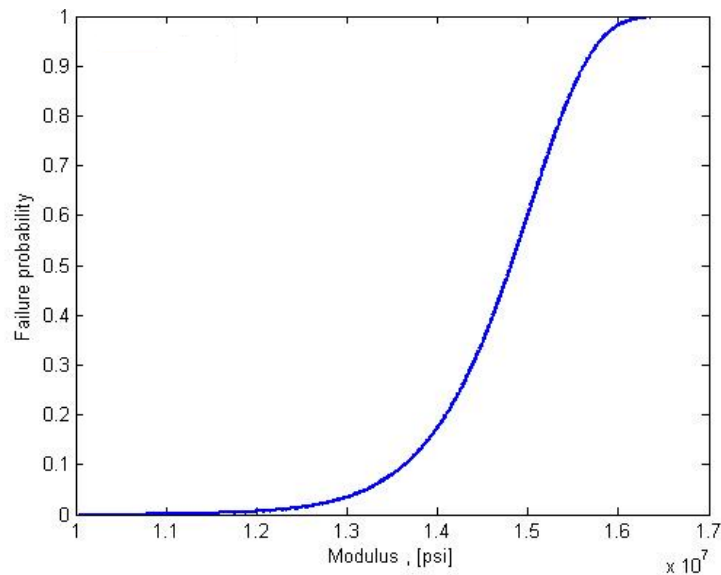


Figure 5-9. CDF plot for probabilistic analysis

Test Case I

This case is to validate the probabilistic analysis implementation in the UMAT subroutine. Some simple checks were performed to validate the model.

The probabilistic analysis is carried out on one model - LG612 [7] that were arbitrarily selected.

Several analyses are carried out to understand the differences between deterministic and probabilistic analyses - (a) all the fabric elements have the lowest E value, (b) all the fabric elements have the highest E value, and (c) finally the E values are as per Weibull distribution. The results are shown in Table 5-7.

Table 5-7. Test Case I Results.

Model (LG612)	Exit Velocity (ft/s)
Low E value	877.8
High E value	701.3
Deterministic	773.4
Probabilistic	737.2
Experimental	822.7

The trends in the results are as expected. However, a more detailed study is needed to develop a methodology for design of containment systems using probabilistic analysis. In the same way, probabilistic nature of the other material parameters such as crimp strain (warp & fill direction), strain at ultimate stress (warp & fill direction) and stress at post peak region are also implemented in the Engine containment model.

Test Case II

LG964 model [7] is considered for the further analysis involving MCS. The LG964 model, because the FE simulation results of this model closely match

with the experimental results and projectile is also contained in this model, so there is no penetration of the model through any layer. Since the difference in the experimental and simulation results is very minor, we expect to see a similar kind of behavior/results using MCS. Different sets of simulations are run and the probability of failure is calculated based on the number of failures over total number of simulations. For each simulation, FE analysis is done in which each shell element is assigned an individual modulus value based on the random number generated. Different simulations are performed by changing the seed value; both the positive and negative seed values are considered. Results for the different sets of simulations are given in Table 5-8. If the projectile exits the fabric, then it is counted as a failure.

Table 5-8. Simulations vs. Probability of failure.

Number of Simulations	Probability of Failure
20	0.0
30	0.0
40	0.0
50	0.0

In all MCS, the projectile is contained and there is no penetration of projectile seen through any layer. This shows that the simulation of LG964 under probabilistic modeling closely matches with the experimental and FE simulation (without probabilistic data) provided the given set of loading conditions, initial projectile orientations, number of fabric layers around the fabric, boundary conditions, initial rigid body acceleration are unaltered when modeling with

Young's modulus (E) as random variable using Weibull 2-parameter distribution.

Test Case III

A small scale impact problem is considered to see the individual and combined effect of material parameters when used as random variable, before actually being implemented in the engine containment model. The impact problem is based on the material model and projectile model as described in the Chapter 4. The schematic diagram of the model (Flat_Impact) and other details are explained below in Figure 5-10 and Table 5-9.

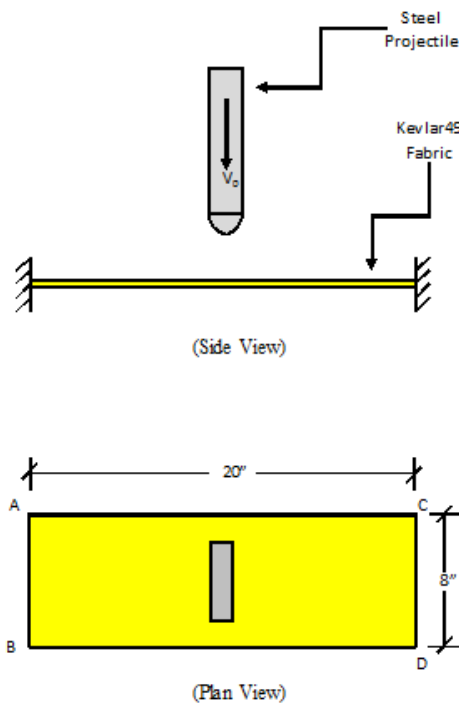


Figure 5-10. Schematic diagram of the FE model

Table 5-9. Flat_Impact Model Description.

FEA Model Information	
Nodes	3421
Solid elements	629

Solid materials	1
Parts	3
Number of shell layers	1
Fabric layers per shell	1
Fabric material	*MAT_USER_DEFINED_MODELS (ASU v 1.3)
Projectile mass (g)	317.8
Initial velocity (in/ms)	2.225
Initial kinetic energy (J)	507.5
Contact damping	2
Partial damping (Fabric only)	10.0
Unit system	in (length), ms (time), lbf (force), msi (stress), lbf-in (energy)

Boundary Conditions: The fabric is completely fixed in all six degrees of freedom along sides A-B and C-D.

Material Card: The material properties used in the analysis are given in the *Table 4-1*.

The material parameters such as Young's modulus, crimp strain, strain at ultimate stress and stress at post peak region are obtained from the experimental data [51]. The appropriate distribution model for the parameters and the corresponding data are explained in *Table 5-10*. The parameters and the corresponding probabilistic models are given below

Table 5-10. Parameters and Distribution Models.

Parameter	Probabilistic Model
Young's Modulus	Weibull 2-parameter
Crimp Strain	Weibull 2-parameter
Strain at Ultimate Stress	Weibull 2-parameter
Stress at Post-Peak Region	Normal

Probabilistic distribution models of all the parameters are provided below

Young's Modulus

$$F(E) = 1 - \exp \left[- \left(\frac{E}{E_0} \right)^m \right] = 1 - \exp \left[- \left(\frac{E_{FE}}{4.726} \right)^{45.906} \right] \quad (5.1.3)$$

Crimp Strain

$$F(\varepsilon_{11}^{crp}) = 1 - \exp \left[- \left(\frac{\varepsilon_{11}^{crp}}{\varepsilon_{11}^{crp} 0} \right)^m \right] = 1 - \exp \left[- \left(\frac{\varepsilon_{11}^{crp}}{0.0089} \right)^{5.407} \right] \quad (5.1.4)$$

$$F(\varepsilon_{22}^{crp}) = 1 - \exp \left[- \left(\frac{\varepsilon_{22}^{crp}}{\varepsilon_{22}^{crp} 0} \right)^m \right] = 1 - \exp \left[- \left(\frac{\varepsilon_{22}^{crp}}{0.0029} \right)^{2.320} \right] \quad (5.1.5)$$

Strain at Ultimate Stress

$$F(\varepsilon_{11}^{\max}) = 1 - \exp \left[- \left(\frac{\varepsilon_{11}^{\max}}{\varepsilon_{11}^{\max} 0} \right)^m \right] = 1 - \exp \left[- \left(\frac{\varepsilon_{11}^{\max}}{0.0228} \right)^{18.7019} \right] \quad (5.1.6)$$

$$F(\varepsilon_{22}^{\max}) = 1 - \exp \left[- \left(\frac{\varepsilon_{22}^{\max}}{\varepsilon_{22}^{\max} 0} \right)^m \right] = 1 - \exp \left[- \left(\frac{\varepsilon_{22}^{\max}}{0.02056} \right)^{21.749} \right] \quad (5.1.7)$$

Stress at Post-Peak Linear Region

$$F(\sigma^*) = \frac{1}{\sqrt{(2\pi)}\sigma_0} \int_0^x \exp \left(- \frac{(\sigma_{FE}^* - \mu)^2}{2\sigma^2} \right) dx \quad (5.1.8)$$

$$F(\sigma^*) = \frac{1}{\sqrt{(2\pi)}0.00045} \int_0^x \exp \left(- \frac{(\sigma_{FE}^* - 0.00956)^2}{2(0.00045)^2} \right) dx \quad (5.1.9)$$

where m is the shape parameter and X_0 is the scale parameter (X corresponds to the random variable). Results for the different sets of simulations are given in Table 5-10. If the projectile exits the fabric, then it is counted as a failure. The number of Monte Carlo simulations is 50 and the exit velocity from the deterministic analysis is 69.6 ft/s.

Table 5-11. Simulation Results of Flat Impact Model.

Probabilistic Parameter	Probability of	Lowest Exit	Highest Exit
-------------------------	----------------	-------------	--------------

	Failure	Velocity (ft/s)	Velocity (ft/s)
<i>Young's Modulus</i>	0.84	10.9	123.1
<i>Crimp Strain</i>	0.74	32.5	122.7
<i>Strain at Ultimate Stress</i>	1.0	61.7	131.6
<i>Stress at Post-Peak Linear Region</i>	0.98	81	101.36
<i>All</i>	0.74	57.8	138.6

The table provide the individual effect of probabilistic parameter and the total effect of the all the parameters. The probabilistic failure is greater than 0.7 in each case showing greater chances of failure. As opposed to deterministic analysis, the probabilistic analysis gives the range of exit velocities along with the probability of failure. The range of exit velocities is huge in all the cases and hence all the parameters are implemented in the engine containment analysis.

Test Case IV

Based on the previous analysis on individual effect of parameters on the model, two LGXXX models are considered from the engine containment system for the further analysis with one showing close resemblance with the NASA experimental data and the other which shows greater deviation from the NASA experimental data in terms of absorbed energy. The two models are LG594 and LG620 and their exit velocity from the deterministic analysis are 484.5 and 580.8 ft/s respectively. Results from MCS are provided in Table 5-12.

Table 5-12. Simulation Results of Engine Containment Models.

Probabilistic Parameter	Probability of Failure	Lowest Exit Velocity (ft/s)	Highest Exit Velocity (ft/s)
<i>LG594</i>	1.0	186.9	715.0
<i>LG620</i>	1.0	503.3	779.4

The following graph (see Figure 5-11 and Figure 5-12) provides the clear view on the exit velocity from probabilistic analysis, deterministic analysis and NASA experimental data. In both the cases, the deterministic analysis under predict the results. The probabilistic analysis provides the range of exit velocity in which the deterministic and probabilistic analysis results fall.

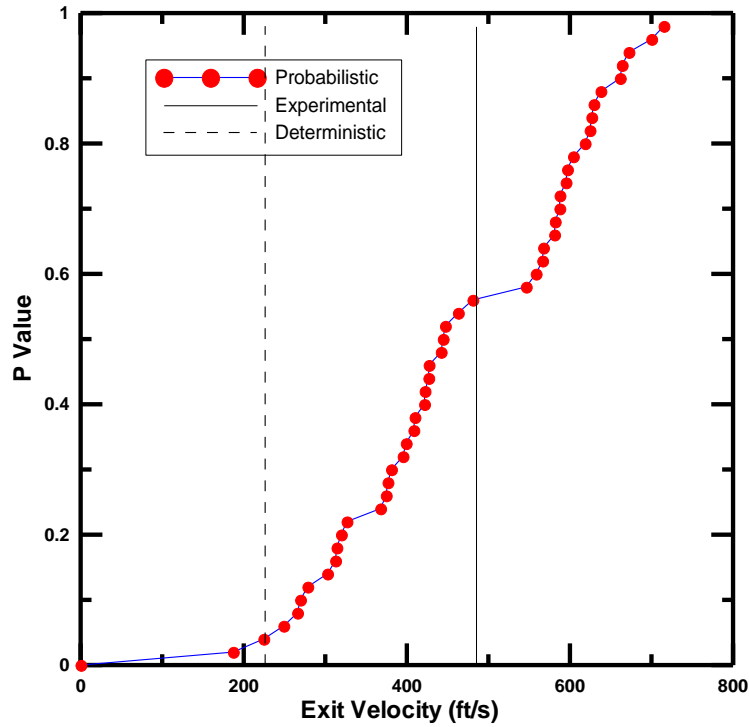


Figure 5-11. CDF plot of exit velocity for LG594

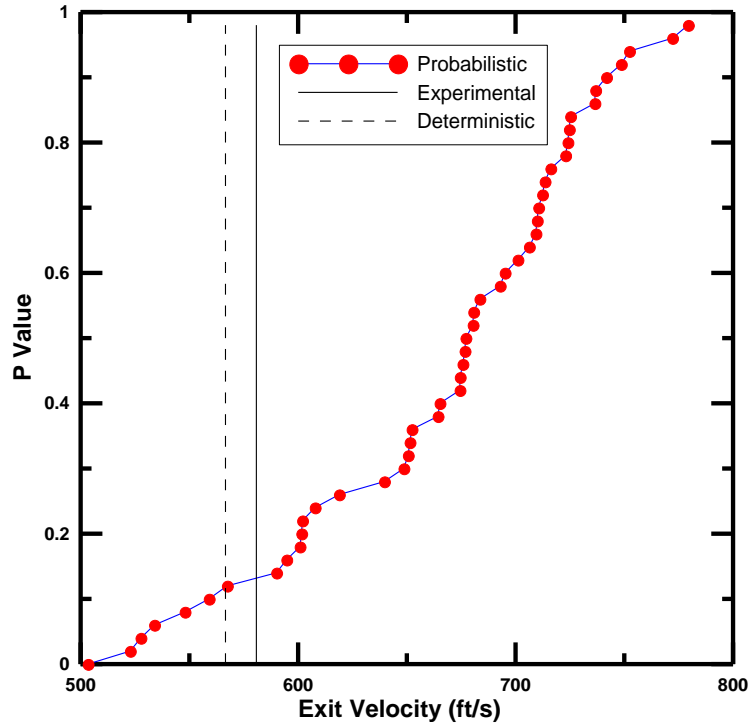


Figure 5-12. CDF plot of exit velocity for LG620

5.2 Truss Designs

A computer program FEAT-EDO is developed using C++ in which reliability algorithm is coupled with finite element analysis and Engineering Design Optimization (EDO) [49] library. The EDO library has a number of numerical optimization techniques for solving nonlinear programming problems (NLP) - method of feasible directions (MFD), genetic algorithm (GA) and differential evolution (DE).

Reliability Analysis using FORM and SORM

Reliability analysis is carried out using FORM, SORM and MCS (1000 simulations) methods. Planar truss problems are solved to study and illustrate the use of FORM and SORM techniques in finite element-based engineering designs. For each problem, the problem formulation (design variables, constraints, FE

model, random variables) is explained. Once the problem is solved, the final values, reliability and probability of failure of the each constraint and for the system are listed. Series failure of system is considered in which the system is considered as failed if any one of the constraints is not satisfied. Only the normal distribution of variables is considered for each problem. Reliability analysis is performed on the DO results by varying the random variable's standard deviation value represented as a percentage of the mean value (such as 2%, 5%, 10% & 15%). Finally, probability of failure versus standard deviation is plotted. The number of random variables range from 8-12 and type of random variables used are load, allowable/yield tensile stress, allowable/yield compressive stress, and Young's modulus with response function as maximum member stress and nodal displacements.

Problem Formulation for Design Optimization

$$\begin{aligned}
 &\text{Find } \mathbf{x}=\{A\} \\
 &\text{to minimize } f(\mathbf{x})=\text{Volume} \\
 &\text{Subject to } \sigma_i^t < \sigma_a^t \\
 &\qquad\qquad\qquad \sigma_i^c < \sigma_a^c \\
 &\qquad\qquad\qquad \delta_k < \delta^a \\
 &i = 1, \dots, \text{members} \\
 &k = \text{DOF at node } k
 \end{aligned}
 \tag{5.2.1}$$

where A is the area of the member, σ_a^c, σ_a^t are the allowable compressive and tensile stresses, δ^a is allowable deflection at a particular node.

Test Problem 1: 2-Bar Truss [52] (Units: in, lb)

For this problem (Figure 5-13) material properties of steel (0.2% C HR, A36 Steel) are used. Material & load data (Table 5-13), problem formulation (Eqn.(5.2.2)) and results (Table 5-14 & Figure 5-14) of this problem are given below.

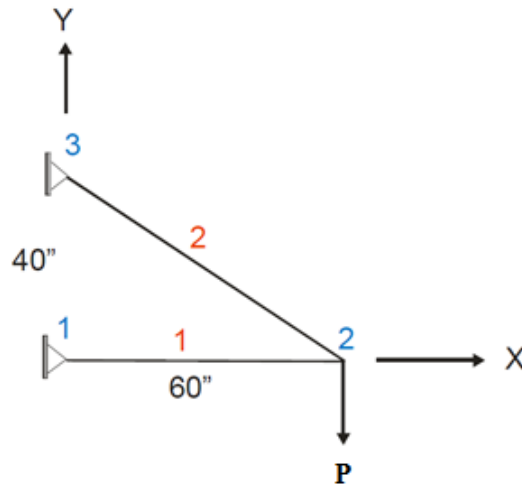


Figure 5-13. 2-bar truss FE model

Table 5-13. 2-Bar Truss Problem Data.

Property	Value
E_1, E_2	30×10^6
$\sigma_y^{t1}, \sigma_y^{t2}$	36300
$\sigma_y^{c1}, \sigma_y^{c2}$	36300
δ_a	0.05
P	10000

$$\begin{aligned}
&\text{Find } \mathbf{x} = \{A_1, A_2\} \\
&\mathbf{X} = \{\sigma_y^{c1}, \sigma_y^{t1}, \sigma_y^{c2}, \sigma_y^{t2}, E_1, E_2, P\} \\
&\text{to minimize } f(\mathbf{x}) = \text{Volume} \\
&\text{subject to } \sigma_i^t < \sigma_y^t \text{ for } i=1,2 \\
&\sigma_i^c < \sigma_y^c \text{ for } i=1,2 \\
&\delta_i < \delta_a \text{ for } i=1,2 \text{ at node 2}
\end{aligned} \tag{5.2.2}$$

Results of the design optimization are as follows:

$$\begin{aligned}
\mathbf{A} &= \{2.208, 2.640\} \text{ in}^2 \\
\text{Volume} &= 322.842 \text{ in}^3 \\
\text{Active Constraint} &: y\text{-displacement constraint at node 2}
\end{aligned} \tag{5.2.3}$$

These optimized values are then used with FORM, SORM and MCS to find the reliability and probability of failure of each constraint.

Table 5-14. 2-Bar Truss Results ($\sigma_x = 5\%$).

Constraint Information	Reliability Index			Probability of Failure		
	FORM	SORM	MCS	FORM	SORM	MCS
Stress in element 1	5.0	5.0	5.0	0	0	0
Stress in element 2	5.0	5.0	5.0	0	0	0
X-Displacement at node 2	5.0	5.0	5.0	0	0	0
Y-Displacement at node 2	0.0087	0.01055	-0.0569	0.4965	0.4957	0.5051

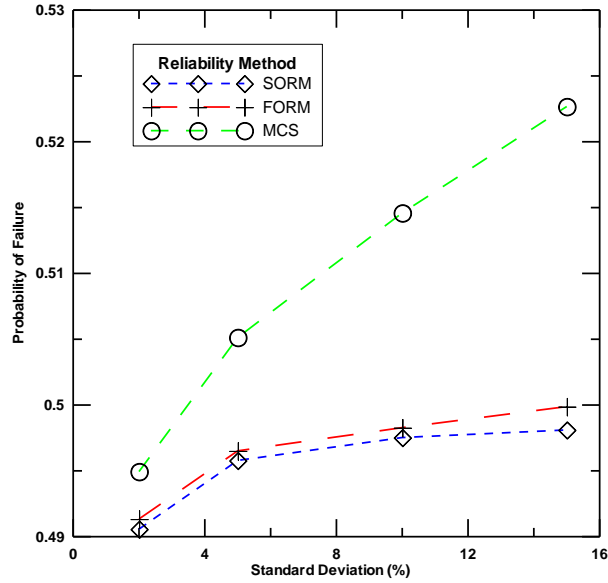


Figure 5-14. Probability of failure vs. σ_x (% of mean)-2-bar truss

From Table 5-14 it can be seen that all the constraints except the y-displacement constraint (critical constraint) at node 2 have high reliability values and less probability of failure. And also difference in results (probability of failure) between FORM and SORM is negligible whereas the difference is huge when the comparison is made between FORM and MCS or SORM and MCS. The Figure 5-14 plots the probability of failure value for the critical constraint versus the standard deviation. Difference in results (probability of failure) computed by MCS and FORM/SORM increases as the standard deviation increases.

Test Problem 2: 6-Bar Truss [42] (Units: in, lb)

For this problem (Figure 5-15) material properties of aluminum are used. Material & load data (Table 5-15), problem formulation (Eqn.(5.2.4)) and results (Table 5-16 & Figure 5-16) of this problem are given below.

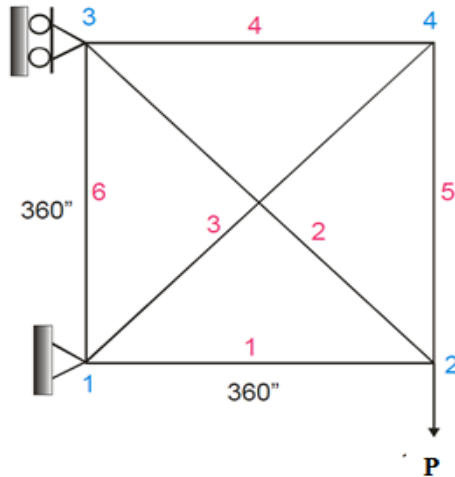


Figure 5-15. 6-bar truss FE model

Table 5-15. 6 Bar-Truss Problem Data.

Property	Value
E	10×10^6
σ_y^t, σ_y^c	21000
P	21000

Find $\mathbf{x} = \{A_1, A_2, A_3, A_4, A_5, A_6\}$

$\mathbf{X} = \{\sigma_y^c, \sigma_y^t, E, P\}$

to minimize $f(\mathbf{x}) = \text{Volume}$

subject to $\sigma_i^t < \sigma_y^t$ for $i=1, \dots, 6$

$\sigma_i^c < \sigma_y^c$ for $i=1, \dots, 6$

$\delta_i < 0.005$ for $i=1, 2$ at node 2

(5.2.4)

Results of the design optimization are as follows:

$$\mathbf{A} = \{3.934, 5.569, 7.057, 4.993, 0.0108, 3.938\} \text{in}^2$$

$$\text{Volume} = 11854.3 \text{in}^3$$

Active Constraint : Stress constraint in element 2

y-displacement constraint at node 2

(5.2.5)

The optimized values are then used with FORM, SORM and MCS to find the reliability value and probability of failure of each constraint.

Table 5-16. 6-Bar Truss Results ($\sigma_x = 5\%$).

Constraint Information	Reliability Index			Probability of Failure		
	FORM	SORM	MCS	FORM	SORM	MCS
Stress in element 1 to 4 & 6	5.0	5.0	5.0	0	0	0
Stress in element 5	0.0213	0.0233	0.0212	0.4915	0.4907	0.4915
X-Displacement at node 2	5.0	5.0	5.0	0	0	0
Y-Displacement at node 2	0.2490	0.2508	0.2464	0.4017	0.4010	0.4027

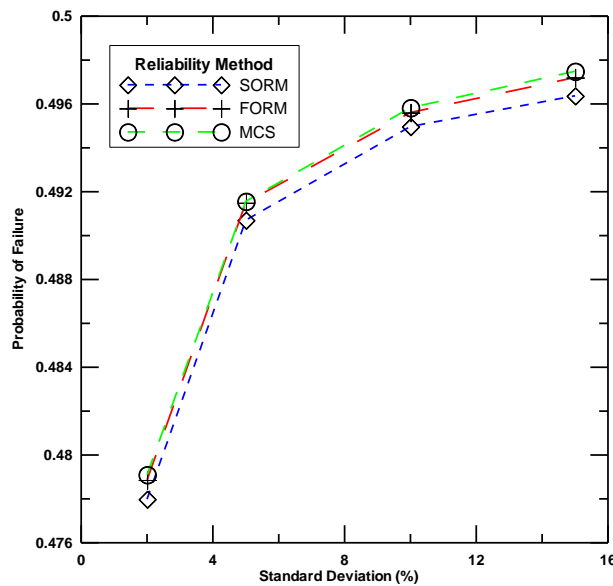


Figure 5-16. Probability of failure vs. σ_x (% of mean) - 6-bar truss

Discussion:

From Table 5-16 it can be seen that all the constraints except the displacement constraint at node 2 and stress constraint in element 5 (which are critical constraints) have high reliability values and less probability of failure. Difference

in results (reliability value/probability of failure) between FORM/SORM and MCS is negligible. The Figure 5-16 plots the probability of failure value for the critical constraint versus the standard deviation.

Test Problem 3: 31-Bar Truss [42] (Units: N, m)

Material & load data (Table 5-17), problem formulation (Eqn.(5.2.6)) & element data (Eqn.(5.2.7)) and results (Table 5-18 & Figure 5-18) of this problem (Figure 5-17) are given below.

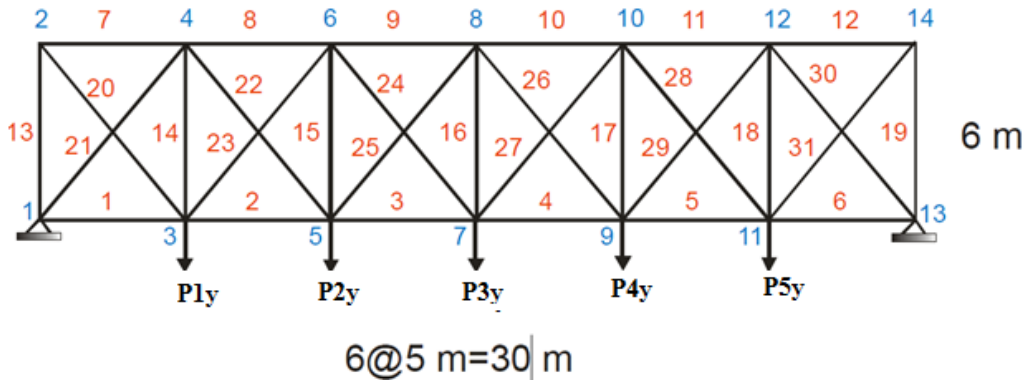


Figure 5-17. 31-bar truss FE model

Find $\mathbf{x} = \{A_1, A_2, A_3, A_4\}$
 $\mathbf{X} = \{\sigma_a^c, \sigma_a^t, E, P\}$
to minimize $f(\mathbf{x}) = \text{Volume}$ (5.2.6)
subject to $\sigma_i^t < \sigma_a^t$ for $i=1, \dots, 31$
 $\sigma_i^c < \sigma_a^c$ for $i=1, \dots, 31$

A_1 – Element 1 to 6
 A_2 – Element 7 to 12
 A_3 – Element 13 to 19
 A_4 – Element 20 to 31

(5.2.7)

Table 5-17. 31-Bar Truss Problem Data.

Property	Value
E	20×10^6
σ_y^t, σ_y^c	2.502×10^8
P	100000

Results of the design optimization are as follows:

$$\mathbf{A} = \{2.942, 10.663, 2.227, 6.489\} \text{ in}^2$$

$$\text{Volume} = 1112.09 \text{ in}^3 \quad (5.2.8)$$

Active Constraint = Stress constraint in element 1,6,8,9,10,11,13,19,21 & 30

These values are then used with FORM, SORM and MCS to find the reliability value and probability of failure of each constraint.

Table 5-18. 31 Bar Truss Results ($\sigma_x = 5\%$).

Constraint Information	Reliability Index			Probability of Failure		
	FORM	SORM	MCS	FORM	SORM	MCS
Stress in element 1 & 6	0.0568	0.0589	0.0593	0.4774	0.4765	0.4764
Stress in element 2 to 5	5.0	5.0	5.0	0	0	0
Stress in element 7	5.0	5.0	5.0	0	0	0
Stress in element 8 & 11	3.910	3.920	3.808	0	0	0
Stress in element 9 & 10	0.112	0.114	0.115	0.4554	0.4558	0.4542
Stress in element 12	5.0	5.0	5.0	0	0	0
Stress in element 13 & 19	0.098	0.099	0.102	0.4610	0.4606	0.4593
Stress in element 14 to 18	5.0	5.0	5.0	0	0	0
Stress in element 21 & 30	0.146	0.148	0.148	0.4420	0.4412	0.4412
Remaining	5.0	5.0	5.0	0	0	0

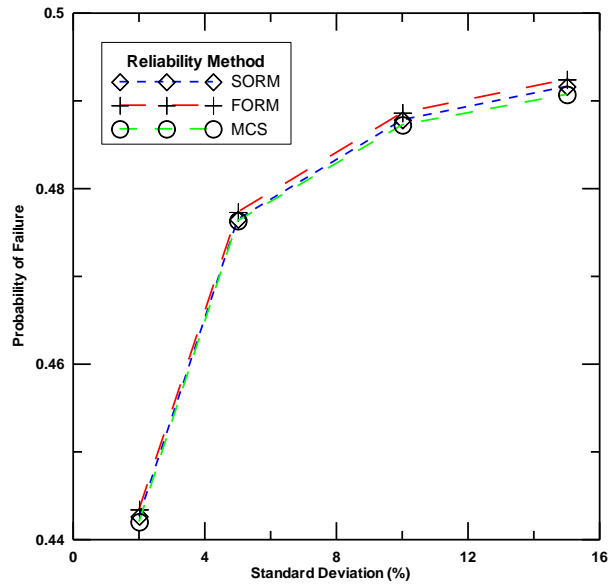


Figure 5-18. Probability of failure vs. σ_x (% of mean) - 31-bar truss

Discussion:

The Figure 5-14, Figure 5-16 and Figure 5-18 give a good view on probability of failure versus index versus S.D (% of mean). The probability of failure increases when the standard deviation increases and this result is reverse when we look in terms of reliability index which decreases when the standard deviation increases. Similar results from the all the methods show that, in all the above problems FORM method works well. The FORM method is preferred over the other two methods due to the following observations a) the drawback of SORM method is that, the method requires lot of function evaluations/computational time in finding the curvature associated with second order approximation b) accuracy of MCS depends on the number of simulations, so the simulation time increases when the random variables and the constraints in the problem increases. From the results (Figure 5-14 - Figure 5-18), we can see

that difference in results (reliability (or) probability of failure) using FORM, SORM and MCS is negligible. So, the FORM method is preferred over the other two methods as there is less number of computational time and function evaluations.

Reliability Based Design Optimization

Example problems involving implementation of the RBDO method as explained in Section 2.7 are illustrated here. RBDO is implemented and tested with (a) truss problems [26] involving linear and nonlinear constraints with normal variables and (b) beam problem [53] involving nonlinear constraints with non-normal variables such as Weibull and lognormal.

Test Problem 4: Cantilever Beam Problem (Units: lb, in)

The cantilever beam (see Figure 5-19) subjected to fatigue loading is discussed here. The problem deals with non-linear constraints, non-normal variables and multi-constraints. Results obtained from the developed algorithm are compared with publicly available results [53].

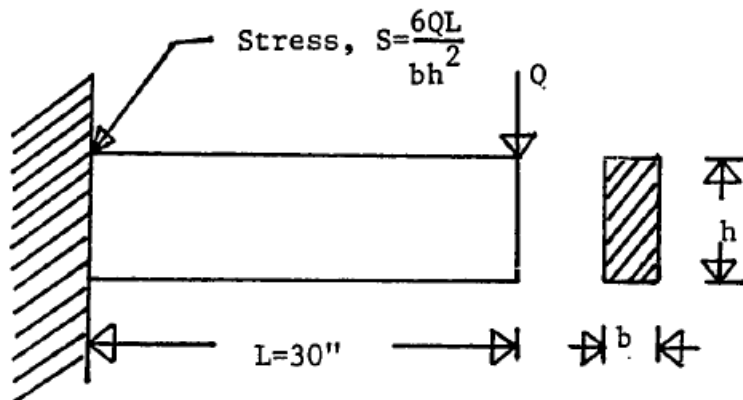


Figure 5-19. Cantilever beam problem [53].

The beam is subjected to a fatigue loading. The problem is to minimize the weight of the structure subjected to maximum stress constraint, fatigue failure and plate buckling. The problem formulation and the random variables associated with the problem are provided below. Random variables are described by their mean and coefficient of variation (COV).

$$\begin{aligned}
 &\text{Find} && \mathbf{x}=(b,h) \\
 &\text{to minimize} && f(\mathbf{x})=\gamma bhl \\
 &\text{subject to} && g_1 \text{ to } g_2 && (5.2.9) \\
 &&& 0.1 \leq b \leq 15 \\
 &&& 0.1 \leq h \leq 15
 \end{aligned}$$

$$g_1 \equiv R - \frac{6Ql}{bh^2} \leq 0 \text{ (Stress constraint)} \quad (5.2.10)$$

$$g_1 \equiv A - N_0 S_R^m \leq 0 \text{ (Fatigue failure)} \quad (5.2.11)$$

$$g_3 \equiv \frac{0.3Eb^3h}{l^2} - Q \leq 0 \text{ (Plate buckling)} \quad (5.2.12)$$

Table 5-19. Beam Problem-Random Variable Data

Random Variable	Distribution	Mean	COV	Scale	Shape
R , yield strength	Weibull	50	0.12	52.58	9.81
A, Fatigue strength coefficient	Lognormal	1.632x10 ¹⁰	0.5	-	-
E, Young's modulus	Normal	30000	0.5	-	-

A static load ($Q=0.5$ kips) is applied and considered in Eqns. (5.2.10) and (5.2.12). An oscillatory loading of 0.4kips is applied for (N_0) 2×10^6 cycles and is considered in Eqn. (5.2.11). The beam is made of ASTM A572-50 High Strength Low Steel Alloy with density of 0.3 lb/in³ and the allowable probability of failure of the structure is 3.333×10^{-4} . The DO results are {0.234393, 3.91691} in².

Results from the RBDO analysis are given below and the results show good comparison with the reference results.

Table 5-20. Beam Problem RBDO Results.

Method	Weight	{b,h}	p_f of g_1	p_f of g_2	p_f of g_3
Source [53]	11.2608	{0.2463,5.08}	2.41×10^{-6}	3.23×10^{-4}	3.51×10^{-8}
RBDO	12.067	{0.2687,4.99}	1.41×10^{-6}	9.33×10^{-5}	2.94×10^{-5}

Test Problem 4: 3-Bar Truss Problem (Units: lb, in)

The problem is shown in Figure 5-20. The design variables are the cross-sectional area of the members. The random variables are material properties (see Table 5-21) and allowable deflection. Random variables are normal and are described by their mean and coefficient of variation (COV) as given in Table 5-22.

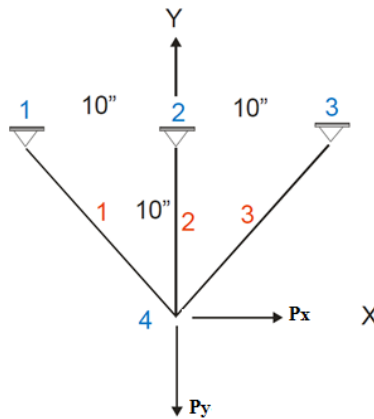


Figure 5-20. 3-bar truss FE model(RBDO)

Table 5-21. 3-Bar Truss Problem Data (RBDO).

Property	Value
E_1	10×10^6
$\sigma_y^{t1}, \sigma_y^{c1}$	5000
P_x, P_y	28284

The problem is to minimize the volume of the structure subjected to stress and displacement constraints.

$$\begin{aligned}
 &\text{Find} && \mathbf{x}=(A_1,A_2) \\
 &\text{to minimize} && f(\mathbf{x})=L(2\sqrt{2}A_1 + A_2) \\
 &\text{subject to} && g_1 \text{ to } g_5 \\
 &&& 0.1 \leq A_1 \leq 15 \\
 &&& 0.1 \leq A_2 \leq 15
 \end{aligned} \tag{5.2.13}$$

$$g_1 \equiv \frac{\sqrt{2}P_x L}{A_1 E} - 0.005 \leq 0 \tag{5.2.14}$$

$$g_2 \equiv \frac{\sqrt{2}P_y L}{(A_1 + \sqrt{2}A_2)E} - 0.005 \leq 0 \tag{5.2.15}$$

$$g_3 \equiv \frac{1}{\sqrt{2}} \left[\frac{P_x}{A_1} + \frac{P_y}{(A_1 + \sqrt{2}A_2)} \right] - \sigma_y^t \leq 0 \tag{5.2.16}$$

$$g_4 \equiv \sqrt{2} \left[\frac{P_y}{(A_1 + \sqrt{2}A_2)} \right] - \sigma_y^t \leq 0 \tag{5.2.17}$$

$$g_5 \equiv \frac{1}{\sqrt{2}} \left[-\frac{P_x}{A_1} + \frac{P_y}{(A_1 + \sqrt{2}A_2)} \right] - \sigma_y^c \leq 0 \tag{5.2.18}$$

Table 5-22. 3 Bar Truss-Random Variable Data.

Random Variable	Distribution	Mean	COV
E	Normal	1×10^7	0.05
σ_a^c, σ_a^t	Normal	5000	0.05
P_x, P_y	Normal	28284	0.05

Area of the member 1 (A_1) is assumed to be same as area of member 3 and the constraints g_1, g_2, g_3, g_4 & g_5 correspond to displacement-x, displacement-y, stress constraint-member-1, stress constraint-member-2 and stress constraint-member-3 respectively. Since the functions are provided explicitly, the number of random variables that control each constraint can be easily identified. Young's modulus doesn't have any impact on stress constraints as there is no E value associated with any of the stress constraints (see Eqn.(5.2.16) through Eqn.(5.2.18)) So load is the only random variable which is associated with all the constraints. Results from the design optimization are $\{7.999, 0.1\}$ in² with the volume as 114.12 in³ and from the FORM, SORM and MCS, reliability of the constraints corresponding to the optimized results are as provided below.

Table 5-23. 3 Bar Truss-Reliability Analysis Results.

Technique\Constraint	g_1	g_2	g_3	g_4	g_5
FORM	-0.0014	0.2476	0.1428	0.2476	>5.0
SORM	-0.0021	0.2497	0.1441	0.2497	>5.0
MCS	-0.0044	0.2460	0.1478	0.2522	>5.0

From the above reliability analysis it can be seen that, from the optimized values through design optimization doesn't provide good reliability with the all the constraints. The most critical constraint (with the least reliability) is the displacement constraint along x-direction. Reliability index value is not provided for g_5 , since the probability of failure is negligible beyond the value of 5.0. The fifth constraint is not considered any further. Results of the structures with various target reliability indices are given in Table 5-25.

Table 5-24. 3 Bar Truss-RBDO Results

Reliability Index	Design Variables	Reliability Index of Constraint			
		g_1	g_2	g_3	g_4
0.5	{8.288, 0.1}	0.5	0.739	0.709	0.739
1.5	{8.897, 0.1}	1.5	1.721	1.825	1.721
2.5	{9.557, 0.1}	2.5	2.703	2.915	2.703
3.0	{9.910, 0.1}	3	3.194	3.452	3.194

From the above results, we can clearly see the effect of random variables on the constraint for the various target reliability index values. As the target reliability index value increases the minimized values also increases and thereby making it more reliable. Since the critical constraint is g_1 , reliability index of the remaining constraints are greater than the target value. In RBDO, reliability index of the critical constraint of the structure is made more reliable by considering reliability constraints.

Test Problem 6: 6-Bar Truss Problem (Units: lb, in)

The problem is same as explained in the Figure 5-15 with the addition of random variables to the problem as given in Table 5-25.

Table 5-25. 6 Bar Truss-Random Variables Data.

Random Variable	Distribution	Mean	COV
E	Normal	1×10^7	0.05
σ_y^c, σ_y^t	Normal	21000	0.05
Load	Normal	21000	0.05

From the sensitivity analysis it was found that the stress constraint depends on the random variable allowable stress and load, and the displacement constraints depend on the Young's modulus and load. Reliability analysis results

are shown in Table 5-26 and RBDO result in Table 5-27 for only the critical constraints whose reliability index values are less than 3.5.

Table 5-26. 6 Bar Truss-Reliability Analysis Results.

Technique\Constraint	g_5	g_8
FORM	0.0023	0.0011
SORM	0.0043	0.00211
MCS	0.0016	-0.00403

The constraint g_5 and g_8 are associated with the stress constraint of member-5 and displacement along y-direction. The RBDO results of the structure is provided which follows the same kind of trend as explained in the previous problem, but the obtained reliability index is greater than the target value.

Table 5-27. 6 Bar Truss – RBDO Results

Reliability Index	Volume	Design Variables	Reliability Index of Constraint	
			g_5	g_8
DO	10594.2	{4.094, 5.809, 6.403, 4.551, 0.01, 3.504}	0.002	0.001
0.5	10786.8	{4.259, 5.591, 6.260, 4.753, 0.01, 4.182}	0.518	0.500
1.5	11252.9	{4.289, 6.022, 6.20, 4.307, 0.01, 4.736}	1.515	1.553
2.5	11788.1	{4.745, 7.042, 6.901, 3.999, 0.01, 4.272}	2.550	2.580
3.5	11959.6	{5.089, 6.802, 6.425, 4.507, 0.01, 4.909}	3.052	3.038

All the problems provide insight into the importance of RBDO in engineering designs. The problems involved nonlinear constraints and non-normal variables.

6. CONCLUSIONS AND FUTURE WORK

6.1 Conclusions

The following are the conclusions based on the current study.

1. The experimental data from the uniaxial tension tests were analyzed and modeled using available statistical models. From the results, it is clear that a majority of the data can be modeled using Weibull distributions. However, for some of the material properties, other distribution models show a better fit.
2. Reliability of the structural designs obtained using DO are computed using the FORM, SORM and MCS techniques. The results indicate that the reliability of some of the constraints are small with a high probability of failure when considering the material properties or/and load acting on the system as being random in nature.
3. From the RBDO examples involving linear and nonlinear constraints, and normal and non-normal variables, it can be seen that the optimized design variable values are different from the DO results. Typically, the objective function value increases with increase in the desired reliability.
4. MCS technique is implemented in finite element model where the experimental properties of the material are modeled as random variables and the probability of failure associated with the structure is computed.

6.2 Future Work

1. Accuracy of MCS purely depends on the number of simulations that were performed to obtain the probability of failure. So, as the simulations increases the accuracy of the method also increases. At the same time, as the simulation increases the computational time associated with it increases and thereby it becomes computationally expensive. More advanced Monte Carlo methods are available [54] in which simulations are performed by selecting the points away from the specified ball of radius. Radius is the reliability value computed by approximation methods. Sampling is done outside the circle shown in Figure 6-1 and the distribution function for the sampling is described below.

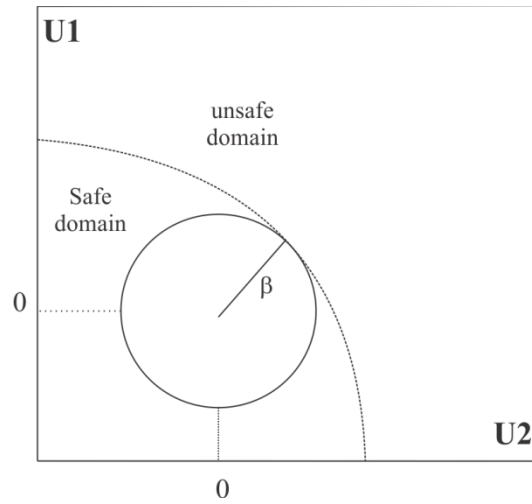


Figure 6-1. Advanced MCS method

The probability density function becomes

$$f_{tr}(U) = \begin{cases} K_{tr} f(U) & \text{if } |U| > \beta \\ 0 & \text{if } |U| \leq \beta \end{cases} \quad (6.2.1)$$

$$K_{tr} = \frac{1}{(1 - \Gamma_k(\beta^2))} \quad (6.2.2)$$

where Γ_k is the cumulative chi-square distribution with k degrees of freedom which are actually number of random variables. MCS with the above mentioned sampling distribution produces accurate results even with less number of simulations.

2. The random variables considered for the reliability analysis and RBDO study is all assumed to be independent, but practically in some cases there exist correlation among variables. Correlation is incorporated in the FORM or SORM analysis by transforming the correlated variable to uncorrelated variable [20]. The uncorrelated variable is given as

$$\mathbf{Y} = \mathbf{L}^{-1}(\mathbf{U})^T \quad (6.2.3)$$

where \mathbf{Y} is the uncorrelated variable, \mathbf{L} is the lower triangular matrix obtained from corrected correlation coefficient matrix (\mathbf{C}') which is calculated as follows

$$\mathbf{C}' = \begin{pmatrix} 1 & \rho_{X_1, X_2} & \cdots & \rho_{X_1, X_{n_{rv}}} \\ \rho_{X_2, X_1} & 1 & 0 & \rho_{X_2, X_{n_{rv}}} \\ \vdots & \vdots & \ddots & \vdots \\ \rho_{X_{n_{rv}}, X_1} & \rho_{X_{n_{rv}}, X_2} & \cdots & 1 \end{pmatrix} \quad (6.2.4)$$

where $\rho_{X_a X_b}$ is the correlation coefficient of X_a and X_b variables. So if the variables are correlated, it is first transformed to uncorrelated variable and then the usual reliability analysis procedure are carried out as explained in the sections 2.4 and 2.5. Incorporating the random variables along with correlation would give a more clear idea on behavior or response of the structure with increases in accuracy.

3. Function evaluation in reliability analysis and RBDO method involves solving finite element related simultaneous equations ($KD = F$) each time which increases the computational time if the number of iterations or populations used in optimization technique increases. Use of response surface method for handling constraint would decrease the computation time enormously. Response surface method creates a response surface (a nonlinear equation) for each of the function evaluation in a problem. Regression runs are performed with lower and upper limit of random variables to obtain the response surface. This method highly depends on the upper and lower limits assumption, so careful considerations have to be taken before assuming the bound limits.

Using the response surface method reduces the function evaluations and computational time, because solving the simultaneous equation is carried out only during the regression analysis. Only the response surface function is called in the subsequent iterations for the function evaluations.

APPENDIX A

Input file format is discussed below. It should be noted that the input needs to be in consistent units. The sample input format for the experimental data analysis is given below.

***heading**

a suitable heading describing the data

***data**

Strength or any parameter corresponding to the sample one per line.

***estimates**

Weibull2p (or) Weibull3p, 0 (or) 1 (1 represents weighted method)
GeneralizedExponential, upper limit (shape parameter)

For other distributions such the distribution name is sufficient and they are gamma, normal, lognormal

***end**

The sample input format for the reliability analysis (FORM, SORM, MCS) and RBDO are given below.

***Reliability_Analysis**

This input signals the beginning of reliability analysis data. The input corresponding to reliability analysis must be specified between reliability_analysis and end_reliability_analysis.

***Reliability_Technique**

Signals the type of reliability technique and followed by number of iterations for each performance function, number of line search, and target reliability value if RBDO is specified as reliability technique. Other types of technique are FORM, SORM and Monte Carlo.

***Random_Variable**

Signals the next few lines of input contain the random variable information. Each data line contains the random variable type and the associated information, and if required, the lower bound the upper bound and the precision. If the type is XSECTION (for element cross sectional area) or MODULUS (for Young's modulus) or COMPRESSIONALLOBALE/TENSIONALLOWABLE (allowable stresses), the next input is the type of distribution (normal/lognormal/weibull/gamma/generalized exponential) then property group number followed by lower bound, upper bound, mean value, standard deviation and parameters for non-normal distribution (scale and shape parameters). If the type is LOAD, the next input is the distribution type followed by load case, node number, direction (1 for x and 2 for y, -ve values for opposite direction), the remaining order is same as other random variables.

***Constraint**

This signals that next few lines of input contain constraint information. Each data line contains the constraint type and the associated information. If the type is STRESS (for stress constraint) the next input is the material group number. If the type is DISPLACEMENT (for nodal displacement constraint) the next inputs are the node number, the degree-of-freedom to use (1 for x, 2 for y) and the allowable displacement value.

***End_Reliability_Analysis**

Specify the end of reliability analysis data

REFERENCES

- 1 Naik, D., Sankaran, S., Mobasher, B., Rajan, S.D. and Pereira, J.M. (2009). "Development of Reliable Modeling Methodologies for Fan Blade-Out Containment Analysis. Part I: Experimental Studies." *J. of Impact Engineering*, 36, 1-11.
- 2 Bansal K. S. (2007). "Development of Micro-Mechanical Model for Dry Fabrics." MS Thesis, Arizona State University.
- 3 Rajan, S.D., Mobasher, B., Sharda, J., Yanna, Y., Deenadayalu, D., Lau, D. and Shah, D. (2004). "Explicit Finite Element Analysis Modeling of Multi-layer Composite Fabric for Gas Turbine Engines Containment Systems. Part 1-Static Tests and Modeling." FAA report DOT/FAA/AR-04/40, P1.
- 4 Revilock, D.M. and Pereira, J.M. (2004). "Explicit Finite Element Analysis Modeling of Multi-layer Composite Fabric for Gas Turbine Engines Containment Systems. Part 2: Ballistic Impact Testing." FAA report DOT/FAA/AR-04/40, P2.
- 5 Rajan, S.D., Mobasher, B., Stahlecker, Z., Bansal, S., Zhu, D., Morea, M. and Dhandapani, K. (2010). "LS-DYNA Implemented Multi-Layer Fabric Material Model Development for Engine Fragment Mitigation. Phase III, Part 2: Fabric Material Tests." FAA Report DOT/FAA/AR-10/23, 2010.
- 6 Vaidya, S.A. (2010). "Improvements in Modeling Techniques for Fabric based Aircraft Engine Containment Systems." MS Thesis, Arizona State University.
- 7 Fein, J. (2012). "Improvements in Numerical Modeling Methodology of Dry Woven Fabrics for Aircraft Engine Containment System." MS Thesis, Arizona State University.
- 8 Basu, B., Tiwari, D., Kundu, D. and Prasad, R. (2009). "Is Weibull the Most Appropriate Statistical Strength Distribution for Brittle Materials?" *Ceramics International*, 35, 237-246.
- 9 Cousineau, D. (2009). "Nearly Unbiased Estimators for the Three Parameter Weibull Distribution with Greater Efficiency than the Iterative Likelihood Method." *British Journal of Mathematical and Statistical Psychology*, 2009, 62, 167-191.

- 10 Cousineau, D. (2009). "Fitting the Three-Parameter Weibull Distribution: Review and Evaluation of Existing and New Methods." *IEEE Transactions on Dielectrics and Electrical Insulation*, 16, 281-288.
- 11 Cousineau, D. (2011). "The Fallacy of Large Shape Parameters when Using the Two-parameter Weibull Distribution." *TBC*.
- 12 Gupta, R.D. and Kundu, D. (2001). "Generalized Exponential Distributions: Different Methods of Estimation." *Journal of Statistical Computations and Simulations*, 69, 315-338.
- 13 Gupta, R.D. and Kundu, D. (2002). "Generalized Exponential Distributions: Statistical Inferences." *Journal of Statistical Theory and Applications*, 1, 101-118.
- 14 Gupta, R.D. and Kundu, D. (2003). "Closeness of Gamma and Generalized Exponential Distributions." *Communications in Statistics – Theory and Methods*, 32, 705-721.
- 15 Gupta, R.D. and Kundu, D. (2004). "Discriminating between Gamma and Generalized Exponential Distributions." *Journal of Statistical Computations and Simulations*, 74, 107-121.
- 16 Faris Dooraki, B., Nemes, J.A. and Bolduc, M. (2006). "Study of Parameters Affecting the Strength of Yarns." *J.Phys.IV France*, 134, 1183-1188.
- 17 Wang, Y., Miao, Y., Yen, C., Cheeseman, B. and Zhenq, J.Q. (2011). "Effects of Fiber Friction Coefficient on Fabric Penetration Resistance." *International Journal on Impact Engineering*, *TBC*.
- 18 Nilakantan, G., Keefe, M., Gillespie, J.W. and Bogetti, T.A. (2008). "Modeling the Material and Failure Response of Continuous Filament Fabrics for Use in Impact Simulation." *International Conference on Textile Composites*, Newark.
- 19 Gu, B. (2004). "Ballistic Penetration of Conically Cylindrical Steel Projectile into Plain-Woven Fabric Target-A Finite Element Simulation." *Journal of Composite Materials*, 2038-2049.
- 20 Haldar, A. and Mahadevan, S. (2000). "Reliability Assessment using Stochastic Finite Element Analysis." John Wiley & Sons Inc.

- 21 Hasofer, A.M. and Lind, N.S. (1974). "Exact invariant Second Moment Code Format." *Journal of the Engineering Mechanics Division*, 100, 111-121.
- 22 Rackwitz, R. and Fiessler, B. (1978). "Structural Reliability under Combined Random Load Sequences." *Computers and Structures*. 9, 484-494.
- 23 Kiureghian, A., Lin, H. and Hwang, S. (1987). "Second Order Reliability Approximations." *Journal of Engineering Mechanics*, 113, 1208-1224.
- 24 Kirughian, A. and Stefano, M. (1991). "Efficient Algorithm for Second Order Reliability Approximations." *Journal of Engineering Mechanics Division*, 117, 2904-2923.
- 25 Liu, P. and Der Kiureghian, A. (1991). "Optimization Algorithms for Structural Reliability." *Structural Safety*, 9, 169-177.
- 26 Thanedar, P.B. and Kodiyalam, S. (1992). "Structural Optimization using Probabilistic Constraints." *Structural Optimization*, 4, 236-240.
- 27 Royset, J.O., Der Kiureghian, A. and Polak, E. (2001). "Reliability Based Optimal Structural Design by the Decoupling Approach." *Reliability Engineering and System Safety*, 73, 213-221.
- 28 Enevoldsen, I. and Sorensen, J.D. (1994). "Reliability Based Optimization in Structural Engineering." *Structural Safety*, 15, 169-196.
- 29 Kuschel, N. and Rackwitz, R. (2000). "A New approach for structural Optimization of Series System." *Application of Statics and Probability*, 987-994.
- 30 Polak, E. Kirinjer-Neto, C. and Der Kiureghian, A. (1997). "Structural Optimization with Reliability Constraints." *Reliability and Optimization of Structural Systems, proceeding to the 7th IFIP WG 7.5 Boulder '96*, Pentagon, Oxford, 17-32.
- 31 Agarwal, H. (2004). "Reliability Based Design Optimization: Formulations and Methodologies." Ph.D. Dissertation, University of Notre Dame.
- 32 Tu, J., Choi, K.K., and Parl, Y.H. (1999). "A New Study on Reliability Based Design Optimization." *Journal of Mechanical Design*, 121, 557-564.

- 33 Mahadevan, S. and Haldar, A. (1988). "Efficient Algorithm for Stochastic Structural Optimization." *Journal of Structural Engineering*, 115, 1579-1598.
- 34 Zou, T. and Mahadevan, S. (2006). "A Direct Decoupling Approach for Efficient Reliability Based Design Optimization." *Struct. Multidisc. Optim*, 31, 190-200.
- 35 Chen, W. and Du, X. (2002). "Sequential Optimization and Reliability Assessment Method for Efficient Probabilistic Design." *Proceedings of DETC'02 ASME 2002 Design Engineering Technical Conferences and Computers and Information in Engineering Conference*, Montreal, Canada.
- 36 Liu, H., Chen, W., Sheng, J. and Chang, H. (2003). "Application of the Sequential Optimization and Reliability Assessment Method of Structural Design Problems." *Proceedings of DETC'03 ASME 2003 Design Engineering Technical Conferences and Computers and Information in Engineering Conference*, Chicago, Illinois.
- 37 Frangopol, M. and Maute, K. (2003). "Life Cycle Reliability Based Optimization of Civil and Aerospace Structures." *Computers and Structures*, 81, 397-410.
- 38 Frangopol, D.M. (1998). "Probabilistic Structural Optimization." *Progress in Structural Engineering and Materials*, 2, 223-230.
- 39 National Institute of Standards and Technology (NIST) (2006). "Engineering Statistics Handbook." <http://www.nist.gov/stat.handbook/>.
- 40 Kundu, D. and Manglick, A. (2004). "Discriminating between the Weibull and Log-Normal Distributions." *Naval Research Logistics*, 51, 893-905.
- 41 Cox, D.R. (1962). "Further Results on Tests of Separate Families of Hypothesis." *Journal of the Royal Statistical Society*, Ser. B, 24, 406-424.
- 42 Dhandapani, K., Jain, R., and Rajan, S.D. (2012). "Engineering Design Optimization (EDO) Workbench User's Manual." SSEBE.
- 43 Rackwitz, R. and Fiesler, B. (1976). "Note on Discrete Safety Checking when using Non-Normal Stochastic Models for Basic Variables." *Load Project Working Session*, MIT, Cambridge, MA.

- 44 Breitung, K. (1984). "Asymptotic Approximations of Multi-Normal Integrals." *Journal of Engineering Mechanics*, ASCE, 110(3), 357-366.
- 45 Montgomery, D.C. (2007). "Design and Analysis of Experiments. 5th edition." John Copyright © 2007, John Wiley & Sons. Inc.
- 46 Pan, B., Quian, K., Xie, H. and Asundi, A. (2009). "Two-Dimensional Digital Image Correlation for in-plane displacement and strain measurement: a review." *Measurement Science and Technology*, 20, 1-17.
- 47 Stahlecker, Z., Mobasher, B., Rajan, S.D. and Pereira, J.M. (2009). "Development of Reliable Modeling Methodologies for Fan Blade-Out Containment Analysis. Part II: Finite Element Analysis." *J. of Impact Engineering*, 36, 447-459.
- 48 LS-DYNA. (2003). "Keyword User's Manual: Version 971." Livermore Software Technology Corp, Livermore CA, 2003.
- 49 Vokshi, E., Deivanayagam, A. and Rajan, S.D. (2010). "Experimental Data Processing (EDP) Program User's Manual." SSEBE.
- 50 Mobasher, Barzin. (2012). "Mechanics of Fiber and Textile Reinforced Cement Composites." Taylor & Francis Group, LLC.
- 51 Zhu, D. (2009). "Experimental Study and Finite Element Modeling of Woven Fabrics." Ph.D Dissertation, Arizona State University.
- 52 Rajan, S.D. (2001). "Introduction to Structural Analysis and Design." John Wiley & Sons Inc.
- 53 Lee, S.J. (1987). "Reliability Based Optimal Structure and Mechanical Design Optimization." Ph.D Dissertation, University of Arizona.
- 54 Harbitz, A. (1986). "An Efficient Sampling Method for Probability of Failure Calculation." *Structural Safety*, 109-115.